Summer 6-21-2022

An Improved Polynomial Chaos Expansion Based Response Surface Method And Its Applications On Frame And Spring Engineering Based Structures

Mhd A. Hafez

AN IMPROVED POLYNOMIAL CHAOS EXPANSION BASED RESPONSE SURFACE METHOD AND ITS APPLICATIONS ON FRAME AND SPRING ENGINEERING BASED STRUCTURES

MHD AMMAR HAFEZ

Bachelor of Science in Civil Engineering

Damascus University

December 2012

Master of Science in Civil Engineering

Cleveland State University

December 2016

submitted in partial fulfillment of requirements for the degree

DOCTOR OF PHILOSOPHY IN ENGINEERING

at the

CLEVELAND STATE UNIVERSITY

AUGUST 2022

We hereby approve this dissertation for

MHD AMMAR HAFEZ

Candidate for the Doctor of Philosophy in Engineering degree

for the Department of Civil Engineering

and the CLEVELAND STATE UNIVERSITY'S

College of Graduate Studies by

Jason P. Halloran, Ph.D, Dissertation Committee Chairperson

Department of Mechanical Engineering, 6/21/2022

Lutful I Khan, Ph.D, Dissertation Committee Member

Department of Civil Engineering, 6/21/2022

Stephen F Duffy, Ph.D, Dissertation Committee Member

Department of Civil Engineering, 6/21/2022

Josiah Sam Owusu-Danquah, Ph.D, Dissertation Committee Member

Department of Civil Engineering, 6/21/2022

Daniel S Munther, Ph.D, Dissertation Committee Member

Department of Mathematics, 6/21/2022

Date of Defense: June 21, 2022

This student has fulfilled all requirements for the Doctor of Philosophy degree

---

Chandra Kothapalli, Ph.D, Doctoral Program Director

ACKNOWLEDGEMENTS

I would like first to thank Allah for giving me the chance to complete my degree. After Allah, I want to thank my parents, who supported me in every possible way and still have their unconditional support.

I would also like to thank my wife, Shaza, and my daughter Rana for the support along this journey. Their support was crucial in motivating me to complete my degree.

Finally, I would like to thank my advisor, Dr. Jason Halloran who supported me making the transition from Civil Engineering and gave me the freedom to research areas I am interested in. I would also thank the department of Civil Engineering for their support, and my committee members for their guidance.

AN IMPROVED POLYNOMIAL CHAOS EXPANSION BASED RESPONSE SURFACE METHOD AND ITS APPLICATIONS ON FRAME AND SPRING ENGINEERING BASED STRUCTURES

MHD AMMAR HAFEZ

Abstract

In engineering fields, computational models provide a tool that can simulate a real world response and enhance our understanding of physical phenomenas. However, such models are often computationally expensive with multiple sources of uncertainty related to the model's input/assumptions. For example, the literature indicates that ligament's material properties and its insertion site locations have a significant effect on the performance of knee joint models, which makes addressing uncertainty related to them a crucial step to make the computational model more representative of reality. However, previous sensitivity studies were limited due to the computational expense of the models.

The high computational expense of sensitivity analysis can be addressed by performing the analysis with a reduced number of model runs or by creating an inexpensive surrogate model. Both approaches are addressed in this work by the use of Polynomial chaos expansion (PCE)-based surrogate models and design of experiments (DoE). Therefore, the objectives of this dissertation were: 1- provide guidelines for the use of PCE-based models and investigate their efficiency in case of non-linear problems. 2- utilize PCE and DoE-based tools to introduce efficient sensitivity analysis approaches to the field of knee mechanics.

To achieve these objectives, a frame structure was used for the first aim, and a rigid body computational model for two knee specimens was used for the second aim. Our results showed that, for PCE-based surrogate models, once the recommended number of samples is used, increasing the PCE order produced more accurate surrogate models. This conclusion was reflected in the R^2 values realized for three highly

non-linear functions (*0.9998*, *0.9996* and *0.9125*, respectively). Our results also showed that the use of PCE and DoE-based sensitivity analyses resulted in practically identical results with significant savings in the computational cost of sensitivity analysis when compared to a traditional quasi-Monte Carlo (MC) approach (95% and 98% reductions in model evaluations for analyses with 10 and 6 uncertain variables, respectively). Finally, the use of D-optimal DoE resulted in a reduction in the number of samples required to perform sensitivity analysis by 64.4%, which reduced the computational burden by 1018 hours.

Table of Contents

List of Tables

List of Figures

CHAPTER I

Introduction and Objectives

1.1 Introduction

In engineering fields, engineers often aim to create models that simulate real world response. In this regard, the Finite Element Method (FEM) is one of, if not the most, widely utilized approaches. FEM includes solving a system of equations, with n represents the degrees of freedom (Logan et al. 2007). For large structures, i.e. a high number of degrees of freedom, the computational cost of solving this system of equations can be burdensome, even for deterministic evaluation of relatively straightforward linear problems. Further compounding computational cost, inherent variability in loads, material and geometric properties (system inputs) requires iterative analysis, which is often needed as a single (or "deterministic") result may not reflect real world failure (Stefanou 2009). Hence, the topic of structural reliability became an established area, which focuses on predicting the probability of failure as a result of variable inputs (Basaga, Bayraktar, and Kaymaz 2012). Stochastic FEM (SFEM) is an umbrella term for this type of analysis and within this Monte Carlo Simulation (MCS) is considered the gold standard, which is based on running a model several hundreds, and likely thousands, of times before reliable calculation of moments of the

output can be realized (e.g., mean, standard deviation). While reliable, a shortcoming of MCS is the slow rate of convergence of $\frac{1}{\sqrt{S}}$, where S is the number of model runs (Xiu 2009). When a problem also requires a high number of degrees of freedom, even one FE model evaluation can be costly and the need for methods with higher rate of convergence become a necessity (Ghanem and Spanos 2012). Polynomial based Stochastic Response Surface Method (RSM-PCE) is a technique that can be used to represent the structural model as a polynomial, which builds a polynomial representation of the "expensive" engineering model with relatively few simulations while still predicting a relatively accurate probability of failure (Rajashekhar and Ellingwood 1993). Polynomial Chaos Expansion (PCE) was introduced by Ghanem and Spanos (Ghanem and Spanos 2012) in the context of Spectral Stochastic Finite Element Modeling (SSFEM) (Ghanem and Spanos 2012; Huang and Kou 2007; Keshavarzzadeh, Fernandez, and Tortorelli 2017), which combine to create one RSM-PCE. In SSFEM, PCE was used to represent the output of interest using Gaussian random variable inputs. SSFEM is considered an intrusive approach (Stefanou 2009; Sudret 2014) as it requires modifications of the FEM partial equations, which presents challenges for complicated problems (Ghanem and Spanos 2012; Xiu 2009) and led to the development of non-intrusive approaches (Stefanou 2009; Sudret 2014; Berveiller, Sudret, and Lemaire 2006). Multiple non-intrusive approaches treat the FEM model as a black-box. Using these methods the analyst can make use of existing deterministic codes, which gives non-intrusive methods one important advantage over intrusive methods. PCE, in particular, can be used as a non-intrusive method, where a corresponding polynomial based model is created that represents each output (e.g., displacement, stress, strain) as a function of the inputs, which in concept is similar to an RSM-PCE. Similar to the highlighted FEM approaches, non-intrusive polynomial based representation of complex engineering problems can equally apply to any "black-box" model that requires relatively efficient representation of a given response. The general area of

computational biomechanics offers numerous possibilities, where even relatively "simple" spring based models may require thousands of simulations to accurately capture the sensitivity of a given model. Potential application areas for efficient representation of biomechanics span many structures, though knee modeling represents a particularly promising area of application. Current approaches for structural knee analysis typically calibrate a given specimen-specific model based on measured kinetic-kinematic (i.e. force-displacement) data. Calculation of a given model's sensitivity, whether performed during or after the calibration process, can require thousands of model evaluations to arrive at reliable results. As a result, it would be beneficial to mitigate computational cost through implementation of RSM-PCE on a knee model of interest (Zaylor, Stulberg, and Halloran 2019), especially if it has the potential to be a resource for both research and clinical questions.

Regardless of the type of underlying model, three solutions are widely used for calculating the polynomial coefficients of a non-intrusive PCE problem: the projection approach, regression approach and stochastic collocation method (Berveiller and Sudret 2004; Xiu 2010; Huang and Kou 2007). In each of these methods, the number of unknown coefficients increases rapidly with the increment of the number of random variables and the order of the PCE. Therefore, work has been performed to improve the efficiency of these solution methods, where one focus has been on reducing the number of required input variables. The focus of this work is on the regression method, and in particular the technique for selection of variables that seek to reduce the required number of model evaluations (e.g., "samples") for improved efficiency. To put the proposed approach in context, stepwise regression has previously been used for variable selection (Blatman and Sudret 2010b; Blatman and Sudret 2010a). However, stepwise regression was not recommended in (Flom and Cassell 2009) because the estimated values of parameters tended to be biased towards zero, which led to the introduction of a variation in the least angle regression (LAR) approach (Efron

et al. 2004; Blatman and Sudret 2011). In LAR independent output random variables were assumed. Although the use of statistical learning tools (e.g., LAR, Lasso) decreases the number of PCE terms significantly, non-linear problems still require a high number of samples to realize accurate results. Highlighting this issue, (Field and Grigoriu 2004) introduced three examples, each of which is a function that includes non-linearity, where both a low rate of convergence and a high PCE order (as well as the required number of terms) were required to realize accurate results, which negatively impacted the attractiveness of this approach. This highlighted, whether an intrusive or non-intrusive approach is used in combination with dimension reduction, nonlinear problems will still require a high number of samples to accurately represent the nonlinear regions of the model. While linear problems can be accurately captured using uniform sampling techniques (e.g., Latin hypercube sampling (LHS)), the increase in the required sample size for nonlinear problems demonstrated that a better design of experiments (i.e. "sampling") is required. "D-optimal" design of experiments is one such possibility to overcome this issue, where input random variables are found through sequential refinement of the sampling space. In this approach, optimization is used to reduce the required number of samples.

First aim

As shown previously, RSM-PCE is a well-established method. However, the literature still lacks clear guidelines, especially for non-expert users, since constructing the surrogate model requires many iterations using different combinations of PCE orders (to capture the behavior of the original model) and number of samples (runs of the original expensive model). Therefore, the first main aim of this work is to provide guidelines that help to reach a reliable RSM-PCE model in the most efficient way possible, in addition, to testing these guidelines in the case of nonlinear functions.

Second aim

Computational knee models, whether are finite elements-based (Harris et al. 2016; Halloran et al. 2005; Halloran, Petrella, and Rullkoetter 2005) or rigid body-based (Zaylor, Stulberg, and Halloran 2019), are often complex, computationally expensive, and include multiple sources of uncertainty. A deterministic analysis fails to capture the effects of these uncertainties, which has implications when drawing conclusions or making decisions based on modeling outcomes. Offering a clear understanding of the impact of these uncertainties, would likely improve the credibility and the potential to be reproduced. Therefore, the second main aim of this work is to show the applicability of RSM-PCE-based sensitivity analysis and D-optimal-based sensitivity analysis to an in-house previously developed rigid-body framework, which was tested and validated against traditional finite element approaches (Zaylor, Stulberg, and Halloran 2019; Zaylor and Halloran 2021). This applicability shows the true value of RSM-PCE in real-world problems by producing accurate results with a low number of model evaluations compared to traditional methods.

1.2 Objectives

To address the research aims, this study has the following objectives:

1- **Guidelines for the use of RSM-PCE (Aim 1):** While RSM- PCE showed promising results in the literature, the literature still lacks an answer to a question that might arise while using this method: what is the fastest way to converge to a MC solution while using this method; is it increasing the PCE order or increasing the number of samples?. Thus, the first objective of this work is to answer this question by introducing RSM-PCE linear solution of a structural frame (**Chapter II**).

Contribution: A Novel study for the convergence of Response Surface Method using Polynomial Chaos Expansion.

2- **Efficiency of RSM-PCE in case of non-linear problems (Aim 1):** Most of engineering problems show high non-linear behavior. Therefore, for the method considered to be useful, an efficient RSM-PCE solution is required for non-linear problems. The second objective of this work is to solve three non-linear functions (Field and Grigoriu 2004) as a proof of concept for the performance of RSM-PCE for the case of highly nonlinear functions (**Chapter III**).

Contribution: A key limitation of PCE based methods was overcome using the proposed method.

3- **RSM-PCE based sensitivity analysis for Biomechanics problems (Aim 2):** Sensitivity analysis is a probabilistic analysis which main purpose is to enhance our understanding of a given model by analyzing the effect of the inputs (independent variables) on the output (dependent variables). Sensitivity analysis becomes a tedious task in the case of computationally and time intensive biomechanics models. Therefore, surrogate models (e.g. RSM-PCE) are desirable alternatives. A RSM-PCE sensitivity analysis for biomechanics problems is introduced in this work. The method is introduced by: first, constructing a biomechanics problem through a calibration of ligament properties using distraction based measurements, which is in itself a novel contribution to the biomechanics field (**Chapter IV**), and second, validating the use of the proposed sensitivity method by investigating sensitivities of the calibrated ligaments properties on knee reaction forces (**Chapter V**). On a specimen-specific basis, this type of capability could efficiently highlight the relative importance each ligament carries using a metric (i.e. knee reactions) that is thought to dictate joint health (objective 4, below, and chapter V) .

Contribution: A new approach to perform sensitivity analysis in biomechanics problems is introduced.

4- **A comprehensive study of Knee Reaction Sensitivity to Properties**

of Ligaments – Application of Distraction Based Models (Aim 2): Use two example calibrated knee models, a study was performed to compare quasi-MC versus PCE-based sensitivity analyses of predicted condylar reactions that include uncertainty in the mechanical parameters of the ligaments. (**Chapter V**).

Contribution: By developing a means to offer direct insight into specimen-specific ligament loading, this work aims to show progress towards simulation-based tools that can potentially be used for research and to support the clinical decision-making process.

5- **Sensitivity to Insertion Site Location for Model-Predicted Ligament and Condylar Loads in Two Knee Specimens: (Aim 1):** Using design of experiments technique and ANOVA statistical analysis, the purpose of this chapter was to introduce an automated framework to perform a sensitivity analysis of femoral insertion site locations of the dominant knee's load-carrying ligaments relevant in arthroplasty (LCL, PCL, and MCL) (**Chapter VI**).

Contribution: A novel approach to select ligaments insertion sites accurately especially in the case of the usage of poor medical images.

1.3 Stochastic Response Surface Method (Overview)

Consider a physical system (frame type structure) that can be represented by a mathematical model M (e.g., finite element):

$$Y = M(X) \tag{1.1}$$

Where X is a vector of random variables inputs (e.g., loads, material properties) with joint probability density function , and is the random output of interest (e.g.,

displacements).

PCE approximation

(Ghanem and Spanos 2012) first introduced PCE concept, equation 1.2 shows PCE formula:

$$U = \sum_{i=o}^{\infty} u_i \psi_i(H) \tag{1.2}$$

Where U is the random output of interest, H is the random inputs vector, u_i are coefficients and ψ_i is the polynomial basis. Equation 1.2 represents an infinite series of terms. However, in practice only finite number of terms is considered (Sudret 2014). Thus, equation 1.2 becomes:

$$U = \sum_{i=o}^{n} u_i \psi_i(H) \tag{1.3}$$

where n is the number of terms. Equation 1.3 is called PCE approximation. In the case of Gaussian random variables, Hermit polynomials are used (Ghanem and Spanos 2012). Table 1.1 shows hermit polynomial for one random variable and first five orders:

p=0	1
p=1	ξ
p=2	ξ^2-1
p=3	ξ^3-3ξ
p=4	ξ^4-6ξ^2+3

Table 1.1: PCE for one random variable and first five orders

where ξ is a standard normal variable.

Since the input variables are not always standardized (centered around zero mean), the following is used for standardization:

$$\frac{X_i - \mu_i}{\sigma_i} \tag{1.4}$$

where μ is the mean and σ is the standard deviation. The number of coefficients (also the number of terms) in Equation 1.3 can be calculated using:

$$n = \frac{(N+P)!}{N!P!} \tag{1.5}$$

where N is the number of random variables and P is the order of PCE. This number increases rapidly when the number of variables and number of terms increase. Table 1.2 shows number of coefficients for different number of random variables and PCE terms:

	p=2	p=3	p=4	p=5	p=6	p=7	p=8
N=2	6	10	15	21	28	36	45
N=3	10	20	35	56	84	120	165
N=4	15	35	70	126	210	330	495

Table 1.2: Number of PCE coefficients

To reduce the computational effort, only important terms of PCE formula are selected. In this work, we use LASSO regression for selecting important PCE terms (see section 1.3).

Detailed descriptions of algorithm specific settings are included in the following sections and an flowchart highlights the workflow 1.1:

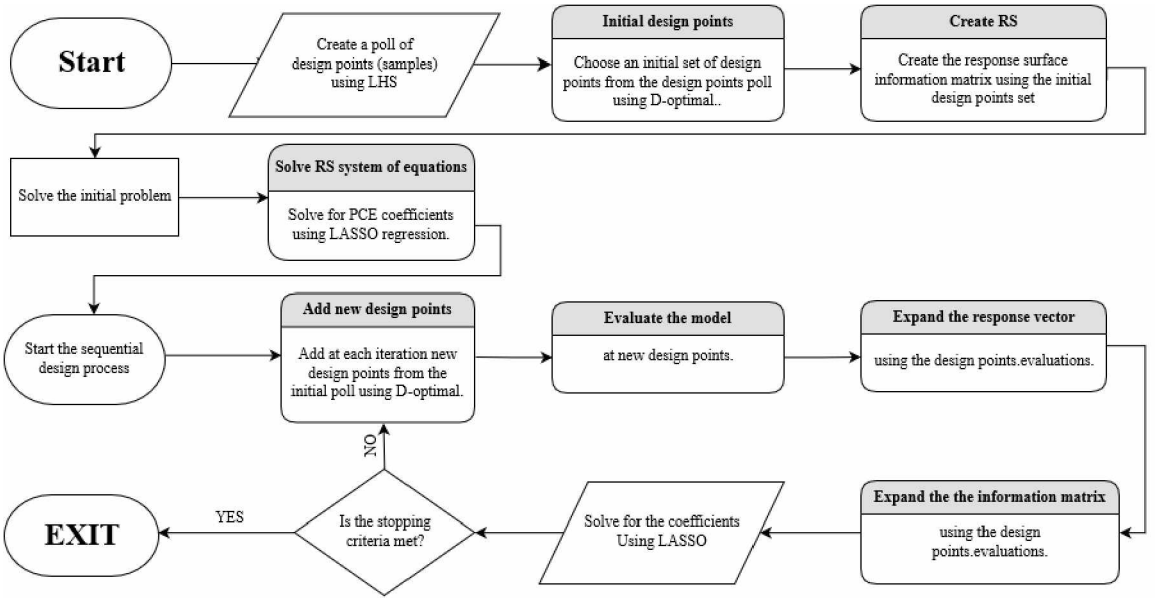

Figure 1.1: The sequential procedure used to implement both LASSO regression and D-optimal design of experiments in the PCE approximation workflow.

The algorithm steps will be discussed further in the following sections.

Sampling method

The main aim of RSM-PCE is to reduce the computational burden and an efficient sampling method is required for RSM-PCE to be feasible. LHS is used in the context of this work. LHS has been shown to converge faster than Monte Carlo sampling (Fajraoui, Marelli, and Sudret 2017; Xiu 2009). In summary, LHS divides the sampling space into equally probable intervals , where one sample is drawn randomly from each interval. To ensure the quality and space filling of our sampling, the "maximin" criteria is used (Morris and Mitchell 1992). The covariance structure (equation 1.6) of LHS samples was assumed to be exponentially decaying (Jalalpour and Tootkaboni 2016).

$$cov_{ij} = \sqrt{var_{ii} var_{jj}} \exp\left(\frac{-||d_i^{'} - d_j^{'}||}{L_{exp}}\right) \tag{1.6}$$

where cov_{ij} is the covariance between elements i and j, var_{ii} is the variance, $d_i^{'}$ is the coordinate for center of element i and L_{exp} is the correlation length. The higher

is L_{exp}, the stronger is the correlation.

LASSO regression:

Equation 1.3 represents a regression problem. The coefficients in equation 1.3 are usually estimated using ordinary least square (OLS). However, OLS estimates suffer from high variance. LASSO deals with the high variance issue by applying the following criterion:

$$\sum_{i=o}^{n} |u_i| \leq t \tag{1.7}$$

where t is a tuning parameter. When t has a large value, the criterion has a low effect and the solution is equivalent to least squares solution. However, LASSO shrinks some coefficients and set others to *0* when t has smaller values. As a result cross-validation (CV) was applied to tune the parameter t and select the best model (Krstajic et al. 2014). In this work, LASSO regression was used to estimate the regression coefficients and select the most important variables (Tibshirani 1996).

Optimal design of experiments

(Zein, Colson, and Glineur 2013) stated the RSM-PCE problem size depends on the number of evaluation that are required to estimate the PCE coefficients, which is not feasible in case of large problems. Many algorithms have been proposed to improve efficiency and reduce the number of model evaluations by incorporating the design of experiments concept. Due to its basis in minimizing the variance in the regression coefficients, D-optimal design criterion was selected in this work. The goal of the optimal design is to select rows from the information matrix A in an optimal way, where A is the matrix of the polynomial basis $\Psi_i(H)$, which was evaluated at each design point. This is accomplished by minimizing the variance of the OLS solution predicted response. Thus, D-optimal is an optimization problem. The solution

of this problem is provided by maximizing the determinant of the $|A^T A|$. In this criterion, the model, the candidate set of design points and the number of optimal design points required from the candidate set are predefined (which makes D-optimal a model dependent design). It was shown that use of the D-optimal algorithm reduces the number of model evaluation by almost three times lower (Zein, Colson, and Glineur 2013) compared to traditional method (Projection method) with good accuracy (difference of 1%-6%). Even though the results from (Zein, Colson, and Glineur 2013) showed measurable improvement the use of statistical tools of variable selection was not used, which may further reduce the computational cost. (Fajraoui, Marelli, and Sudret 2017) introduced an algorithm that couples the benefits from the statistical learning tools in addition to the design of experiments tools. Two design of experiments tools were used, D-optimal design criterion and S-optimal design criterion (Shin and Xiu 2016). In the proposed algorithm, a sequential design of experiments was also added, which works by:

1- Selecting an initial set of design points using any sampling method (i.e., LHS).

2- A variable selection procedure is used to reduce the information matrix dimensions.

3- A set of design points is selected by using a design of experiment criterion.

4-Using the information collected by the set from the previous step, more design points are added to the initial set, and this process is repeated until the number of design points desired by the user is reached.

Since D-optimal criterion is a well-established and easy to implement method, it was selected for this work.

CHAPTER II

Guidelines for the use of RSM-PCE

2.1 Introduction

RSM-PCE is a well established method in the literature, however, a systematic approach for use of this method has not been established. With this consideration, this work will attempt to answer the following question: what is the fastest way to create a reliable RSM-PCE model compared to MC solution; Is it increasing the PCE order or increasing the number of samples? Thus, the aim of this chapter will answer this question by systematically evaluating the order of polynomial and the number of required samples for RSM-PCE representations of a linear 2D frame structure.

2.2 Problem Description

A structural frame with eight elements subjected to seven normally distributed loads R_i was defined to represent a hanger structure. Figure 2.1

$$R_i \; N(\mu, \sigma^2) : i = 1, 2, ..., 7 \tag{2.1}$$

Where $\mu = 1000N$, $\sigma = 2000N$, $E = 2.1 * 10^6 Mpa$, $A = 4000mm^2$ and $I = 1.33 * 10^8 mm^4$

A static linear analysis was performed using an in house developed FE code that has been verified by OpenSees software (McKenna, Fenves, and Scott 2000; Mazzoni et al. 2007).

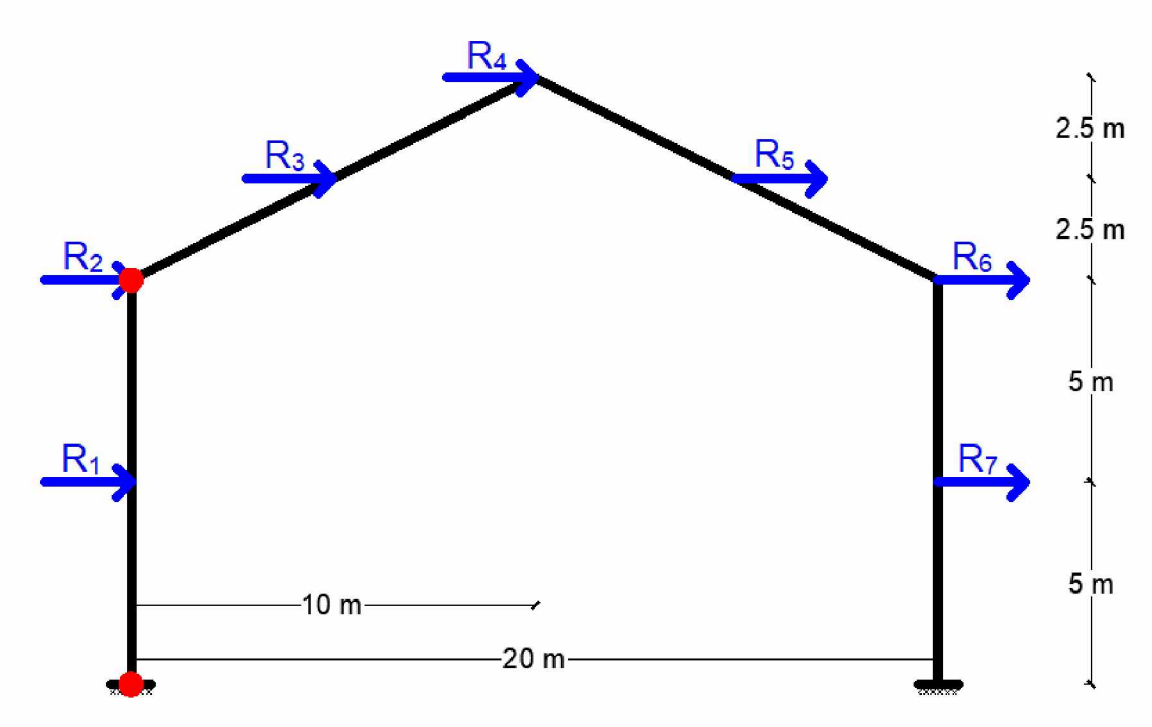

Figure 2.1: Structural Frame subjected to static point loads.

In this example, two responses were considered. First, the horizontal displacement at R_2, which will be referred to as *"$R_{2h.}$"* Second, the moment at the fixed end, *"$R_{AM.}$"* These two responses were chosen to demonstrate the behavior of RSM-PCE in different range of response magnitude. Monte Carlo simulation with 10^6 samples was performed as a validation for the proposed method. In this example, we assess the performance of RSM-PCE approximation by 1) comparing the error between the statistics found using MC simulation versus those from RSM-PCE approximation and 2) specific evaluation of the ability of RSM-PCE to capture the tails of the corresponding MC simulations. Evaluation of the tails has relevance for questions that require prediction of probability of failure at the extremes of a given response.

2.3 Methods and Results

We start by investigating the effect of increasing the order of PCE on analysis results accuracy. The frame was analyzed with 2^{nd}, 3^{rd}, and 4^{th} PCE order. The number of LHS samples for each order is twice the number of the PCE coefficients and with a correlation length L_{exp} set to 5000 to ensure a strong correlation. For the R_{2h} response all PCE orders gave a good approximation for the mean values (in order of $10^{-}3$) compared to MC results. For the standard deviation the 4^{th} order PCE gave the best approximation with 1% error, while the error was 1.5% and 3% for the 2^{nd} the 3^{rd} order respectively. The same behavior was observed for the R_{AM} response for both the mean and standard deviation values 3% for the 2^{nd} order PCE, 1.6% for the 3^{rd} PCE order and 1% for the 4^{th} PCE order)

This investigation continued by increasing the number of samples using the same PCE order. The frame was analyzed using the 2^{nd} order PCE for 18, 36 and finally 72 samples. The correlation length, L_{exp}, was set to 50000 to ensure a strong correlation. Results of this exploration showed that increasing the number of samples using same PCE order did not improve the results. Although the mean values yielded acceptable approximations compared to those obtained from MC simulation for both cases, the standard deviation values did not improve the by increasing the number of samples. Note the errors were approximately 4% for 18 and 36 samples and 3% for the 72 samples for the R_{2h} and the R_{AM} (Tables 2.1, 2.2 ,Figures 2.2,2.3).

R_{2h} (mm)						
	MC	PCE_2nd(18)	PCE_2nd(36)	PCE_2nd(72)	PCE_3rd(240)	PCE_4th(660)
Mean	16.052	16.0519	16.0518	16.05183692	16.03825056	16.05066602
% Error between MC and RSM-PCE	0.0000	-6.23E-04	-1.25E-03	-1.02E-03	-8.57E-02	-8.31E-03
STD	2.9333	2.8153	2.8193	2.8457	2.8900	2.9024
% Error between MC and RSM-PCE	0.0000	-4.0228	-3.8864	-2.9874	-1.4770	-1.0526

Table 2.1: The error between MC simulation and RSM-PCE approximation for R_{2h}. PCE with different orders (number of samples between parentheses) were used. The error shows an improvement by increasing the PCE order used in the approximation against increasing the number of samples used.

R_{AM} (N.mm)						
Mean	2.0E+08	2.0E+08	2.0E+08	2.0E+08	2.0E+08	2.0E+08
% Error between MC and RSM-PCE	0.0000	0.0000	0.0000	-0.0011	-0.1019	-0.0082
STD	3.7E+07	3.5E+07	3.5E+07	3.6E+07	3.6E+07	3.7E+07
% Error between MC and RSM-PCE	0.0000	-3.874	-5.015	-3.059	-1.667	-0.980

Table 2.2: The error between MC simulation and RSM-PCE approximation for R_{AM}. PCE with different orders (number of samples between parentheses) were used. The error shows an improvement by increasing the PCE order used in the approximation against increasing the number of samples used.

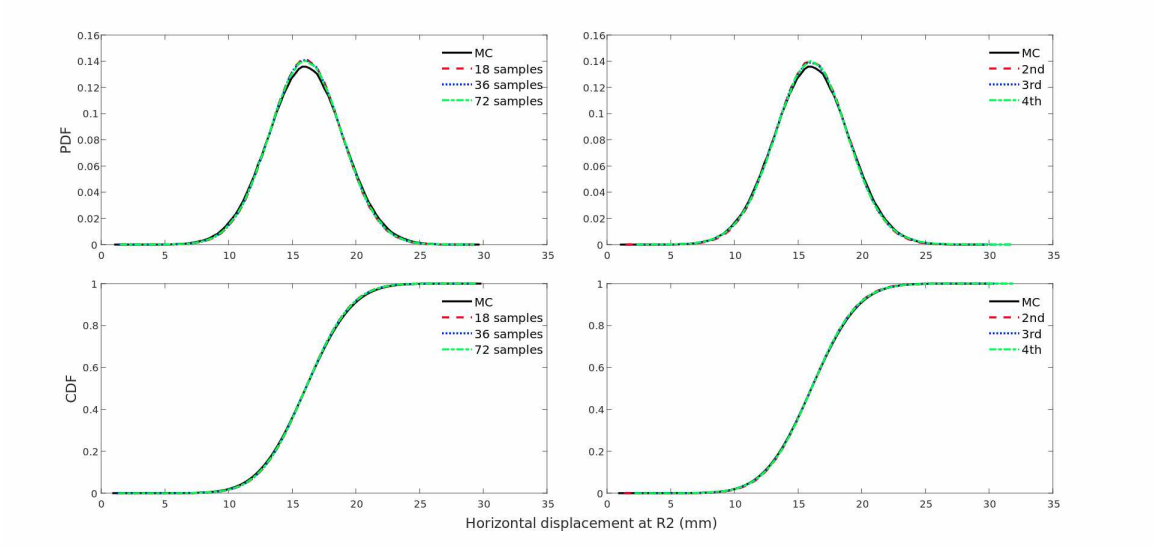

Figure 2.2: The upper two figures show the Probability distribution functions (PDF) for R_{2h} with different number of samples using the 2nd order PCE (upper left) and using different PCE orders (upper right). The lower two figures show the Cumulative distribution functions (CDF) for R_{2h} with different number of samples using the 2nd order PCE (upper left) and using different PCE orders (upper right).

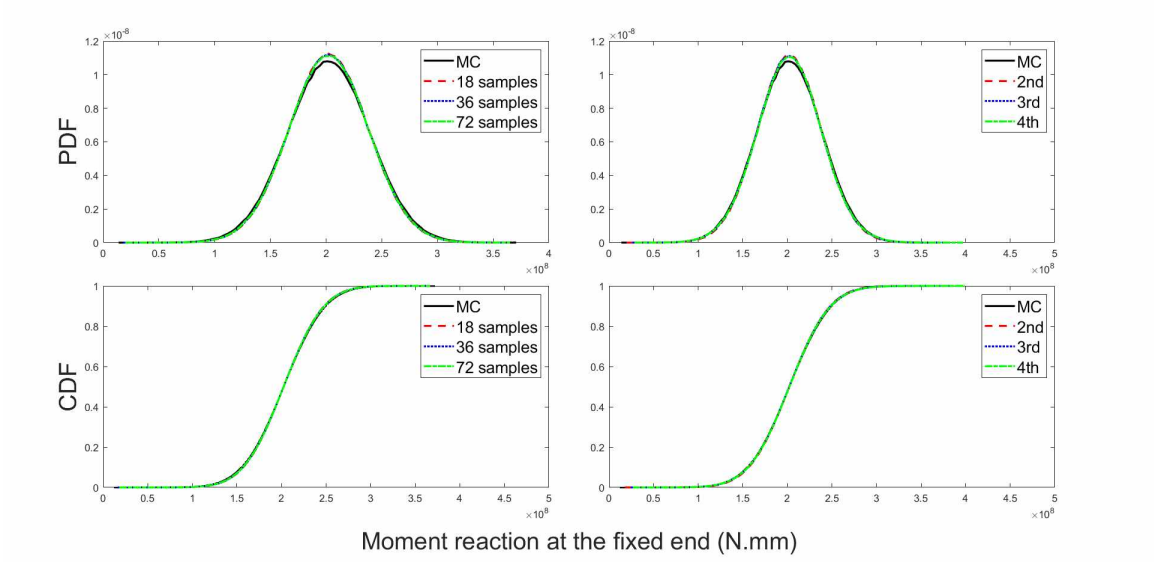

Figure 2.3: The upper two figures show the PDFs for R_{AM} with different number of samples using the 2nd order PCE (upper left) and using different PCE orders (upper right). And the lower two figures show the CDFs for R_{AM} with different number of samples using the 2nd order PCE (upper left) and using different PCE orders (upper right).

In addition to the good approximation of the mean the standard deviation values according to the used criteria, increasing the PCE order from 2^{nd} to the 3^{rd} and finally to the 4^{th} PCE order showed a better behavior by following the tails of the MC simulation, which has implications for assessing design values when low probability of failure is required (e.g. in case of designing important structures). However, 3^{rd} order PCE was sufficient for this specific problem while using the 4^{th} PCE order overestimated the MC solution. This result was also due to the efficiency of the variable selection process, where the 2nd order PCE used eight variables while eleven was needed for 3^{rd} and 4^{th} PCE approximations (Figures 2.4, 2.5)

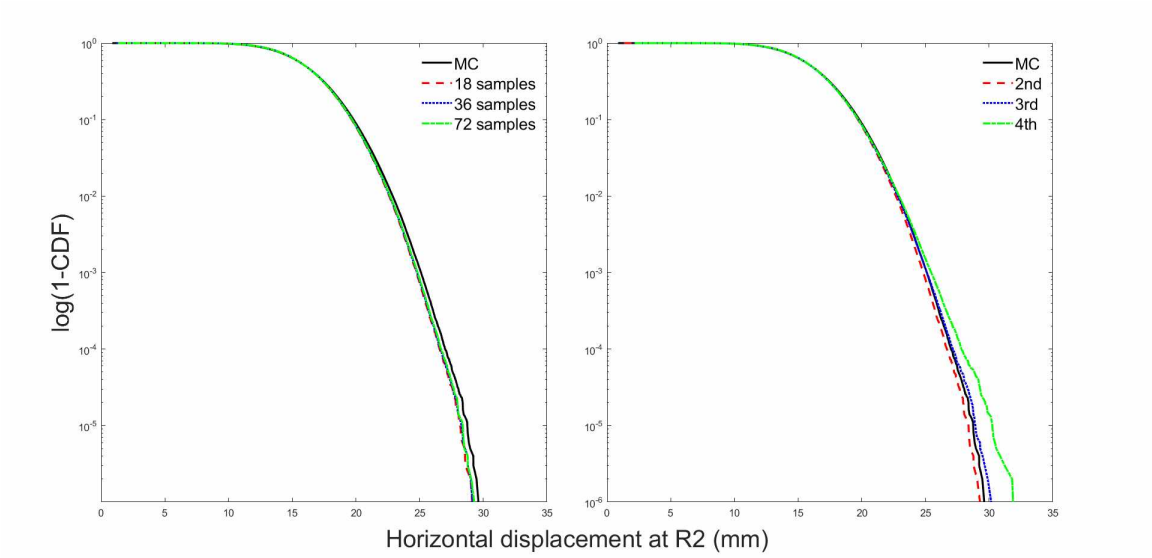

Figure 2.4: The complementary of the CDF plotted in logarithmic scale for R_{2h} with different number of samples using the 2^{nd} order PCE (left) and using different PCE orders (right). The left figure shows that using the 2^{nd} order PCE did not recreate a reliable approximation. i.e. it underestimated the response. compared to the MC solution because it could not predict the tail of R_{2h} when compared to the MC solution. even when higher number of samples was used. However. increasing the order of PCE used did create a reliable model compared to MC solution in both 3^{rd} PCE order and more conservative approximation by using 4^{th} PCE order.

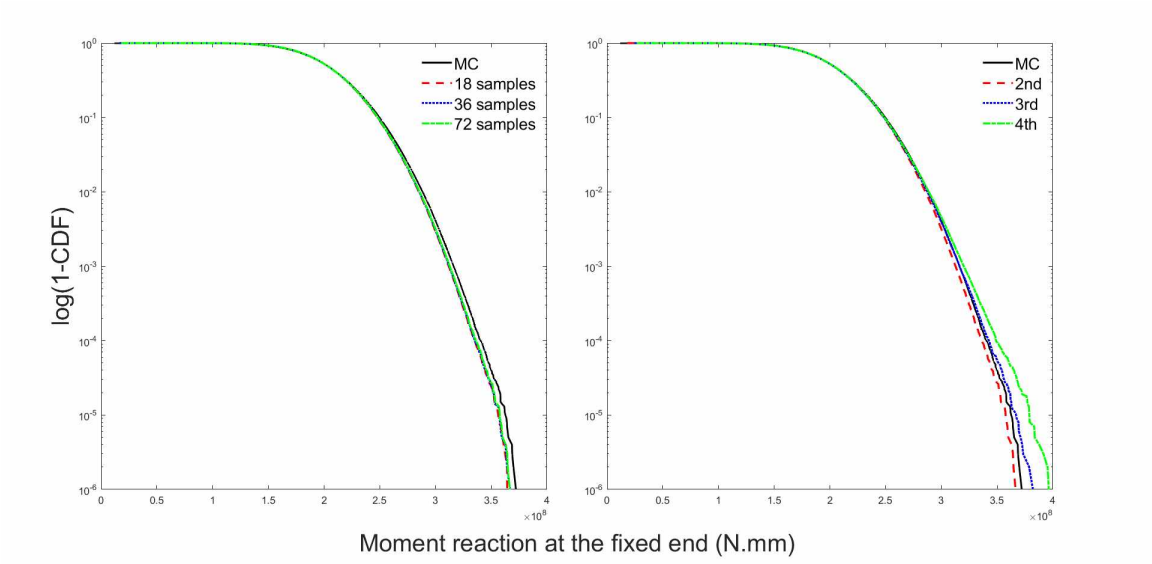

Figure 2.5: The complementary of the CDF plotted in logarithmic scale for R_{AM} with different number of samples using the 2^{nd} order PCE (left) and using different PCE orders (right). The left figure shows that using the 2^{nd} order PCE did not recreate a reliable approximation, i.e. it underestimated the response, compared to the MC solution because it could not predict the tail of R_{AM} when compared to the MC solution, even when higher number of samples was used. However, increasing the order of PCE used did create a reliable model compared to MC solution in both 3^{rd} PCE order and more conservative approximation by using 4^{th} PCE order.

2.4 Conclusion and Contribution

In this chapter, a structural frame subjected to correlated Gaussian random variable inputs was analyzed using RSM-PCE. LASSO regression was used to find PCE coefficients and select the important variables. The results show that increasing the number of LHS samples with fixed PCE order was not sufficient to create a reliable model compared to MC solution. However, increasing the PCE order was sufficient to create a reliable model, as reflected by a more conservative representation of the tail of the distributions (Figures 2.4, 2.5). As for criteria for the comparison between RSM-PCE and MC solutions, we used the error between the mean and standard deviation values approximated by RSM-PCE solution and the ones obtained by MC simulations as the first criterion, and the ability of RSM PCE solution to follow the

tails of the MC solution as a second criterion. The ability of following the tails is important because the tails include the extreme design values that are required to be included in the design process for a reliable probabilistic design. These results are due to the efficiency of the sampling method and the variable selection process performed by LASSO regression and Cross validation. The aim of this chapter was to fill a gap in the literature by introducing a few guidelines that help the users of this method to get faster and more accurate results.

CHAPTER III

Application of RSM-PCE on Nonlinear Functions

3.1 Abstract

RSM-PCE is a well established method in the literature, however, it still has a few shortcomings. One of these shortcomings is the high computational demand in case of highly nonlinear problems. Addressing such shortcomings is important because most of real-world engineering problems show one or multiple aspects of nonlinearity.

The aim of this chapter is to solve three nonlinear functions (Field and Grigoriu 2004) as a proof of concept for the performance of RSM-PCE approximation with low computational demand. The results showed that the algorithm also produced excellent results (high R^2 values) for the evaluated nonlinear functions, which also realized a reduction of the required PCE coefficients by half in some cases.

3.2 Introduction

Most of engineering problems show nonlinear behavior. Therefore, a good behavior for RSM-PCE in nonlinear condition is a requirement for the method to be practical.

(Field and Grigoriu 2004) highlighted a limitation in PCE approximation for nonlinear behavior; a high PCE order is required for nonlinear problems, which also

results in a high number of coefficients needed for acceptable results. In the case of non-intrusive methods, that was directly related to the required number of samples which reflects to the high computational demand. However, (Field and Grigoriu 2004) use of the PCE approximation did not include the use of variable selection and the design of experiment concepts, which reduces the computational demand dramatically. Thus, the aim of this chapter is to solve three nonlinear functions (Field and Grigoriu 2004) as a proof of concept for the performance of RSM-PCE approximation with low computational demand by reducing the number of samples required and the number of PCE coefficients needed to be calculated.

3.3 Problems description

The behavior of the proposed algorithm for three non-linear functions was evaluated. The three functions from (Field and Grigoriu 2004) were considered: $Y_1 = \exp(z)$, $Y_2 = F_y^{-1} \cdot \Phi(Z)$ and $Y_3 = |Z|$, where $Z \sim N(0,1)$ is normally distributed random variable and F_y is CDF of a uniformly distributed random variable. In this chapter, the coefficient of determination R^2 is used. R^2 is measurement of how well a model can predict the data, which takes values between 0 and 1. The higher the value of R^2, the better the RSM-PCE approximation fits the true mapping of a given function (Y_1, Y_2 and Y_3 in this case).

3.4 Results

In all three examples, without using D-optimal design criterion and the LASSO regression, thousands of model evaluations were needed to approximate the functions sufficiently. While incorporating the steps included in this work, only 42 model evaluations were needed to approximate Y_1 with 5^{th} order PCE, and 60 model evaluations for Y_2 and Y_3 with 9^{th} order PCE. In all three examples the RSM-PCE approximation was able to follow the true mapping of the considered function, including the tails

with high R^2 values (*0.9998*, *0.9996* and *0.9125* for Y_1, Y_2 and Y_3, respectively).

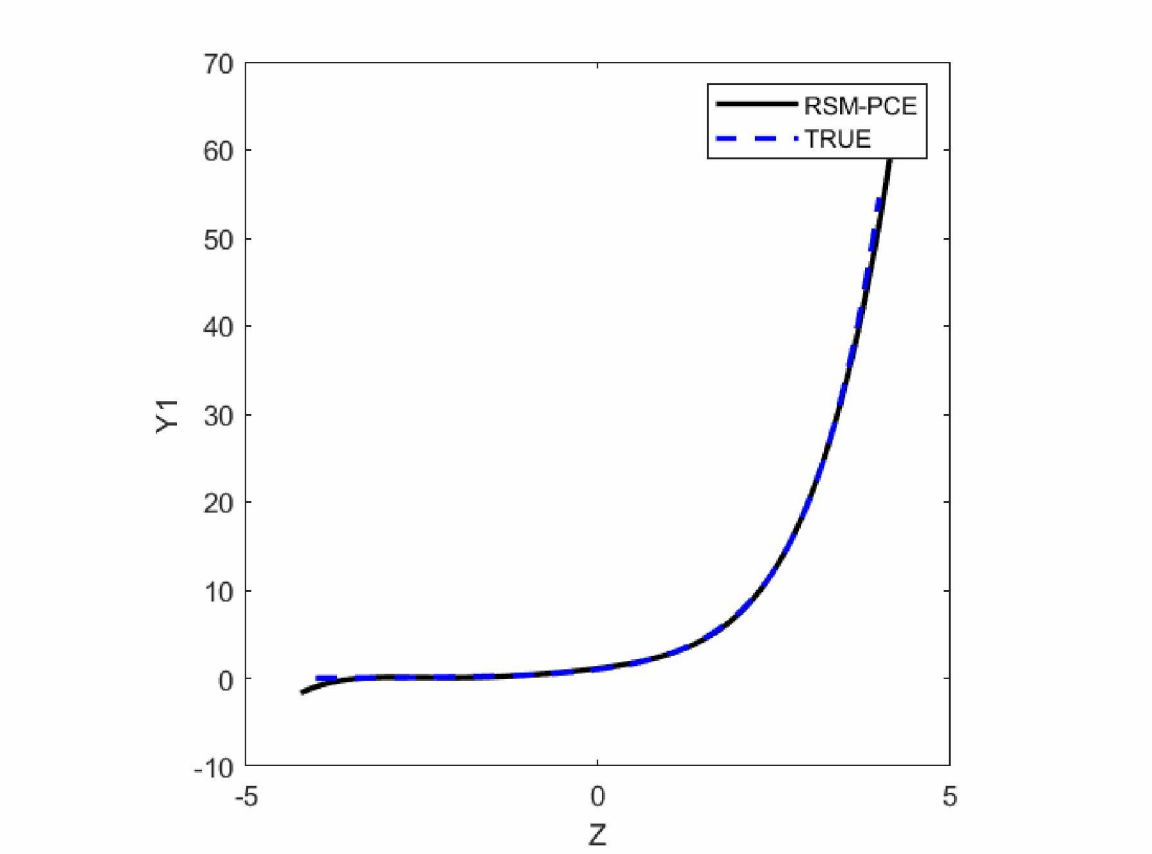

Figure 3.1: Exact and PCE approximation mapping of Y_1. RSM-PCE approximation is almost exactly following the true mapping by using only 30 LHS samples and 5^{th} PCE order.

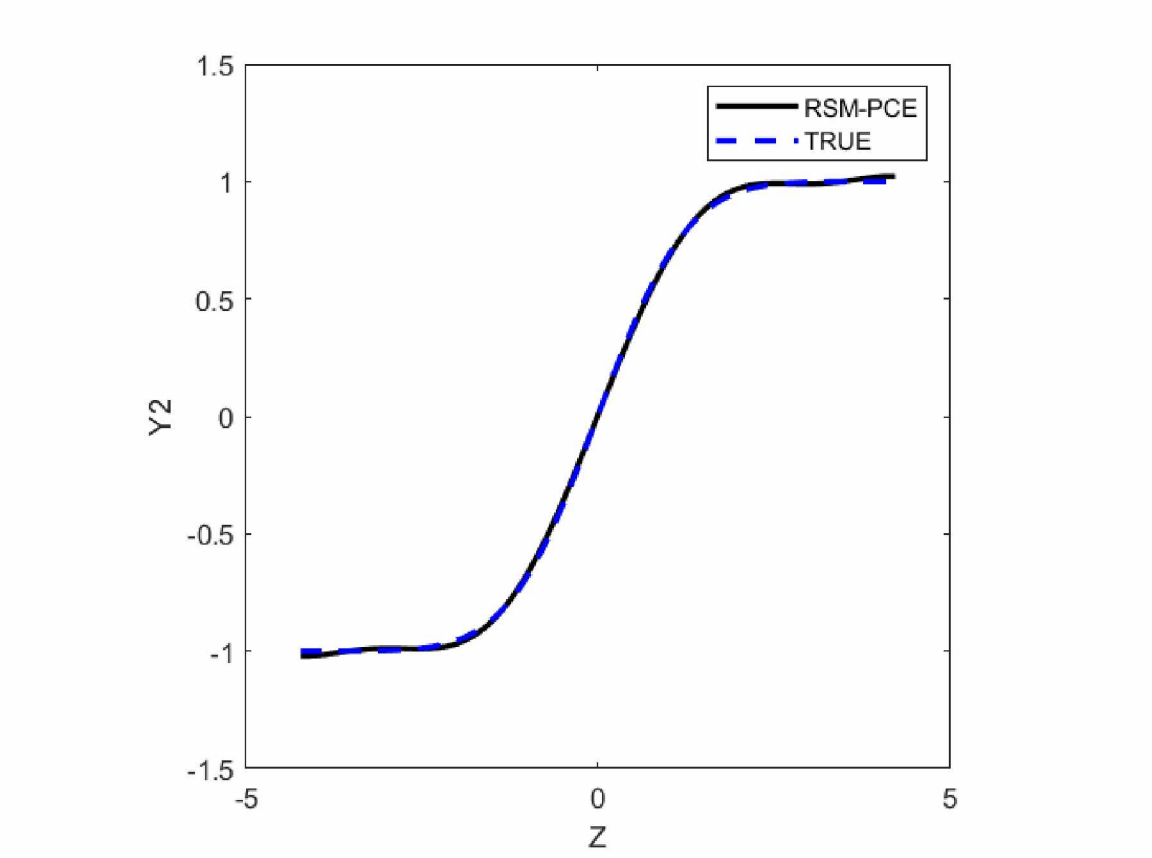

Figure 3.2: Exact and PCE approximation mapping of Y_2. RSM-PCE approximation is almost exactly following the true mapping by using only 60 LHS samples and 9^{th} PCE order.

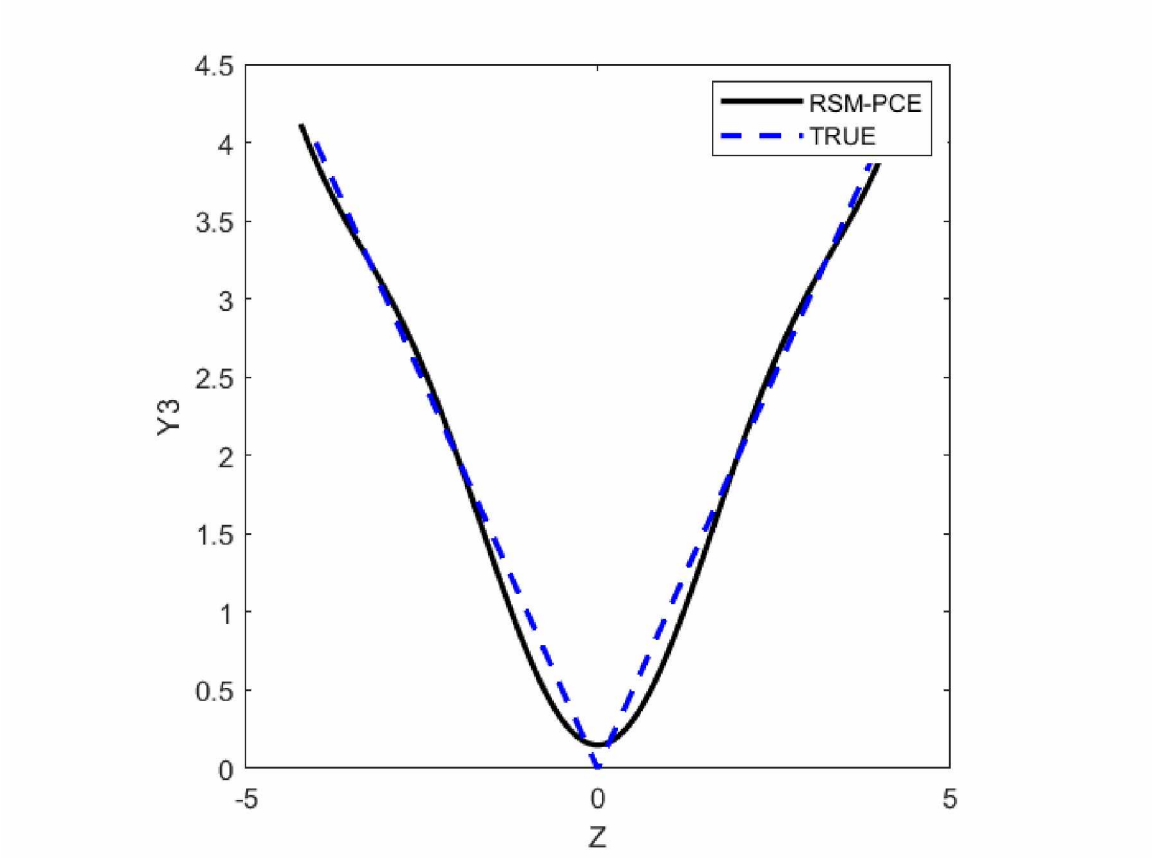

Figure 3.3: Exact and PCE approximation mapping of Y_3. RSM-PCE approximation is almost exactly following the true mapping by using only 60 LHS samples and 9^{th} PCE order.

3.5 Conclusion and Contribution

In this chapter, three examples were tested to demonstrate the efficiency of the algorithm used in this work. The results showed that the algorithm also produced excellent results (high R^2 values) for the evaluated nonlinear functions, which also realized a reduction of the required PCE coefficients by half in some cases. Although; high PCE order was required for good representation of the functions, real world examples with many inputs will have a cross terms in low orders (e.g, 3^{rd}, 4^{th}), which will capture the behavior of the function in interest without the requirement of high PCE order. This chapter results show that RSM-PCE approximation is a promising method for probabilistic analysis (e.g., sensitivity analysis) even in case of non-linear

models (e.g, biomechanics models).

CHAPTER IV

Calibration of Ligament Properties Using Distraction Based Measurements Across Multiple Specimens

4.1 Abstract

Total knee arthroplasty (TKA) success is thought to be tied to stability of the implanted joint, where a key aspect of TKA is achieving balanced ligament loading. Indirect knowledge of patient-specific ligament forces can be captured using devices that measure condylar reactions during intraoperative distraction of the joint. These measurements, while useful, do not provide direct quantification of ligament-specific forces. Specimen-specific, calibrated computational models can estimate these forces by attempting to recreate measured condyle reactions. Hence, using two cadaveric specimens, the goal of this study was to develop and assess a computational framework for calibration of ligament mechanical properties when condylar reactions and kinematics were known. Testing was composed of application of condylar reactions and measurement of kinematics at 10°, 45°, and 90° flexion, which were performed once with the posterior cruciate ligament (PCL) intact and repeated after PCL resection. Tests at 10° and 90° flexion were used for calibration while 45° flexion was retained for validation. Overall, calibrated knee models recreated measured condylar

reactions, realizing root mean square errors from 10 to 40 N. This study is the first to calibrate knee models when condylar reactions were known, which offers the potential to accommodate patient-specific tissue mechanics during TKA.

4.2 Introduction

The success of total knee arthroplasty (TKA) is thought to be tied to stability of the implanted joint, where a key aspect of this process is achieving balanced ligament recruitment throughout flexion. The means to realize this "balance" is typically achieved through experiential knowledge related to classification of knees based on morphology and their disease state, which influence implant selection and placement followed by possible intraoperative ligament releases (Hirschmann and Behrend 2018; Tanzer and Makhdom 2016). Within this paradigm, the role of ligaments in stabilizing the knee are important in the long-term success of joint replacements (Cho, Seon, Jang, et al. 2018; Babazadeh et al. 2009). On a patient-specific basis, indirect knowledge of ligament loading is currently captured using various approaches to assess flexion and extension gaps, and possibly with a device that measures the force-displacement response of the condyles (D'Lima and Colwell 2017; Shalhoub, Moschetti, Dabuzhsky, et al. 2018; Völlner, Weber, and Weber 2019). Related measurements, while useful, do not provide direct quantification of ligament-specific loading. Such knowledge may be helpful for both targeted patient-specific balancing procedures and as a basis to create fundamental knowledge about ligament-specific behavior across patient types.

Many studies have investigated the role of ligament balancing on the degree of success in TKA. For example, Unitt et al. (Unitt et al. 2008b) performed a study on 526 total knee replacements one year after implantation. The study concluded soft tissue balancing significantly improved short-term outcomes, where post-operative flexion angle increased from 90.5° to 103°. Using 32 patients another study concluded

balancing may play a role in joint kinematics and implant failure (Wasielewski, Galat, and Komistek 2005a). In addition to impacting range of motion, joint kinematics and potential implant failure, improper balancing may cause joint stiffness or instability (Verstraete et al. 2017). The importance of soft tissue balancing has been identified as a primary factor in the postoperative performance of TKA. Achieving desirable balance, however, is challenging and may be bolstered through awareness of knee-specific ligament response (Griffin, Insall, and Scuderi 2000a).

Computational models provide a tool that can enhance our understanding of the role of soft tissues in the success of TKA by providing the ability to 1) quantify the load sharing across the ligaments and 2) test conditions that may be otherwise infeasible in vitro or in vivo. As a result, computational modeling has been the primary approach to complement measured mechanical response of a given joint. Typically, specimen-specific ligament properties are estimated using an optimization scheme where the properties are iteratively adjusted until the error between model-predicted and experimentally measured joint mechanics are minimized (Baldwin et al. n.d.; Blankevoort and Huiskes 1996; Ewing, Kaufman, Hutter, et al. 2016; Harris et al. 2016; Mommersteeg, Blankevoort, Huiskes, et al. 1996). One underlying assumption of this approach is that the known externally applied loads balance with the unknown internal loads at a given joint position (Blankevoort and Huiskes 1996). The unknown internal loads are comprised of both articular contact and ligament forces; however, the complexity of the overall system could be reduced by utilizing measurements of articular contact forces.

As opposed to considering the complexity of both condylar and ligament interactions, recent work focused on the possibility of specimen-specific model calibration when the articular surfaces were physically removed (Zaylor, Stulberg, and Halloran 2019). Such an approach, which utilized external loads supplied by a robotic test frame to distract the joint, may be adapted to scenarios when internal loads

are known, as would be the case for measured force-displacement response of flexion and/or extension gaps during arthroplasty procedures (Figure 4.1). Hence, using two cadaveric specimens, the goal of this study was to develop and assess a computational framework for calibration of ligament-specific mechanical properties when condylar reactions and kinematics were known. The framework can serve as the basis for 1) future work related to prediction of patient-specific ligament loads during arthroplasty procedures and 2) a framework to create calibrated knee models across a range of knee types.

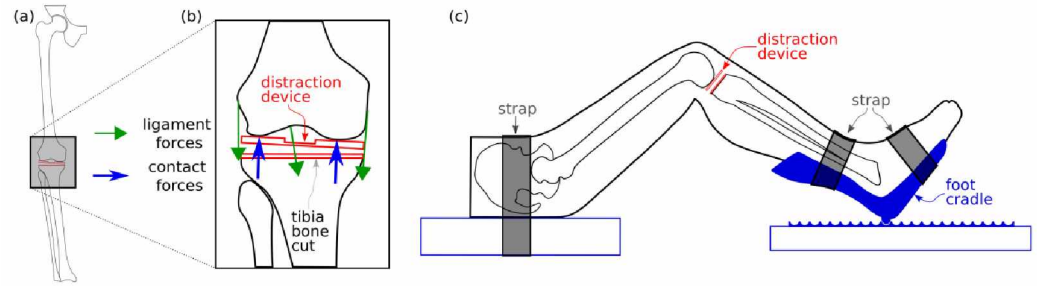

Figure 4.1: (a) Coronal view of a leg with an abstraction of a distraction device. (b) Close up of the knee with arrows that represent the applied condylar contact forces (blue) and the resulting ligament forces (green). After tibial bone cuts were performed, a proprietary distraction device was inserted into the joint. The device can distract and rotate about the anterior-posterior axis of the bone cut to apply desired condyle-specific forces. (c) Schematic of a leg with the distraction device and the foot cradle. Straps were used to secure the hip to an operating table and the foot to a moveable cradle. The foot cradle was moved toward or away from the hip to achieve the desired knee flexion angle.

4.3 Methods

Specimen Preparation

One female and one male hip to foot specimens were acquired from Science Care (Phoenix, AZ). The female specimen ("specimen 1") had a BMI of 18, was age 61 with a height of 160 cm and had no history of knee injury, surgery or chemotherapy. The male specimen ("specimen 2") had a BMI of 27, was age 57 with a height of 173 cm and no history of knee injury, surgery, chemotherapy or arthritis. Prior to testing,

specimens were imaged using CT in accordance with preoperative Mako Robotic-Arm Assisted Surgery System (Stryker) TKA protocols (Grau, Lingamfelter, Ponzio, et al. 2019). Per the Mako Robotic-Arm Assisted Surgery System (Stryker) procedure, the specimen geometry was segmented, anatomical landmarks were used to define local bone-specific anatomical coordinate systems, and an implant preplan was defined. Standard intraoperative procedures were followed to register both the specimen and cutting tool in the Mako Robotic-Arm Assisted Surgery System (Stryker) (Grau, Lingamfelter, Ponzio, et al. 2019). A mechanically aligned posterior cruciate ligament (PCL) retaining tibial bone cut was performed, which removed approximately 10 mm of the tibial plateau. For re-creation of the bone cuts in the specimen-specific models (Figure 4.3), spatial coordinates in a tibial anatomical coordinate frame for three points on the tibial bone cut were probed using the Mako Robotic-Arm Assisted Surgery System (Stryker). To reflect expected in vivo conditions, the ACL was resected in both specimens while all other ligaments remained intact. The quadextensor mechanism also remained intact throughout testing.

Experimental Data

A research-focused proprietary distraction device was used to apply condyle-specific reactions at flexion angles of 10°, 45° and 90° (Figure 4.1). In this testing, equal reactions in both condyles were applied from 5 lbf to 50 lbf in 5 lbf increments (10 total loading increments). Use of the device requires the tibial bone cut to be performed, which provides the space for the device to be inserted into the joint. Measurements were acquired using the native femoral articular surfaces. During application of the distraction, loads straps were used to secure the hip to a table and the foot in a cradle. To achieve the desired knee flexion angle (as measured using the Mako Robotic-Arm Assisted Surgery System, (Stryker)), the foot cradle allowed the ankle to be set at a fixed distance from the hip (Figure 4.1). The leg

was also manually guided in the medial-lateral direction to approximate the planned varus-valgus alignment of the tibia and femur during application of the distraction load increments. Relative tibiofemoral kinematics were defined with respect to an anatomical joint coordinate system (Grood and Suntay 1983) and were recorded by the Mako Robotic-Arm Assisted Surgery System (Stryker) at each of the loading increments. Additionally, joint gaps were calculated based on the femoral anatomy, planned construct thickness, and the plane of the tibial bone cut. To summarize, at each of the distraction loading increments, experimental results included: medial and lateral condyle reaction force magnitude, medial and lateral joint gaps, and the corresponding tibiofemoral kinematics. To evaluate the effect of removing the PCL, the experiment was performed twice, once with PCL intact and again with the PCL resected.

Model Description

Bone Anatomy and Coordinate Frames

Magnetic resonance imaging (MRI) and computed tomography (CT) images were used to create three-dimensional models of both specimens. An automated routine defined osseous femoral and tibial surfaces from the CT images, where registration with experimental data was dictated by alignment of point clouds collected using the Mako Robotic-Arm Assisted Surgery System (Stryker) during experimentation. As a result, anatomically defined embedded bone-specific coordinate systems could be registered between model and experimental coordinate frames (Grood and Suntay 1983). MRI was utilized to define ligament insertion site locations (details below), which were registered to the CT-defined bone anatomy to align the MR determined femur and tibia ligament insertion sites. To accomplish this, points on the femoral and tibial bone anatomy from the MR images were aligned by minimizing the distance between these points and the CT-defined femoral and tibial surfaces.

Ligaments

To define relevant soft tissues, MRIs were used to locate the insertion sites for all included ligaments. Each ligament was modeled as a set of nonlinear elastic springs (Figure 4.2). For every bundle, two points on both the femur and tibia were utilized (four points total) that approximated the longest width of each insertion site. As a result, bone-specific insertion points effectively defined a line for each bundle's insertion site, where each connected an insertion point on the femur with the corresponding point on the tibia.

At all applied tibiofemoral kinematic positions, fiber-specific wrapping points around each bone were used to define the shortest distance between femoral and tibial insertions points, including wrapping, for every ligament fiber (Zaylor, Stulberg, and Halloran 2019). An algorithm was utilized, which performed iterative analysis to define lines of action that realized the shortest femur to tibia distance for every fiber. Calculation of forces generated by the ligaments included contributions of both wrapping across the femur and the insertion site itself (tibia wrapping was neglected).

Ligaments were modeled as bundles of 25 nonlinear springs (i.e. the "fibers"). The force-length relationship for every spring was defined by three parameters, (1) slack length (Len_{Slack}), (2) linear region stiffness, and (3) toe-region end value (Figure 4.2.b). Each ligament bundle was assigned two slack length values to allow for nonuniform application of slack length across the ligament bundle. The two values specified the slack lengths of the fibers at the margins of the each bundle (Figure 4.2.c). The corresponding ligament fiber insertion-to-insertion lengths in the CT image joint position were used to determine the pre-strain needed for the margin fibers to have the specified slack lengths. Linear interpolation of the pre-strain values was used to define slack lengths for the remaining 23 fibers. The equivalent stiffness (K) of the ligament was defined, and each ligament fiber was assigned a stiffness value of K/25.

The following ligaments were included: PCL, medial collateral ligament (MCL), lateral collateral ligament (LCL) and the oblique popliteal ligament (OPL) (LaPrade et al. n.d.). Additionally, the PCL was modeled as two bundles, which included the anterolateral and posteromedial portions (alPCL, pmPCL) (Anderson et al. 2012). Finally, the MCL was modeled using three bundles: the proximal and distal superficial MCL (sMCLProx, sMCLDist) and the deep MCL (dMCL) (LaPrade et al. 2015) (Figure 4.2).

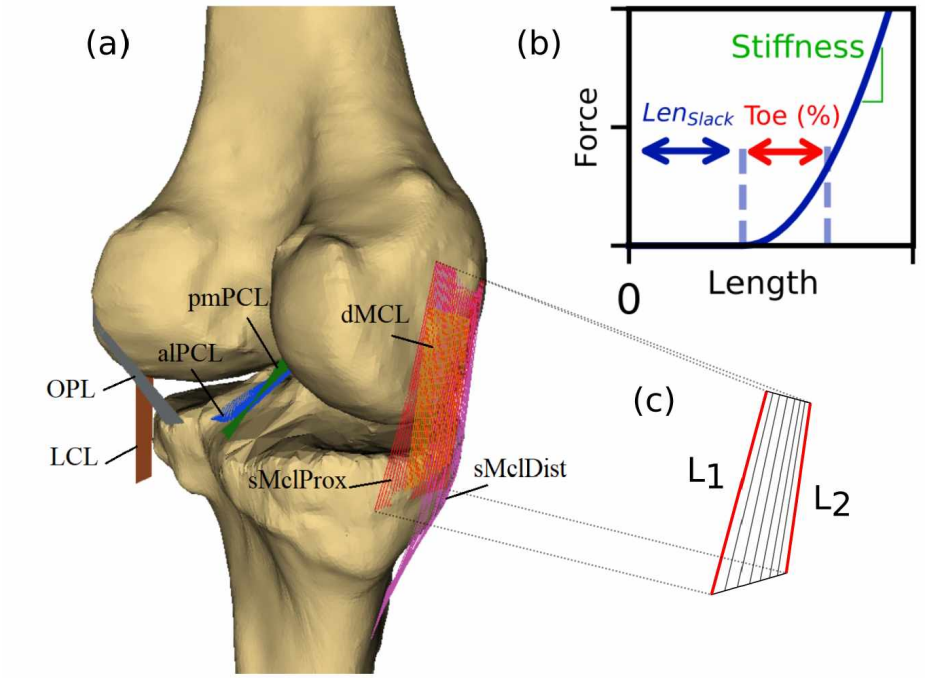

Figure 4.2: (a) The specimen 2 knee model with all included ligaments. The same ligaments were included in both specimens. (b) Properties used to define the nonlinear behavior of each ligament bundle included the slack length (Len_{Slack}), toe region percent and linear stiffness. (c) Abstraction of the sMCLProx bundle, which shows the two slack lengths, L_1 and L_2, that defined the margin "fibers" for this bundle. 23 nonlinear springs were spaced between the margins of each bundle where the force production of each was defined by the fiber-specific wrapping distances and material properties.

Computational Framework

A modified version of the computational framework developed by Zaylor et al. was used to model the two specimens (Zaylor, Stulberg, and Halloran 2019). In

summary, the Python-based code applied kinematics to define a given tibiofemoral position while the force produced by each ligament bundle could be summed to any desired coordinate frame. In this study, at a given joint position and set of ligament properties the computational model determined the sum of forces and moments the ligaments imparted onto the femur, which were resolved to the condyle-specific contact forces needed to maintain static equilibrium. Specifically, at each loading increment (and relative tibiofemoral position) a unique orientation of the simulated plane of the distraction device was defined by the tibial bone cut and a rotation about an axis defined by projecting the tibial anterior-posterior axis onto a plane coincident with the tibial cut (Figure 4.3). The plane's rotation about this axis was iteratively evaluated until the distance between the plane and nearest medial and lateral femoral points were equal. The resulting orientation of the plane and the nearest points on the medial and lateral condyles were used to define the locations and direction of the contact forces. The plane's normal was defined as the direction of each condyle's contact force. Predicted condyle-specific forces effectively represented reactions that would be required to maintain static equilibrium with the forces imparted by the ligaments, which in concept was similar to previous work but extended to three-dimensional analysis (Stoltze, Rasmussen, and Skipper Andersen 2018).

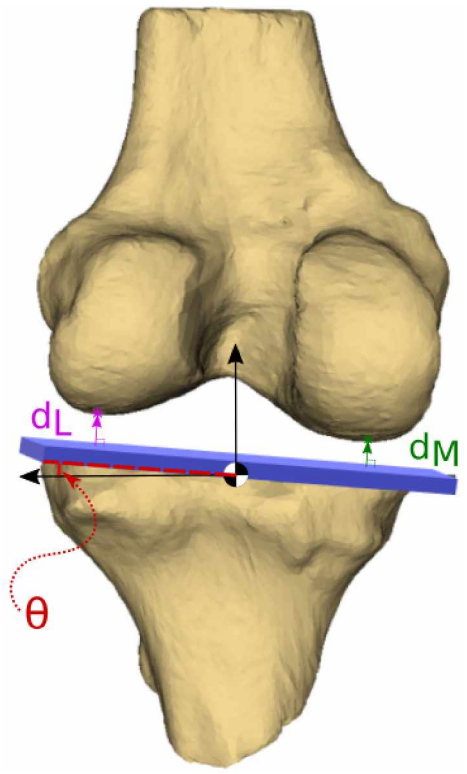

Figure 4.3: The simulated distraction plane (shown in blue). θ is the angle of rotation that was used to define contact points on the condyles. d_L and d_M are the distances between the plane and the lowest points on the lateral and medial condyles, respectively, and the direction of applied forces were normal to the plane.

Calibration

Specimen- and bundle-specific material properties were calibrated using optimization, which minimized the difference between experiment and model predicted condyle reactions. Twenty-eight total variables were calibrated, including the slack lengths (for the two fibers that defined the margins), the stiffness and the toe region of each bundle. Initial guesses for slack length values were defined as 0.98% of the maximum length of each bundle throughout the tests included in the optimization, while the stiffness values were initially based on the literature (Zaylor, Stulberg, and Halloran 2019) and 0.06 was used as initial value for toe region. Bounds were set to 0.5 and 3 of the initial guesses for stiffness (Table 4.1) and 0.03 and 0.08 for toe region, while the slack lengths were bounded between 10 mm and 100% of the maximum length

throughout the tests included in the optimization. The relatively large bounds for stiffness were due to the wide range of reported values in the literature (Blankevoort and Huiskes 1996; Ewing, Kaufman, Hutter, et al. 2016; Harris et al. 2016)

alPCL	dMCL	pmPCL	sMCLProx	sMCLDist	,LCL	OPL
5625	1000	3375	1375	1375	2000	1000

Table 4.1: Initial guesses of the stiffness (N/ϵ)).

The optimization problem minimized the following objective function:

$$\sum_{i=1}^{2}\sum_{j=1}^{2}\sum_{k=1}^{n}\sum_{l=1}^{2}(M_{ijkl} - E_{ijkl})^2 \tag{4.1}$$

where M is the model predicted contact force, E is the experimentally measured contact force, i is the test case (PCL resected and PCL intact), j is flexion angle, k is the index of the point in the loading cycle, and l are the medial and lateral condyles. The 10° and 90° flexion angles were included in the calibration.

To avoid possible convergence to local minima (Ewing, Kaufman, Hutter, et al. 2016), the covariance matrix adaptation evolution strategy (CMA-ES) optimization approach was used to calibrate the ligament properties. CMA-ES is an evolutionary algorithm that has shown good performance for nonlinear multidimensional problems (Hansen and Ostermeier 2001; Posik, Huyer, and Pal 2012). For each loading increment in the calibration and to focus on the loaded response, experimental results associated with the highest five applied condyle reactions were considered in the objective (i.e. approximately 30 to 50 lbf).

Validation

To evaluate the performance of the calibration results, experimental data at 45° flexion for both PCL intact and resected cases were left out of the calibration. The

calibrated, specimen-specific models were run using the kinematics data at 45° and the predicted condylar reaction loads were compared with experimental results.

Evaluation of Model Calibration

To assess the calibration and validation results, root mean square errors (RMSE) between model predicted and experimental condylar reactions were calculated. RMSE values were calculated for the utilized points in the objective (i.e. the highest five applied loading increments) as well as across all loading increments. The lower the RMSE, the better the agreement between experimental and predicted condylar reactions.

Computational Cost

All computations were performed on an Intel workstation with dual Xeon 2.4 GHz processors and 64 Gb of RAM. To assess the computational cost, wall clock time was assessed for both specimens, where times were recorded for both the wrapping and calibration procedures.

4.4 Results

Specimen 1

The model for specimen 1 recreated condyle specific reactions with RMSE 23.03 N and 9.15 N for the PCL intact case at 10° and 90° flexion angles, respectively. For the PCL resected case, RMSEs of 24.02 N at 10° and 19.00 N at 90° were realized. For the non-calibrated 45° flexion angle, model predictions realized RMSEs of 30.83 N and 47.12 N for the intact and resected cases, respectively (Figures 4.4, 4.5). Contact forces were generally recreated, with trends and peak values displaying similar behavior (Figures 4.4, 4.5). For both the PCL intact and resected cases, at 10° the LCL and sMCLDist carried the majority of the loads. At the 90° flexion and for the

intact case, the PCL bundles were recruited along with the LCL. The PCL resected case distributed loads between MCL bundles and the LCL. The 45° validation case loaded the same ligaments as 10° with the exception that the pmPCL was loaded in the intact case. Notably, for both the PCL intact and the resected cases, the LCL was predicted as the dominant load-carrying structure on the lateral side, even at low flexion (Table 4.2).

Ligaments	Slack length(fiber 1)	Slack length(fiber 2)	Stiffness	Toe region
alPCL	38.84	41.55	7601.69	0.03
pmPCL	37.95	39.05	7397.66	0.06
dMCL	41.42	35.90	2657.13	0.07
sMCLProx	46.21	49.77	2236.54	0.06
sMCLDist	85.85	85.81	4112.22	0.08
LCL	56.59	53.46	4620.94	0.08
OPL	58.77	45.99	5608.17	0.06

Table 4.2: Calibrated properties (slack lengths in mm and stiffness in N/ϵ) for specimen 1.

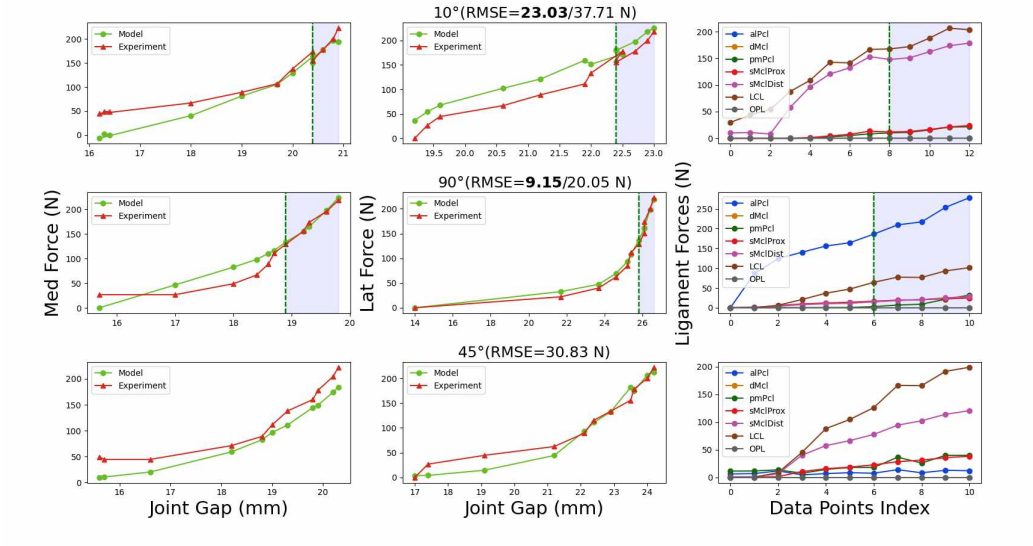

Figure 4.4: Model predicted versus experimental medial and lateral condylar loads as a function of joint gap for specimen 1 and the PCL intact case at 10°, 90° and 45° of flexion. The five highest loads in 10° and 90° cases were used in the calibration (shaded in light blue) while 45° was retained for validation. RMSE for both the calibrated set (in bold) and all data points were provided at each flexion angle. Bundle-specific load predictions at each flexion angle were plotted as a function of data point (right column) to highlight the loaded response..

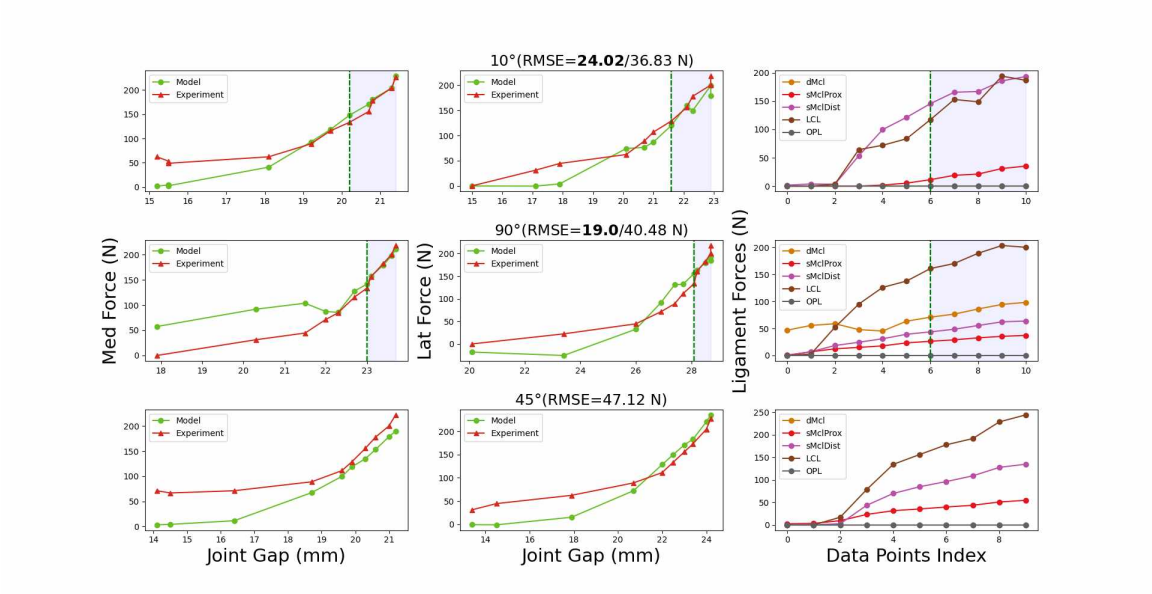

Figure 4.5: Model predicted versus experimental medial and lateral condylar loads as a function of joint gap for specimen 1 and the PCL resected at 10°, 90° and 45° of flexion. The five highest loads in 10° and 90° cases were used in the calibration (shaded in light blue) while 45° was retained for validation. RMSE for both the calibrated set (in bold) and all data points were provided at each flexion angle. Bundle-specific load predictions at each flexion angle were plotted as a function of data point (right column) to highlight the loaded response.

Specimen 2

Similar to the first specimen, the model for the second specimen successfully recreated condyle specific reactions with average RMSE of 20.45 N and 12.47 N for the PCL intact case 10° and 90° flexion, respectively. The PCL resected case performed similarly with RMSEs of 28.0 N at 10° flexion and 21.9 N at 90°. For the non-calibrated 45° data, across all loading increments the calibrated properties realized 40.76 N and 30.49 N for the intact and resected cases, respectively (Table 4.3). As in specimen 1, contact forces were generally recreated, with trends and peak values displaying similar behavior (Figure 4.6).

For specimen 2 predicted ligament forces at 10° were similar for both the PCL intact and resected cases with the OPL and dMCL carrying the majority of the loading. For the 90° intact case the alPCL, dMCL and sMCLProx bundles were

loaded while the LCL dominated the contribution for the lateral structures. Loads were predominantly distributed between the LCL, dMCL, and sMCLProx for the PCL resected case at 90° flexion. Finally at 45° flexion and both the intact and resected cases the dMCL and sMCL structures shared the loads on the medial side while the LCL and OPL carried loads on the lateral side. As compared to specimen 1 (Table 5.3), relatively high stiffness values and lower overall loads for the PCL bundles were realized (Table 4.3).

Ligaments	Slack length(fiber 1)	Slack length(fiber 2)	Stiffness	Toe region
alPCL	38.54	45.95	15159.28	0.06
pmPCL	32.34	35.68	8489.57	0.03
dMCL	38.87	32.67	2736.84	0.05
sMCLProx	44.92	51.73	1652.06	0.04
sMCLDist	92.22	90.29	2126.61	0.05
LCL	52.54	52.92	1511.97	0.07
OPL	52.74	34.00	2097.21	0.05

Table 4.3: Calibrated properties (slack lengths in mm and stiffness in N/ϵ) for specimen 2.

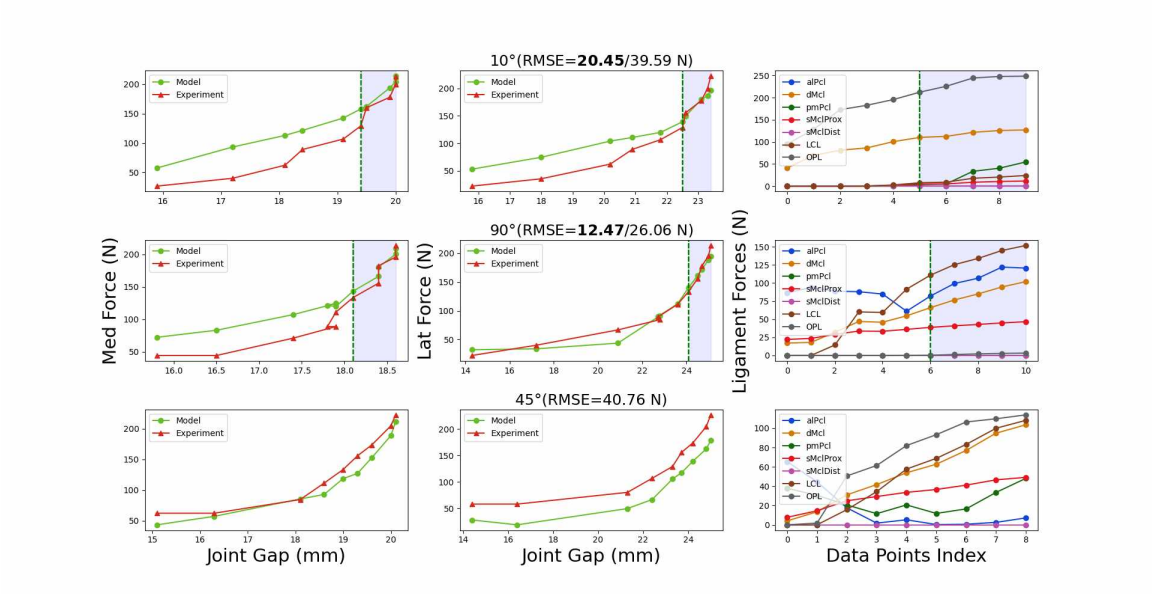

Figure 4.6: Model predicted versus experimental medial and lateral condylar loads as a function of joint gap for specimen 2 and the PCL intact case at 10°, 90° and 45° of flexion. The five highest loads in 10° and 90° cases were used in the calibration (shaded in light blue) while 45° was retained for validation. RMSE for both the calibrated set (in bold) and all data points were provided at each flexion angle.Bundle-specific load predictions at each flexion angle were plotted as a function of data point (right column) to highlight the loaded response.

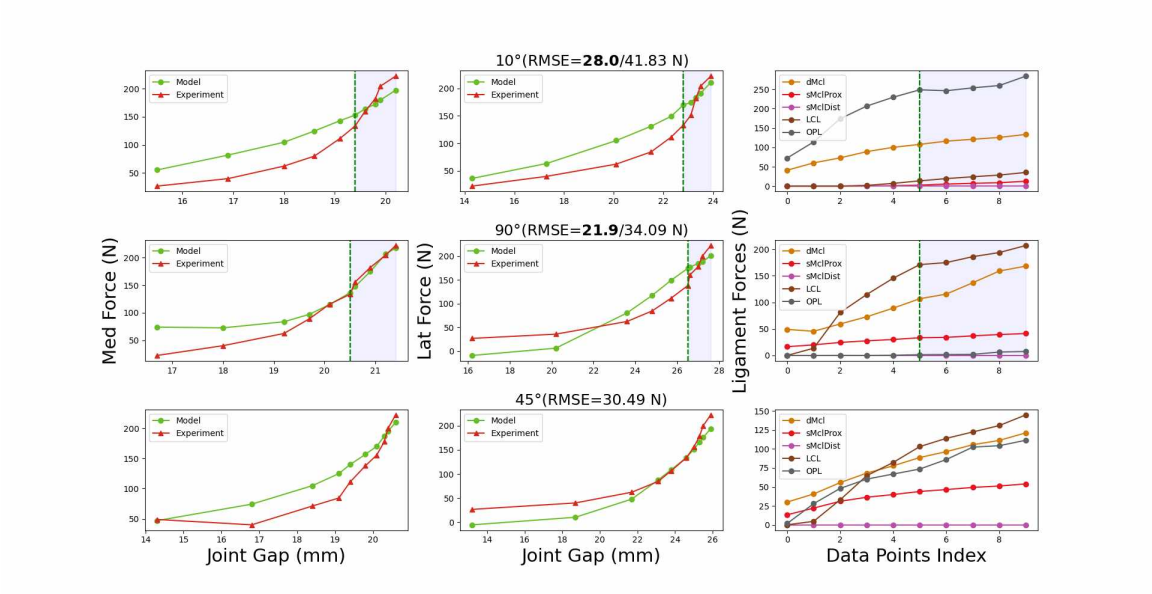

Figure 4.7: Model predicted versus experimental medial and lateral condylar loads as a function of joint gap for specimen 2 and the PCL resected case at 10°, 90° and 45° of flexion. The five highest loads in 10° and 90° cases were used in the calibration (shaded in light blue) while 45° was retained for validation. RMSE for both the calibrated set (in bold) and all data points were provided at each flexion angle. Bundle-specific load predictions at each flexion angle were plotted as a function of data point (right column) to highlight the loaded response.

Computational Cost

Wall clock time for each calibration ranged from 60 to 70 minutes while the wrapping algorithm required approximately 7 minutes per specimen.

4.5 Discussion

Measurements of the joints internal loads during distraction offers a useful yet indirect means of understanding ligament loading. Computational models can provide complementary knowledge of patient-specific measurement of knee mechanics, though distraction inspired models are only a recent development (Zaylor, Stulberg, and Halloran 2019). The purpose of this study was to evaluate the use of experimentally measured specimen- and condyle-specific distraction forces during calibration of

nonlinear ligament properties for two specimens. Overall, experimentally measured condyle reactions were generally recreated across both specimens and the calibration and validation load cases, as reflected by the relatively low RMSE values and reproduction of trends in the force-displacement response (Figure 4.4-4.7). Corresponding predictions of the loads carried by each ligament offer insight into specimen-specific response, which may provide an avenue to accommodate patient-specific tissue mechanics during TKA procedures.

An important consideration in this study was the data used for model development and calibration were based on possible pre- and intraoperative measurements and imaging. The lone exception to this statement is that MRI was utilized to determine specimen-specific ligament insertion sites, though methods are currently being evaluated to overcome this bottleneck. Beyond this exception, bone anatomy and registration were based on CT imaging, kinematics were measured using the Mako Robotic-Arm Assisted Surgery System (Stryker), and the force-gap measurements were found using a prototyped research focused device. It is important to emphasize the focus of this study was assessment of the computational framework while explicit evaluation of the force-gap measurement device will be summarized in future work. Application of this framework remains a research tool, though it is possible to envision utilization for either intraoperative assessment or to catalog and classify patient- and/or specimen-specific joint mechanics. Future work will look to streamline the framework, especially regarding computational efficiency and development of automated approaches for model setup (e.g., determination of ligament insertion sites without use of MRI).

As opposed to traditional gradient-based approaches, the presented calibration procedure utilized the evolutionary based CMA-ES optimization approach, which was adopted to avoid potential issues related to dependence on the initial guess and realizing solutions at a local minimum (Ewing, Kaufman, Hutter, et al. 2016). While

CMA-ES is attractive due to its efficiency over other global approaches, it does have a stochastic component to its evaluation, where subsequent calibrations are not guaranteed to arrive at consistent solutions. Preliminary assessment (not presented) revealed effectively similar results for successive calibration runs and future work will systematically evaluate the reliability of CMA-ES for this application. Another consideration, in spite of the method being classified as a global approach, is that realizing a true global optimum is always a concern. CMA-ES was adopted over traditional global approaches due to its relative efficiency and apparent robustness, where significantly higher computational expense would have been required if other "global" approaches had been adopted (e.g. simmulated annealing or quasi-Monte Carlo sampling). In spite of the this possible shortcoming, encouraging results indicated the suitability of this approach across the two evaluated specimens.

Related to prediction of specimen-specific load distribution across the ligament bundles, numerous considerations are warranted. First, as opposed to including all available loading points, the five highest experimental data points for the PCL intact and resected at 10° and 90° cases were included in the calibration. This decision was made to emphasize the loaded state of each specimen, which presumably realized sufficient recruitment of the ligaments while minimizing the impact of external loading during the tests. While attempts were made to minimize external loading at all load increments (e.g. manual guidance of the leg), it is expected the effects of these unknown loads would have a greater impact at lower load values. Possibly more important, without direct measurement of specimen-specific tissue recruitment, establishing the validity of predicted ligament loads remains an ongoing challenge. Such measurements are both difficult and likely to result in a high degree of uncertainty. It is for this reason, as well as to realize the goal of developing a framework based on clinically feasible data, that computational models are used to complement force-displacement measurements of a given joint. To gain confidence in the predictions,

indirect validation in this study was accomplished by not including 45° in the calibration procedure. The resulting RMSE for the non-calibrated data were relatively low, which increased confidence the framework may provide a basis for development of a tool that is able to predict appropriate specimen-specific ligament loading (Figures 4.4-4.7).

Comparisons with previous work are another avenue to address validity of the predicted load sharing. The importance of the PCL, and its recruitment with flexion, is relatively well established (Papannagari, DeFrate, Nha, et al. 2007; Li et al. 2004). Both specimens demonstrated recruitment of one or both PCL bundles at 90°, though specimen 1 clearly relied more heavily on this structure. This stated, it is important to highlight this study is the first to evaluate ligament loading during application of internal distraction loads, which complicates comparison with previous work that included compressive joint forces and intact articular surfaces. All previous modeling studies relied on comparing model-predicted versus experimental kinematics, as opposed to reaction forces. As a result, the magnitudes of RMSE found in this study could be perceived as high, though it is important to highlight that relatively small changes in joint kinematics (i.e. less than 1.5 mm and 1.2°) can lead to relatively large changes in predicted reactions (up to 186 N and 2.9 Nm) (Zaylor, Stulberg, and Halloran 2019).

In this work, predicted ligament loading varied between the female ("specimen 1") and male ("specimen 2") specimens. The dMCL was the primary load carrying structure on the medial side in all tests and flexion angles in the male specimen. Regarding this finding, it is important to consider both the presence and role of the dMCL in natural and implanted mechanics could be questioned. We anticipate evaluating the specific role of the dMCL in future studies. The female specimen, however, recruited the superficial portions of the MCL while loading of the dMCL was limited to the PCL resected surgical state at 90° flexion. As for the PCL, the

alPCL was loaded in both specimens at 90° (Figures 4.4, 4.6). Interestingly, the male specimen required loading of the OPL to realize acceptable overall response, especially at 10° and 45°, while the female demonstrated little to no recruitment of this structure. More will be learned as validity is further established and additional specimens are evaluated, including those in various cohorts (e.g., male versus female, arthritic versus healthy, etc.).

One final limitation in this study is the cadaveric nature of the work and its corresponding potential for translation to in vivo TKA patients. The tested knees were from relatively healthy subjects, which may behave differently than knees with advanced stage osteoarthritis (OA). Similarly, post-mortem changes may impact the mechanics of ligaments while both OA and age-related changes can influence the quality of ligamentous structures (Loeser et al. 2012). Despite these limitations the overall force-displacement response of TKA patients is likely to behave similarly to the presented cadaveric results. We expect the modeling framework will adequately capture additional subjects, including in vivo data, and this will be evaluated in future studies.

The overarching goal of this work was to evaluate prediction of internal joint reactions as well as preliminarily assess the predictive capacity of the proposed custom simulation framework. The framework successfully recreated measured condyle-specific reactions while predicting possible specimen-specific load sharing across the included ligaments. The computational efficiency of the approach lends itself to analysis of additional subjects, where corresponding sensitivity analysis has the potential to highlight both important modeling assumptions and surgical factors that affect implant performance. Supporting measurement of knee-specific mechanics, whether in a research or clinical setting, with quantification of ligament loading across a larger cohort of knees will provide a basis to understand both typical and abnormal ligament response during arthroplasty procedures.

4.6 Acknowledgements

Stryker Orthopaedics for funding this study.

CHAPTER V

A Comprehensive Study of Knee Reaction Sensitivity to Properties of Ligaments – Application of Distraction Based Models

5.1 Abstract

Computational knee models have shown that predicted condylar reactions are sensitive to the utilized ligament mechanical parameters. These models, however, are computationally expensive with multiple sources of uncertainty. Traditional uncertainty analysis using Monte-Carlo (MC) inspired methods are costly to perform. The purpose of this study was to use two example calibrated knee models to compare quasi-MC versus polynomial chaos expansion (PCE) sensitivity analyses of predicted condylar reactions that included uncertainty in the mechanical parameters of the ligaments. PCE was practically identical versus quasi-MC with 95% and 98% reductions in model evaluations for analyses with 10 and 6 uncertain variables, respectively.

5.2 Introduction

Computational models have helped establish our understanding of knee mechanics by simulating the structural response, which can be summarized as attempting to quantify the load sharing between the articular surfaces and the surrounding soft

tissues. A direct benefit of such models is the ability to enhance our understating of the role of soft tissues, and specifically the ligaments, in healthy, diseased, and surgically reconstructed conditions (Mommersteeg et al. 1996; Ewing et al. 2016). For example, both computational and experimental studies have shown that ligament loading, i.e., the "balance" between ligaments, is tied to the success of surgical interventions, including total knee arthroplasty (TKA) (Unitt et al. 2008a; Wasielewski, Galat, and Komistek 2005b; Verstraete et al. 2017; Griffin, Insall, and Scuderi 2000b). Similarly, computational models have shown the reaction forces at the condyles are sensitive to the applied kinematics as well as the assumed (or calibrated) ligament mechanical parameters (Zaylor, Stulberg, and Halloran 2019; Smith et al. 2016b). Condylar reaction forces are of interest due to their apparent importance in assessing cartilage mechanics in healthy and diseased knees and the performance of implants in arthroplasty. Such models, whether developed for general use or subject-specific applications, offer the possibility to test conditions that are either difficult or impossible to explore using in vitro or in vivo approaches.

These models, however, are complex, often computationally expensive, and include multiple sources of uncertainty. These include assumptions related to the boundary conditions, material properties of the individual model components, and geometric representation of the anatomy. A deterministic analysis fails to capture the effects of these uncertainties, which has implications when drawing conclusions or making decisions based on modeling outcomes. Offering a clear understanding of the impact of these uncertainties would likely improve the credibility and the potential to be reproduced. The transition from a deterministic to probabilistic analysis substantially increases the cost, complexity, and subsequent interpretation of the modeling effort. It is for this reason relatively straightforward fully-randomized methods such as Monte Carlo (MC) simulation have been adopted in knee modeling, where studies have highlighted the potential effects of key modeling assumptions. For example,

Baldwin et al. (Baldwin et al. 2009) performed 200 MC trials for anterior-posterior (AP) and internal-external (IE) laxity tests to quantify the uncertainty of predicted kinematics. Zaylor et al. (Zaylor, Stulberg, and Halloran 2019) applied 1000 MC perturbations to experimentally measured kinematics to assess their effect on predicted reaction loads. Smith et al. performed 2000 MC trials and found a high degree of uncertainty in predicted tibiofemoral contact forces due to uncertainty in the assumed ligament properties (Smith et al. 2016a). In each of these studies, the number of MC simulations was likely limited due to the computational expense of the models, which will be compounded as models increase in complexity.

Sensitivity analysis quantifies the relative or absolute importance of each uncertain input on the resulting distribution of model prediction(s). One can reduce the computational burden of uncertainty analysis, the prequisite step for sensitivity analysis, using one of two approaches, 1) reducing the number of required model evaluations or 2) replacing the "expensive" simulation with an efficient surrogate representation. The first approach can be accomplished using a probabilistic method such as quasi-MC sampling, which utilizes quadrature-based random sampling to improve the slow rate of convergence of traditional fully randomized MC sampling. Alternatively, a deterministic approach such as Design of Experiments (DOE) (Borgonovo and Plischke 2016) perturbs single variables (or a combination) a set amount above and/or below their assumed values. The DOE-based Taguchi method is typically termed a "local" approach and has the 'goal of extracting as much information as possible' (Giunta, Wojtkiewicz, and Eldred 2003) using a reduced number of simulations. For example, Yao et al. used the Taguchi method (Taguchi, Chowdhury, and Taguchi 2000) for selecting control variables and DOE to plan a controlled study to evaluate the sensitivity of material properties in a finite element knee model (Yao et al. 2006). Global approaches, conversely, such as the Morris, mean value, and variance-based methods like Sobol's method (Sobo 2001), represent modeling inputs as probabilities. Global

approaches require a probabilistic uncertainty analysis (e.g., quasi-MC) and are beneficial in that the relative and/or absolute impact each input has on the predictions can be quantified using the resulting distribution(s) of a given model's output(s). These approaches typically require a high number of model evaluations, which motivates the adoption of a surrogate representation of the expensive simulation. If accurate, the surrogate model can be used to run MC or quasi-MC simulations in a reduced timeframe.

A Polynomial Chaos Expansion (PCE)-based surrogate model is one such approach to reduce the potentially high computational cost of probabilistic analysis. PCE is a technique that builds a polynomial representation of the "expensive" biomechanics model using relatively few simulations. PCE has many applications, one of which is sensitivity analysis (Ghanem and Spanos 2012). Once a PCE surrogate model is created, performing a sensitivity analysis becomes a significantly less expensive task compared to conventional MC or quasi-MC simulation. Hence, the purpose of this study was to use two example calibrated knee models to compare quasi-MC versus PCE-based sensitivity analyses of predicted condylar reactions that include uncertainty in the mechanical parameters of the ligaments. In both quasi-MC and PCE-based sampling, Sobol's sensitivity method was used to quantify the relative importance of each ligament's mechanical parameters. Sobol's method was adopted for multiple reasons. First, it provides a convenient way to rank the importance of each parameter once the uncertainty in the outputs has been quantified. Second, it has been used widely, from engineering (Blatman and Sudret 2010a) to pharmacology (Zhang et al. 2015), but to our knowledge has not yet been adopted in biomechanics.

5.3 Methods

Overview

The methods are broken down into three primary sections. The first summarizes the main components of a PCE-based surrogate model (including Sobol's sensitivity approach). The second describes the calibrated knee models. The final section describes the specific workflow used for PCE-based sensitivity analysis of ligament-specific mechanical parameters in the calibrated knee models.

Components of a PCE-Based Surrogate Model

Mathematical Model

Consider a physical system (e.g., a knee model) that can be represented by a model, M:

$$Y = M(X) \tag{5.1}$$

where $X = [X_1, X_2, ..., X_r]$ is a vector of random variables inputs (e.g., ligament mechanical properties) with joint probability density functions and Y is the random output of interest (e.g., joint reaction forces).

PCE approximation

The PCE formula for an infinite number of terms is as follows (Ghanem and Spanos 2012):

$$U = \sum_{i=o}^{\infty} u_i \psi_i(H) \tag{5.2}$$

Where U is the output of interest, H is a vector of random inputs, u_{i} are coefficients and ψ_{i} is the polynomial basis. In practice only finite number of terms are considered (Sudret 2014). Thus, equation 5.2 becomes:

$$U = \sum_{i=o}^{n} u_i \psi_i(H) \tag{5.3}$$

where n is the number of terms. Equation (5.3) is called PCE approximation. In the case of Gaussian random input variables Hermite polynomials are typically used (Table 5.1) (Ghanem and Spanos 2012).

p=0	1
p=1	ξ
p=2	ξ^2-1
p=3	ξ^3-3ξ
p=4	ξ^4-6ξ^2+3

Table 5.1: PCE for one random variable and first five orders where ξ is a standard normal variable.

The number of coefficients (also the number of terms) in Equation (5.3) can be calculated using:

$$n = \frac{(N+P)!}{N!P!} \tag{5.4}$$

where N is the number of random variables and P is the order of PCE. This number increases rapidly when the number of variables and the number of terms increase (Table 5.2).

	p=2	p=3	p=4	p=5	p=6	p=7	p=8	p=9	p=10
N=2	6	10	15	21	28	36	45	55	66
N=5	21	56	126	252	462	792	1287	2002	3003
N=10	66	286	1001	3003	8008	19448	43758	92378	184756

Table 5.2: The number of PCE coefficients as a function of the number of random variables, N, and the polynomial order, p.

Sampling Method

The main aim of a surrogate model is to reduce the computational burden. Therefore, an efficient sampling method is required to build the PCE surrogate model. Latin Hypercube Sampling (LHS) was utilized in this study due to its convergence

versus Monte Carlo sampling and proven ability to capture nonlinear behavior (Fajraoui, Marelli, and Sudret 2017; Xiu 2009). In summary, LHS divides the sampling space into equally probable intervals, where one sample is drawn randomly from each interval (McKay, Beckman, and Conover 2000).

LASSO Regression

Equation (5.3) represents a regression problem. The coefficients in equation (5.3) are typically estimated using ordinary/linear least square (OLS). However, OLS estimates suffer from high variance. LASSO deals with the high variance issue by applying the following criterion to reduce the number of coefficients in the PCE model:

$$\sum_{i=o}^{n} |u_i| \leq t \tag{5.5}$$

where t is a tuning parameter and u_i are the polynomial coefficients in equation 5.3. When t has a large value, the criterion has a low effect and the solution is equivalent to the least-squares solution. LASSO shrinks (reducing the effect) or eliminates coefficients (equation 5.5). Cross-validation (CV) was used to tune t and to eliminate polynomical coefficients by selecting the model with the lowest error (best fit) (Krstajic et al. 2014). Effectively, LASSO regression was used to estimate the regression coefficients and select the most important variables (Tibshirani 1996).

Sensitivity Analysis using Sobol's Method

After uncertainty analysis, the output variance can be decomposed into the relative contributions of each input using Sobol's method. For a model, M (equation 5.1), the Sobol's first-order sensitivity index is as follows:

$$S_i = \frac{V[E(Y|X_i)]}{V(Y)} \tag{5.6}$$

where S_i is the first order Sobol index for the random input variable, X_i. $V[E(Y|X_i)]$ is the variance of the random output of interest, Y, given a fixed value of input, X_i (equation 5.1). The sum of sensitivity indices for all inputs equals 1. Effectively, each S_i quantifies the relative influence of each input, X_i, on the output, Y. An S_i value of 1 indicates sole influence of a given input, X_i, while 0 means that input was found to have no impact on the output.

Description of Calibrated Knee Models

Experimental Data

Two lower limb cadavers were used for experimental testing. Specimen 1 was female, had a BMI of 18, was age 61 with a height of 160 cm, and had no history of a knee injury, surgery, or chemotherapy. The initiation of osteoarthritis was visually confirmed on the femoral condyles. Specimen 2 was male, had a BMI of 27, was age 57 with a height of 173 cm, and had no history of a knee injury, surgery, chemotherapy, and no signs of osteoarthritis.

The experimental procedure used a research-focused proprietary distraction device to apply ramped medial and lateral contact loads at 10°, 45°, and 90° of flexion. Before testing with the distraction device, each knee was registered in a Mako Robotic-Arm Assisted Surgery System (Stryker) using standard intraoperative procedures (Grau et al. 2019). To allow insertion of the distraction device into the joint tibial bone cuts representative of a mechanically aligned, posterior cruciate-retaining knee replacement procedure were performed using the Mako Robotic-Arm Assisted Surgery System (Stryker). The femoral bone and cartilage remained intact during testing. A custom fixation device held each leg at the desired knee flexion angle and the leg was manually guided to realize the planned post-operative varus-valgus alignment. At each flexion angle, measurements were acquired with the distraction device in 5 lbf increments from approximately 5 to 50 lbf, which were applied equally in

both condyles (results reported in Newtons). Kinematics at each loading state were captured using a Mako Robotic-Arm Assisted Surgery System (Stryker). Tests were repeated for both PCL intact and PCL resected cases.

Model Description

Specimen-specific bone anatomy and anatomical landmarks were defined using preoperative CT images, per the Mako Robotic-Arm Assisted Surgery System (Stryker) procedure (Grau et al. 2019). Magnetic resonance images (MRI) of each knee were also acquired and used to locate the insertion sites for all included ligaments, which were rigidly transformed onto the CT-based bone anatomy by minimizing the distance between the triangular mesh-based bone surfaces and sets of specimen-specific MRI-defined point clouds. To define ligament insertion sites, two points were found on the femur and two on the tibia for each included bundle (four points total). Each set of two points approximated the longest width of an insertion site. The ligament and bone-specific insertion points defined the "margins" of each bundle, where the insertion point on the femur connected with the corresponding point on the tibia (Figure 5.1.a). The Posterior Cruciate Ligament (PCL), Medial Collateral Ligament (MCL), Lateral Collateral Ligament (LCL), and Oblique popliteal ligament (OPL) were included in each model (LaPrade et al. 2003). The PCL was modeled as two bundles, the anterolateral PCL (alPCL) and posteromedial PCL (pmPCL) (Anderson et al. 2012). The MCL was modeled as three bundles, the proximal and distal superficial MCL (sMCLProx, sMCLDist) and the deep MCL (dMCL) (LaPrade et al. 2007a). Similar to previous work, the computational model uses equilibrium equations to calculate medial and lateral condylar reactions, with the ligaments forces being the knowns and condylar forces being the unknowns (Figure 5.1.b) (Stoltze, Rasmussen, and Skipper Andersen 2018). Each ligament was modeled as a set of nonlinear elastic springs (Figure 5.1.c).

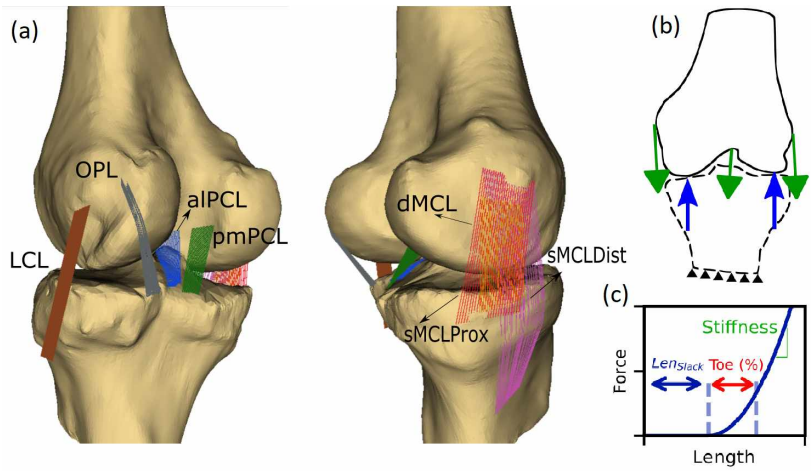

Figure 5.1: (a) Medial and lateral views of the specimen 2 computational model with all included ligaments. The same ligaments were included in specimen 1. (b) Abstraction of knee computational model, when ligament forces are known (green arrows) and condyle's forces (blue arrows) are calculated. (c) Each ligament bundle was modeled using sets of 25 nonlinear elastic springs, which are defined by their slack length, toe region percent, and linear stiffness values. Slack length values were linearly interpolated between the margin fibers and the overall bundle stiffness value (Tables) was equally distributed between each fiber. Toe region was set at a constant 6%.

Model Calibration

Using a custom kinematics driven framework (Zaylor, Stulberg, and Halloran 2019) with ligament wrapping (Zaylor and Halloran 2021), bundle-specific stiffness values and slack lengths were calibrated using optimization. Initial guess values for the slack lengths were set to 98% of the maximum length of each bundle's margin fibers across the calibration data. Bounds for the slack lengths were set to 10 mm up to 100% of the maximum length across all calibration data. Bounds for the stiffness values were based on the literature (Smith et al. 2016b, table 1). As it has demonstrated promising results for nonlinear multidimensional problems, the covariance matrix adaptation evolutionary strategy (CMA-ES) optimization approach was used to minimize the squared difference between measured and predicted condylar loads (i.e., the "objective") (Hansen and Ostermeier 2001). The calibration procedure

included PCL intact and resected data at 10° and 90° while 45° was retained for validation (Tables 5.3, 5.4 and Figures 5.2, 5.3, 5.4, 5.5). To focus on the loaded response of the joint, the objective was minimized using the highest five applied condylar reactions (i.e., 30 to 50 lbf).

Model Calibration Results

The model recreated the trend of experimental data with root mean squared errors(RMSE) ranging from ~10 to 60 N (Table 5.5).

Ligaments	Slack length(fiber 1)	Slack length(fiber 2)	Stiffness
alPCL	38.45	42.53	9091.46
pmPCL	32.07	36.16	3839.80
dMCL	42.93	36.33	4336.12
sMCLProx	46.19	45.22	880.00
sMCLDist	82.02	87.31	3519.99
LCL	55.78	52.87	2880.00
OPL	53.97	45.94	1613.66

Table 5.3: Calibrated properties (slack lengths in mm and stiffness in N/ϵ) for specimen 1.

Ligaments	Slack length(fiber 1)	Slack length(fiber 2)	Stiffness
alPCL	38.95	44.25	9120.00
pmPCL	31.95	34.21	3840.00
dMCL	38.75	31.89	2699.58
sMCLProx	45.04	50.57	880.00
sMCLDist	80.10	87.58	3519.99
LCL	64.10	47.31	2800.43
OPL	49.97	40.27	3200.00

Table 5.4: Calibrated properties (slack lengths in mm and stiffness in N/c) for specimen 2.

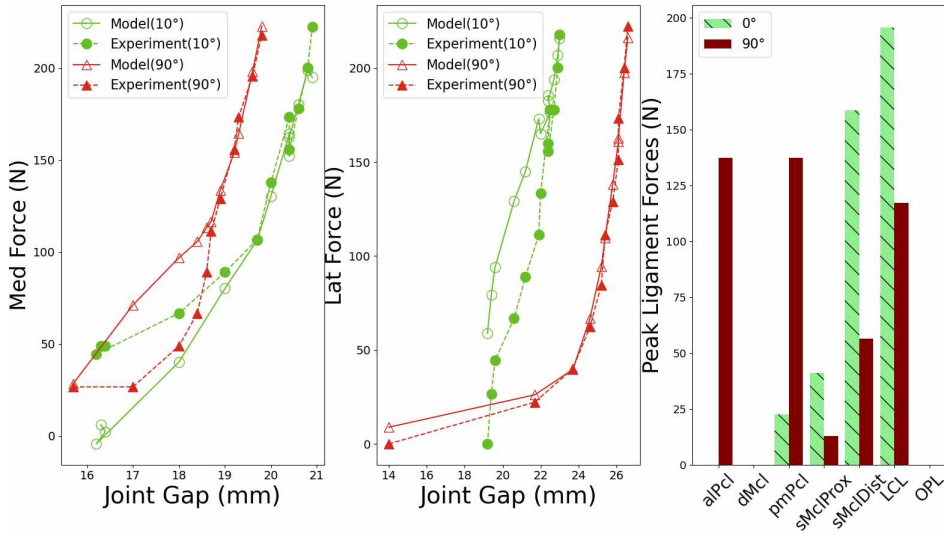

Figure 5.2: Model predicted versus experimental results for specimen 1 with the PCL intact. Medial ("Med") and lateral ("Lat) condylar reactions are plotted as a function of joint gap at 10° and 90° knee flexion. Joint gap is the distance between the tibial bone cut and the low point on the medial or lateral femoral condyle. (right) Ligament forces at peak condyle reactions.

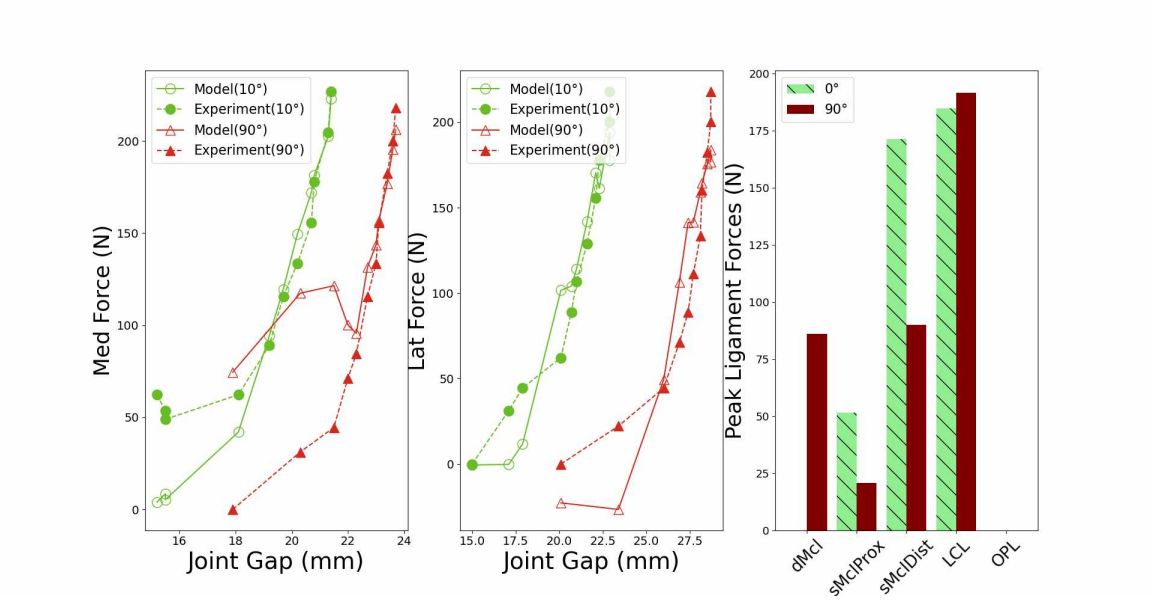

Figure 5.3: Model predicted versus experimental results for specimen 1 with the PCL resected. Medial ("Med") and lateral ("Lat) condylar reactions are plotted as a function of joint gap at 10° and 90° knee flexion. Joint gap is the distance between the tibial bone cut and the low point on the medial or lateral femoral condyle. (right) Ligament forces at peak condyle reactions.

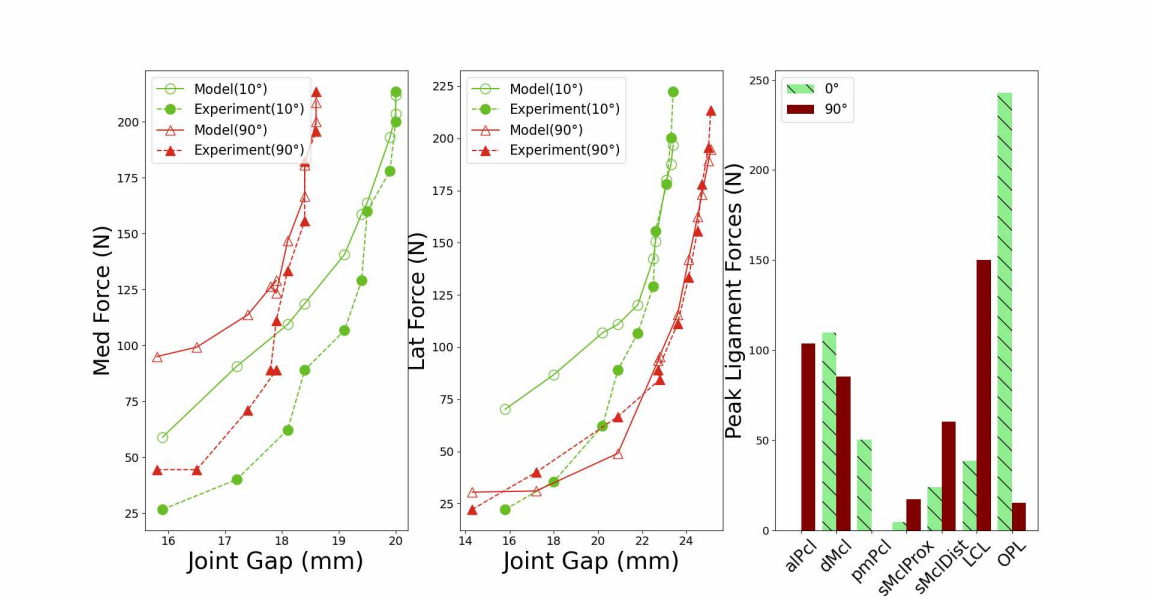

Figure 5.4: Model predicted versus experimental results for specimen 2 with the PCL intact. Medial (¨Med¨) and lateral (¨Lat) condylar reactions are plotted as a function of joint gap at 10° and 90° knee flexion. Joint gap is the distance between the tibial bone cut and the low point on the medial or lateral femoral condyle. (right) Ligament forces at peak condyle reactions.

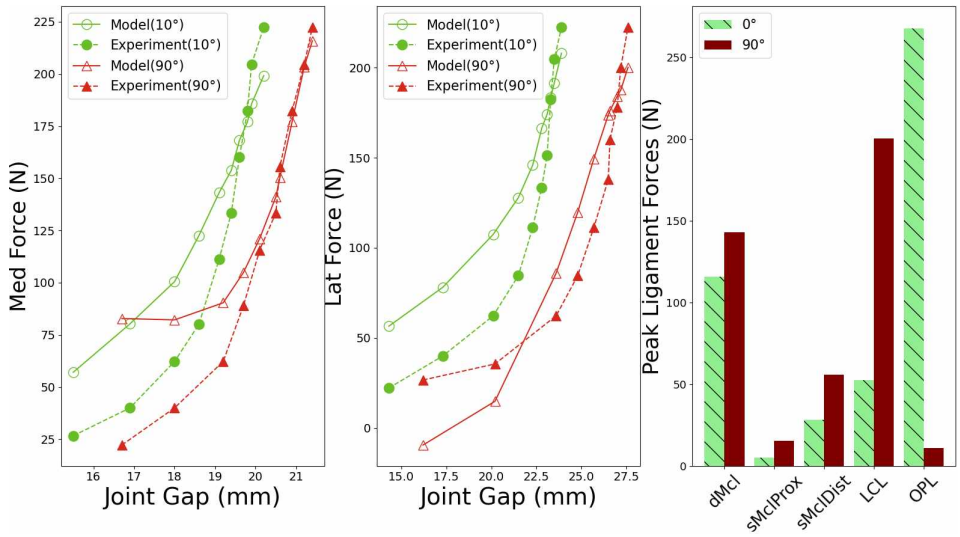

Figure 5.5: Model predicted versus experimental results for specimen 2 with the PCL resected. Medial ("Med") and lateral ("Lat) condylar reactions are plotted as a function of joint gap at 10° and 90° knee flexion. Joint gap is the distance between the tibial bone cut and the low point on the medial or lateral femoral condyle. (right) Ligament forces at peak condyle reactions.

Specimen	10°	90°	45°
First (PCL intact)	22.37	9.67	49.56
First (PCL resected)	23.9	24.43	42.75
Second (PCL intact)	21.14	14.05	59.59
First (PCL resected)	24.97	18.61	43.86

Table 5.5: Root Mean Square Error (RMSEs)(N) between predicted and experimental medial and lateral condylar loads for specimen 1 and 2. Errors are reported for the calibration (10° and 90°) and validation load cases (45°).

Senstivity Analysis of Primary Ligament Mechanical Properties - PCE and Validation with Quasi-MC sampling

Sensitivity Analysis Inputs

The two specimen-specific, kinematics controlled knee models M were utilized to evaluate the relationship between the calibrated mechanical properties of the primary ligament bundles, X_i, and corresponding condyle-specific loads, Y. In the two utilized sensitivity analyses, PCE and quasi-MC (see 5.3 and Figure 5.6), variability was assigned to slack and stiffness values. 10 input variables for the PCL intact cases were required while 6 were included for PCL resected cases (1 slack length and 1 stiffness for every major ligament bundle, Tables 5.6 and 5.7). Across all bundles, uniform distributions were assigned (Nowak and Collins 2000). Slack lengths bounds were set to 0.95 to 1.05 of the calibrated values. Bounds for the stiffness values were consistent with a previous MC sensitivity analysis (Smith et al. 2016b, Tables 5.6, and 5.7).

Ligaments	Slack length(fiber 1)		Slack length(fiber 2)		Stiffness	
	low	high	low	high	low	high
alPCL	36.53	40.37	40.41	44.66	2280	9120
pmPCL	30.47	33.68	34.35	37.97	960	3840
dMCL	40.79	45.08	34.52	38.15	1120	4480
sMCLProx	43.87	48.50	42.96	47.48	880	3520
sMCLDist	77.92	86.12	82.95	91.68	880	3520
LCL	52.99	58.56	50.51	55.51	720	2880

Table 5.6: Lower and higher bounds for specimen 1 properties (slack lengths in mm and stiffness in N/ϵ).

Ligaments	Slack length(fiber 1)		Slack length(fiber 2)		Stiffness	
	low	high	low	high	low	high
alPCL	37.00	40.90	42.04	46.46	2280	9120
pmPCL	30.35	33.54	32.50	35.92	960	3840
dMCL	36.82	40.69	30.30	33.49	1120	4480
sMCLProx	42.79	47.29	48.04	55.10	880	3520
sMCLDist	76.10	84.11	83.20	91.96	880	3520
LCL	60.90	67.31	44.94	49.68	720	2880

Table 5.7: Lower and higher bounds for specimen 2 properties (slack lengths in mm and stiffness in N/ϵ).

PCE-Based Sensitivity Analysis

The specimen-specific PCE-based surrogate models for the primary ligament bundles (Tables 5.6, and 5.7) were created using Python package Uncertainpy (Tennøe, Halnes, and Einevoll 2018), which was based on Chaospy (Feinberg and Langtangen 2015) and SALib (Factorial, Herman, and Usher 2018) packages (Figure 5.6). LASSO regression was used to calculate the surrogate model's coefficients (5.3), which was implemented after incorporating it into the Uncertainpy package using Python's scikit-learn (Pedregosa et al. 2011).

The PCE-based sensitivity analysis was performed using the following two assumptions (Figure 5.6): 1) 10000 MC samples were applied to the PCE-based surrogate model and 2) the experimental kinematics associated with the highest applied condyle reaction forces were used to calculate the sensitivity of each input variable using normalized Sobol's indices (Figures 5.2, 5.3, 5.4, and 5.5) (Saltelli et al. 2010).

Convergence Analysis to Determine PCE order

The computational expense for a PCE based model is strongly associated with the PCE order (Table 5.2). Therefore, a convergence study was performed to select the PCE model order. Mean Squared Error (MSE) was calculated for PCE based sensitivity indices for increasing PCE order using:

$$MSE^j = (\frac{1}{n}) \sum_{i=1}^{n} (S_{i_{PCE}}^{j+1} - S_{i_{PCE}}^{j})^2 \tag{5.7}$$

where j is the PCE order used to create the surrogate model, n is the number of model inputs and $S_{i_{PCE}}$ is the Sobol sensitivity index calculated using PCE based method. The order of PCE was increased until convergence, which was defined as an *MSE* less than 0.01 (Table 5.8).

abs(MSE^1-MSE^2)	0.0529
abs(MSE^2-MSE^3)	0.0470
abs(MSE^3-MSE^4)	6.72 10^{-7}

Table 5.8: Absolute differences for MSE values for increasing PCE order and the PCL intact case at 10° flexion for specimen 1. A 3^{rd} order polynomial was used in this study across both specimens.

Validation Study

To compare the PCE-based sensitivity analyses with a standard approach, quasi-MC sampled sensitivity analyses were performed using the calibrated models (Figure 5.6) (Sobo 2001; Saltelli et al. 2010). Based on the convergence rate of quasi-MC, which considers the number of uncertain variables, 12000 and 8000 quasi-MC samples were generated for the PCL intact and resected surgical cases, respectively. As in the PCE-based approach, at the highest applied condylar loads Sobol indices were calculated to determine the relative contribution of each uncertain variable to the predicted condyle-specific reactions (figure 5.6, 5.3). This resulted in the possibility

to perform a direct comparison between Sobol's indices predicted by the PCE-based sensitivity analysis versus the quasi-MC sensitivity analysis, which were evaluated using the percent difference.

Computational Expense

For both specimens, 574 model evaluation were needed to create 3^{rd} PCE surrogate model for the PCL intact cases and 170 model evaluations were needed for the PCL resected case. As specified, for the Quasi-MC based method, 12000 and 8000 model evaluations were utilized for PCL intact and PCL resected cases, respectively (Section 5.3).

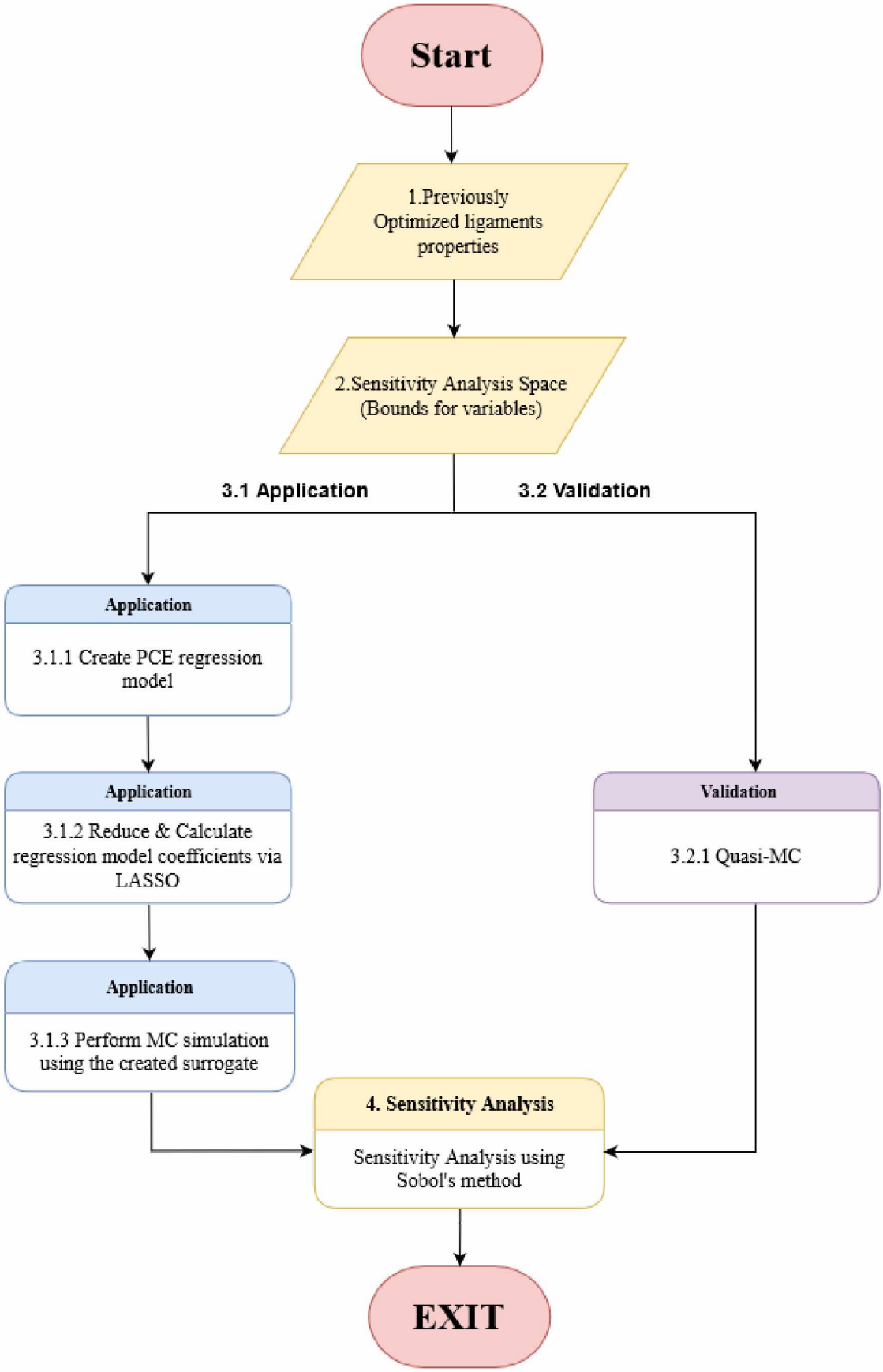

Figure 5.6: A flow chart for the steps used to perform the two sensitivity analysis. The left side (3.1 Application) describes the PCE-based approach and the right (3.2 Validation) is the traditional quasi-MC sampled uncertainty analysis. The two calibrated knee models, with the assigned variability in the ligament mechanical pa-

5.4 Results

For specimen 1, the error between PCE and quasi-MC Sobol indices ranged from -1.1% (slack length of the alPCL, Figure 5.8) up to 0.9% (stiffness of the sMCL, Figure 5.7). For the PCL intact case at 10° flexion, the most dominant variable for the medial condyle force was the slack length of the sMCL with a Sobol index above 0.6 and agreement between PCE and quasi-MC results at 0.4%. The primary contributors to the lateral force for the PCL intact case at 10° flexion were the slack and stiffness of the LCL, where both analyses agreed within 0.8% (Figure 5.7). With the PCL intact at 90° flexion case, the error for the most dominant variable (slack of the alPCL) was 0.3% for the medial force and 0.7% for the lateral force (slack of the LCL, Figure 8). For the PCL resected case at 10° flexion (Figure 5.9), errors for the highest Sobol indices were 0.05% (medial force, slack of the sMCL) and 0.1% (lateral force, slack of the LCL). At 90° flexion the errors for the highest Sobol indices were 0.7% (slack of the dMCL) and 0.04% (slack of the LCL, Figure 5.10).

For specimen 2, the error between PCE and quasi-MC Sobol indices ranged from -0.7% (slack length of the dMCL, Figure 5.7) up to 0.9% (stiffness of the dMCL, Figure 5.10). For the PCL intact case at 10° flexion the most dominant variable for the medial condyle force was the slack length of the dMCL with Sobol index close to 0.4 and agreement between PCE and quasi-MC results at 0.4%. The primary contributors to the lateral force for the PCL intact case at 10° flexion were the slack and stiffness of the LCL, where both analyses agreed within −0.03% for the slack length and 0.8% for the stiffness (Figure 5.7). With the PCL intact at 90° flexion case, the error for the most dominate variable (slack of the dMCL) was 0.4% for the medial force and 1.3% for the lateral force (slack of the LCL, Figure 5.8). For the PCL resected case at 10° flexion (Figure 5.9), errors for the highest Sobol indices were 0.7% (medial force, stiffness of the dMCL) and 0.3% (lateral force, slack of the LCL).

At 90° flexion the errors for the highest Sobol indices were 0.6% (slack of the dMCL) and 0.06% (stiffness of the LCL. Figure 5.10).

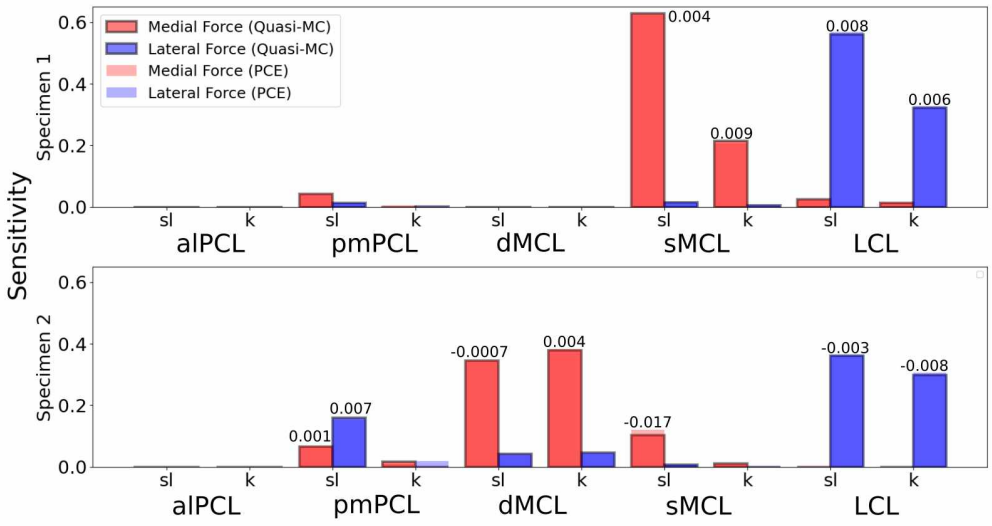

Figure 5.7: A comparison between PCE-based sensitivity analysis and quasi-MC based sensitivity analysis for PCL intact at 10° flexion for specimen 1 (top row) and specimen 2 (bottom row). 'sl' denotes the slack length while 'k' is the stiffness parameter. Differences between the two methods were reported when the sensitivity index is higher than 0.05.

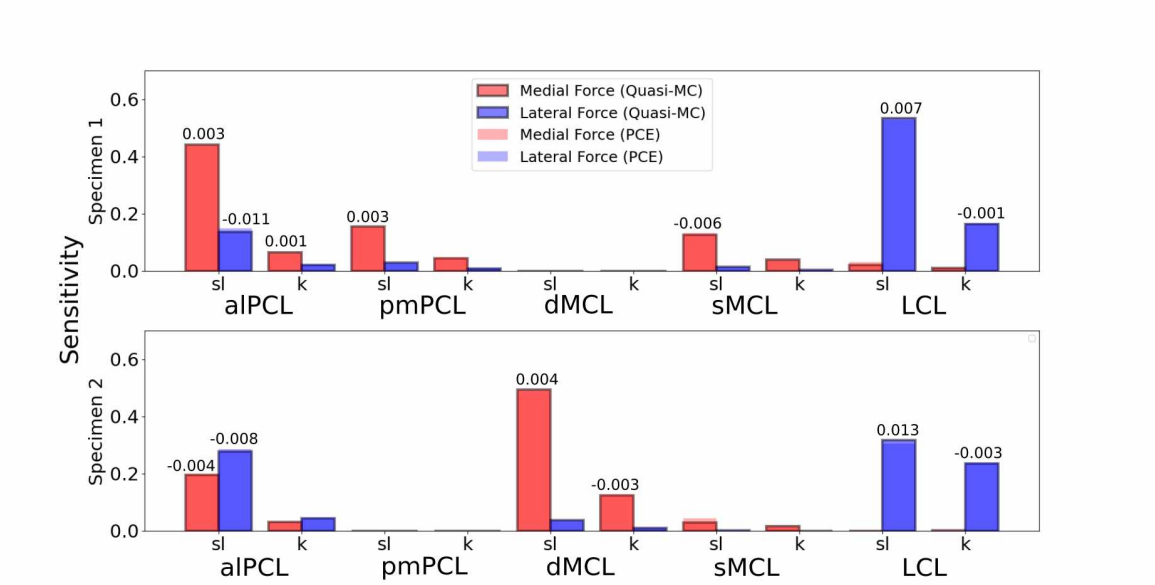

Figure 5.8: A comparison between PCE-based sensitivity analysis and Quasi-MC based sensitivity analysis for PCL intact at 90° flexion for specimen 1 (top row) and specimen 2 (bottom row). 'sl' denotes the slack length while 'k' is the stiffness parameter. Differences between the two methods were reported when the sensitivity index is higher than 0.05.

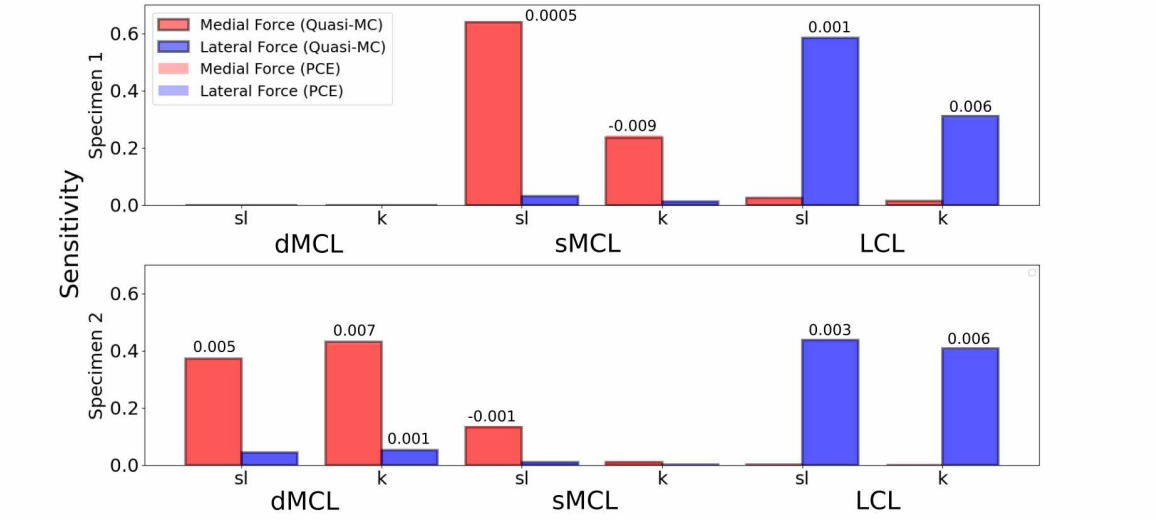

Figure 5.9: A comparison between PCE-based sensitivity analysis and Quasi-MC based sensitivity analysis for PCL resected at 10° flexion for specimen 1 (top row) and specimen 2 (bottom row). "sl" denotes the slack length while "k" is the stiffness parameter. Differences between the two methods were reported when the sensitivity index is higher than 0.05.

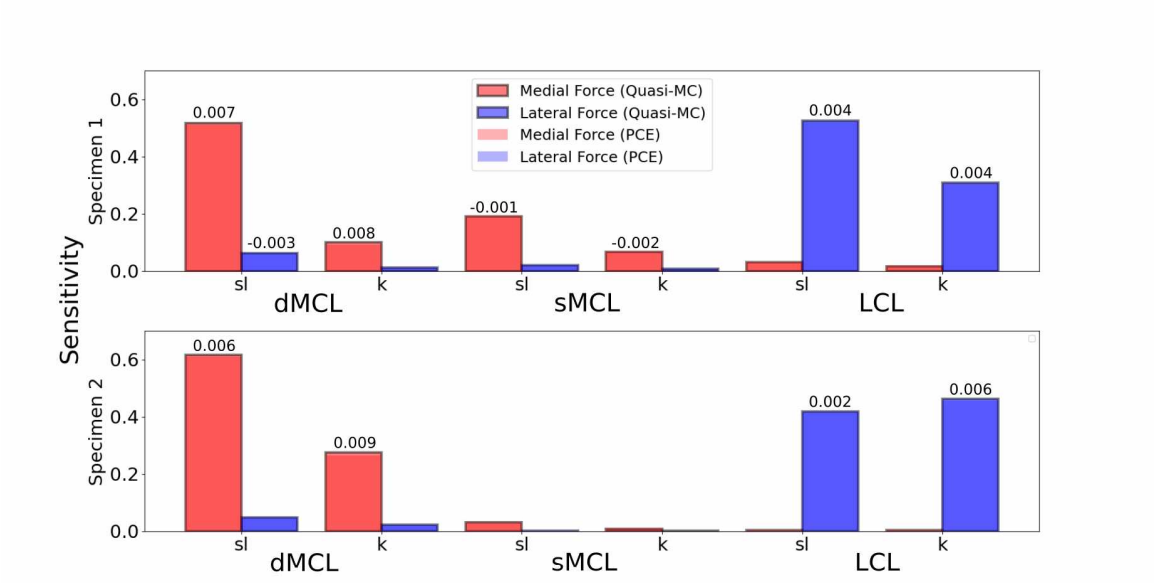

Figure 5.10: A comparison between PCE-based sensitivity analysis and Quasi-MC based sensitivity analysis for PCL resected at 90° flexion for specimen 1 (top row) and specimen 2 (bottom row). "sl" denotes the slack length while "k" is the stiffness parameter. Differences between the two methods were reported when the sensitivity index is higher than 0.05.

5.5 Discussion

In this work, two calibrated models were evaluated to assess the sensitivity of condyle-specific loads to the mechanical properties of primary ligaments in the knee. In both knee models the polynomial chaos expansion (PCE) surrogate modeling approach was able to predict accurate Sobol sensitivity indices using a relatively low number of model evaluations. The number of model evaluations was reduced by 95% for the PCL intact cases and 98% for the PCL resected cases compared to the quasi-MC-based method. These findings are especially beneficial considering the model complexity and the number of uncertain variables. Encouragingly, the relatively small differences also did not affect the relative ranking of any variable (Figures 5.7, 5.8, 5.9, and 5.10).

Quasi-MC-based sensitivity analysis was adopted to assess the performance of the PCE-based approach. The quasi-MC approach is well established with many

applications through a wide variety of fields. Quasi-MC, however, requires thousands of model runs to converge. Although an already fast and efficient rigid-body model was picked as the comparison simulation (i.e. "M" in equation 5.1), it is important to note the PCE-based surrogate model can be executed in a fraction of the time versus the rigid-body based model. The benefits of this approach will be even more evident when a computationally expensive simulation is required, as would be the case for finite-element simulations of knee mechanics that aim to predict soft-tissue mechanics (Harris et al. 2016). Regarding the comparison between PCE and quasi-MC, the important step of selecting the order of the PCE surrogate model depends on many factors such as the complexity of the model and computational resources. In this study, the goal was to select a PCE order that balanced the non-linear behavior of the models while also attempting to reduce the computational expense (the main concern in using polynomial-based regression models). The combination of a 3^{rd} order PCE surrogate model and the adoption of the LASSO technique further reduced the complexity of the PCE-based approach through informed removal of unimportant terms in the realized polynomial-based models.

While not a primary focus of the current work, the results revealed differences between the specimens that could only be found using sensitivity analysis, especially with regards to understanding the relative contribution of slack length versus stiffness of the ligament mechanical parameters. For example, in specimen 1 the PCL intact case at 10° the sMCL and the LCL slack lengths showed the most contribution in the condyle reaction forces on the medial and lateral condyles, respectively. However, the contribution of the stiffness increased in specimen 2 where the dMCL primarily influenced the medial contact force (Figure 5.7). The same pattern was observed for the PCL resected cases at 10°, where the sMCL and dMCL were the primary ligaments contributing to the condyle reactions on the medial side with the LCL dominating in both specimens on the lateral (Figure 5.9). At 90° of knee flexion, reaction forces

for specimen 1 were primarily dictated by the alPCL slack length while specimen 2 relied on a combined contribution from the alPCL and the dMCL slack lengths for the medial side and the PCL intact cases (Figure 5.8). The PCL resected cases, however, showed combined contributions of the sMCL and dMCL for specimen 1 compared to specimen 2 (Figure 5.10). At 90° flexion, the lateral side contact force was dictated by the alPCL and the LCL for specimen 2 and the LCL in specimen 1 for intact cases (Figure 5.8), with the LCL as the primary contributor for both specimens for resected cases (Figure 5.10). Interestingly, the LCL's contribution was dictated by both the slack and stiffness values in all tested cases.

This study has multiple limitations worth discussing. First, while the provided examples revealed the differences between specimens, evaluation across two specimens and the lack of direct validation data limits the conclusions that can be drawn regarding knee-specific behavior. This limitation is further confounded by the performance of the calibration routine, which yielded multiple ligament properties at the bounds of calibration parameters (Tables 5.3 and 5.4). While these considerations are certainly important when drawing insight within or across a set of knees, the presented sensitivity analysis is an important step in establishing the relative importance of modeling assumptions. For example, future experimental work will benefit from a targeted collection of validation data (e.g., measurement of properties or loads of important ligaments). From a model development perspective, the combined benefit of calibration followed by sensitivity analysis also reveals the ligaments, and their corresponding properties, that offer the most value in potentially improving model performance. As a result, future work will evaluate the mechanical and physical representation of the ligaments that drive the predictions. While this could potentially be viewed as obvious, efficient sensitivity analysis provides the means to rapidly inform modeling decisions. Another consideration, the introduced PCE-based method suffers from an exponential increase in the required number of model evaluations as

the number of uncertain inputs grows (Table 5.2). Thus, the efficiency of the proposed method will only be realized when the number of uncertain variables can be limited (e.g., <20).

Sensitivity analysis is an important tool to enhance our understanding of the uncertainty in modeling predictions. Such analysis gives the ability to quantify the output variability while also providing the means to make informed modeling decisions to realize useful representations of knee-specific behavior. Overall, this study presents a viable and novel surrogate-based approach to perform expedited sensitivity analysis in biomechanical simulations. The PCE-based surrogate model has an additional benefit of low memory size, which makes it easy to share, disseminate, and embed with other frameworks when a high number of model evaluations may be required (e.g., coupling with musculoskeletal simulations). The specific example used in this work shows the potential to understand the impact of calibrated (or assumed) ligament material properties on predicted articular contact forces.

5.6 Acknowledgments

Stryker for funding initial development of the calibrated models.

5.7 Declaration of interest statement

Authors have no conflict of interest.

CHAPTER VI

Sensitivity to Insertion Site Location for Model-Predicted Ligament and Condylar Loads in Two Knee Specimens

6.1 Abstract

Developing knee computational models requires defining ligaments insertion locations, which is typically accomplished through manual interpretation of medical images. Insertion site location has been shown to influence ligament recruitment patterns in calibrated, specimen-specific models. The purpose of this study was to perform a sensitivity analysis of insertion site locations of the dominant load carrying ligaments for two knee specimens. An experiment with 220 design points was designed using D-optimal design of experiments, and the experiment outcome was then analyzed using ANOVA. Results showed the effect of insertion site location was knee specific. One specimen ("specimen 1") realized significant effects of the LCL alone and had an interaction between the LCL and PCL locations. The second specimen ("specimen 2") found no significant effects of insertion site locations.

6.2 Introduction

Computer models are important tools to enhance our understanding of knee function and to help inform specimen-specific surgical planning (Mootanah et al. 2014). Developing such models requires defining ligament insertion locations, which is typically accomplished through manual interpretation of medical images with the help of existing literature to define the area which the ligament occupies (LaPrade et al. 2003, LaPrade et al. 2007b, Anderson et al. 2012). Many factors affect the accuracy of insertion site locations, such as the quality of the medical images and user experience. These factors add uncertainty to the computational model inputs which affect the accuracy and quality of the model's output as mentioned in (Ali et al. 2017), where their analysis showed that insertion site location has been shown to influence ligament recruitment patterns in calibrated, specimen-specific models.

Uncertainty related to MRI-determined insertion site locations was investigated by Rachmat et al. by conducting a study to " evaluate the intra- and inter- observer variability when determining knee ligaments attachment sites based on MRI scans, as this variability may have a considerable effect on the biomechanical behavior of computational models." Their analysis showed that depending on the ligament, ligament site locations could be determined within a range from 5 to 10 mm and up to 23.39 mm for some ligaments (Rachmat et al. 2014). To address this uncertainty, (Innocenti et al. 2016) introduced a framework to select cruciate and collateral ligament insertion sites accurately. In short, their approach works by defining the ligament insertion area by selecting points that identify that area or by selecting the center of that area. Their approach resulted in intra-observer variability with a mean of less than 1.5 mm and inter-observer variability with a mean of less than 2.5 mm except for the medial collateral ligament on the tibia which was 6.7 mm.

While Innocenti et. al. approach reduced the uncertainty significantly, it is still

a deterministic approach that requires multiple steps to identify the best possible ligament insertion area. Therefore, the purpose of this study was to introduce an automated framework to analyze uncertainty related to ligaments insertion sites by performing a sensitivity analysis of femoral insertion site locations of the dominant knee's load-carrying ligaments relevant in arthroplasty (LCL, PCL, and MCL) . An experiment was designed using D-optimal design of experiments and two previously developed knee models based on novel measurement of condyle-specific loads and joint kinematics during distraction of the joint, as could be collected during arthroplasty.

6.3 Methods

Description of Calibrated Knee Models

Pre-calibration analysis

Two previously calibrated, kinematics controlled knee models were utilized to evaluate the relationship between the mechanical properties of the primary ligaments and corresponding condyle-specific loads. Calibration was based on experimental data from a custom-designed distraction device, which measured condyle-specific reaction forces in the two cadaver specimens (one male, one female). Specimen 1 ("the female specimen") had a BMI of 18, was age 61 with a height of 160 cm, and had no history of knee injury, surgery, or chemotherapy. Specimen 2 ("the male specimen") 48 had a BMI of 27, was age 57 with a height of 173 cm, and no history of knee injury, surgery, chemotherapy, or arthritis. The experiment included application of ramped medial and lateral contact loads at 10°, 45°, and 90°of flexion. Measurements were acquired in 5 lbf increments from approximately 5 to 50 lbf, which were applied equally in both condyles (results reported in Newtons). Kinematics at each loading state were captured using a Mako Robotic-Arm Assisted Surgery System (Stryker) (Grau et al. 2019). Tests were repeated for both PCL intact and PCL resected cases. Compu-

tational models, which were calibrated using a custom kinematics driven framework (Zaylor, Stulberg, and Halloran 2019) were developed for the two specimens. The Posterior Cruciate Ligament (PCL), Medial Collateral Ligament (MCL), Lateral Collateral Ligament (LCL), and Oblique popliteal ligament (OPL) were included in each model (LaPrade et al. 2003). The PCL was modeled as two bundles, the anterolateral PCL (alPCL) and posteromedial PCL (pmPCL) (Anderson et al. 2012). The MCL was modeled as three bundles, the proximal and distal superficial MCL (sMCLProx, sMCLDist) and the deep MCL (dMCL) (LaPrade et al. 2007a). Each ligament was modeled as a set of nonlinear elastic springs (Figure 6.1).

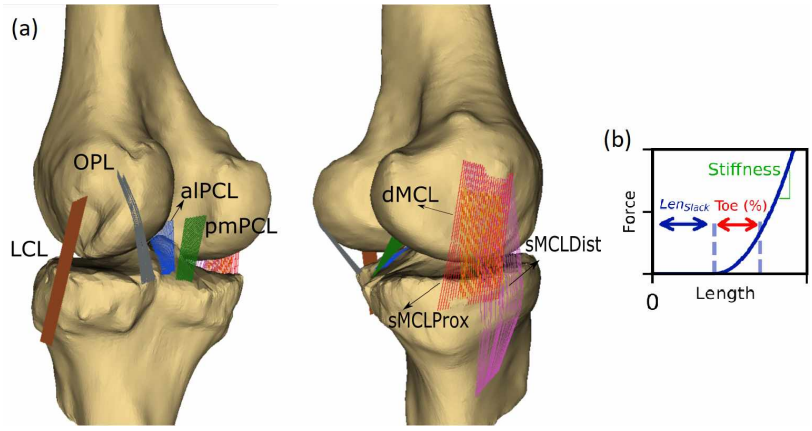

Figure 6.1: (a) Medial and lateral views of the second specimen computational model with all included ligaments. Same ligaments were included in the first specimen. (b) Ligaments were modeled as nonlinear elastic springs. Their behavior was defined by slack length, toe region percent and linear stiffness.

Calibration

For the two knee models used in this work, Ligament-specific stiffness values and slack lengths were calibrated to minimize the difference between measured and predicted condylar loads. Calibration included intact and resected data at 10°and 90°while 45°was retained for validation (Tables 6.1, 6.2 and Figures 6.2, 6.3, 6.4, 6.5).

Ligaments	Slack length(fiber 1)	Slack length(fiber 2)	Stiffness	Toe region
alPCL	38.84	41.55	7601.69	0.03
pmPCL	37.95	39.05	7397.66	0.06
dMCL	41.42	35.90	2657.13	0.07
sMCLProx	46.21	49.77	2236.54	0.06
sMCLDist	85.85	85.81	4112.22	0.08
LCL	56.59	53.46	4620.94	0.08
OPL	58.77	45.99	5608.17	0.06

Table 6.1: Calibrated properties (slack lengths in mm and stiffness in N/ϵ) for the first specimen.

Ligaments	Slack length(fiber 1)	Slack length(fiber 2)	Stiffness	Toe region
alPCL	38.54	45.95	15159.28	0.06
pmPCL	32.34	35.68	8489.57	0.03
dMCL	38.87	32.67	2736.84	0.05
sMCLProx	44.92	51.73	1652.06	0.04
sMCLDist	92.22	90.29	2126.61	0.05
LCL	52.54	52.92	1511.97	0.07
OPL	52.74	34.00	2097.21	0.05

Table 6.2: Calibrated properties (slack lengths in mm and stiffness in N/ϵ) for the second specimen.

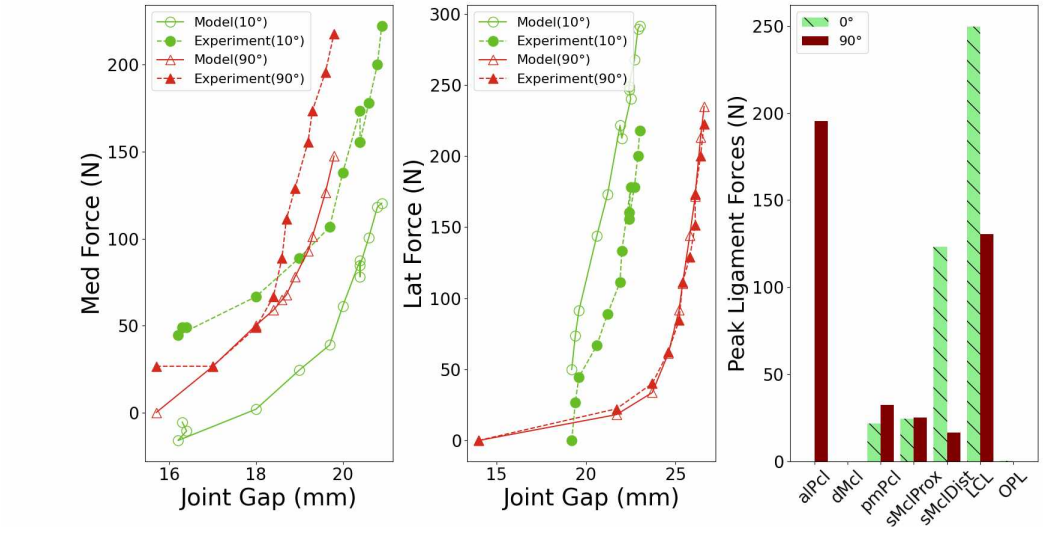

Figure 6.2: Model predicted versus experimental results for PCL intact first specimen (female specimen) as a function of joint gap at 10°and 90°at the medial (Med)-first figure from the right- and the lateral (Lat)-second figure from the right- sides. First figure from the left shows ligament forces at peak condyle reactions.

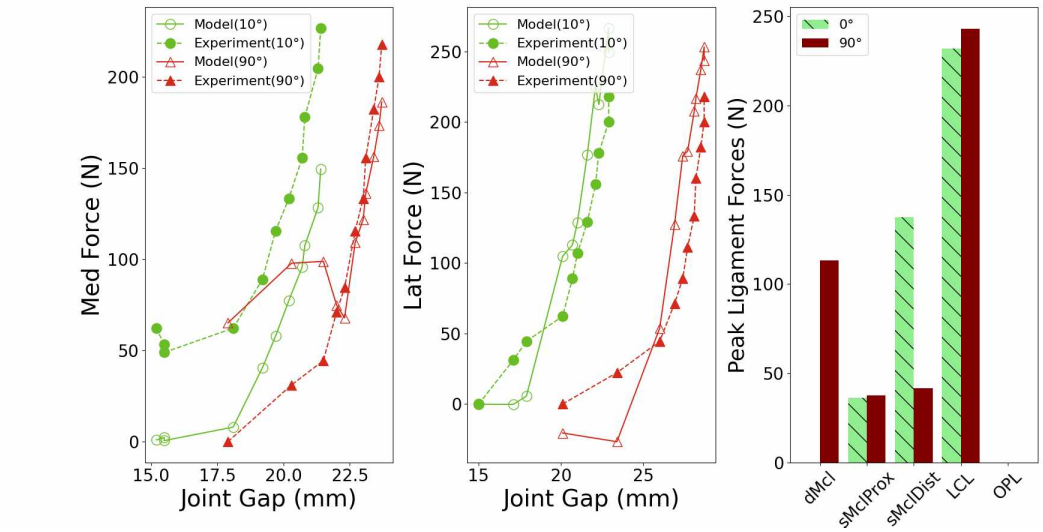

Figure 6.3: Model predicted versus experimental results for PCL resected first specimen (female specimen) as a function of joint gap at 10°and 90°at the medial (Med)-first figure from the right- and the lateral (Lat)-second figure from the right- sides. First figure from the left shows ligament forces at peak condyle reactions.

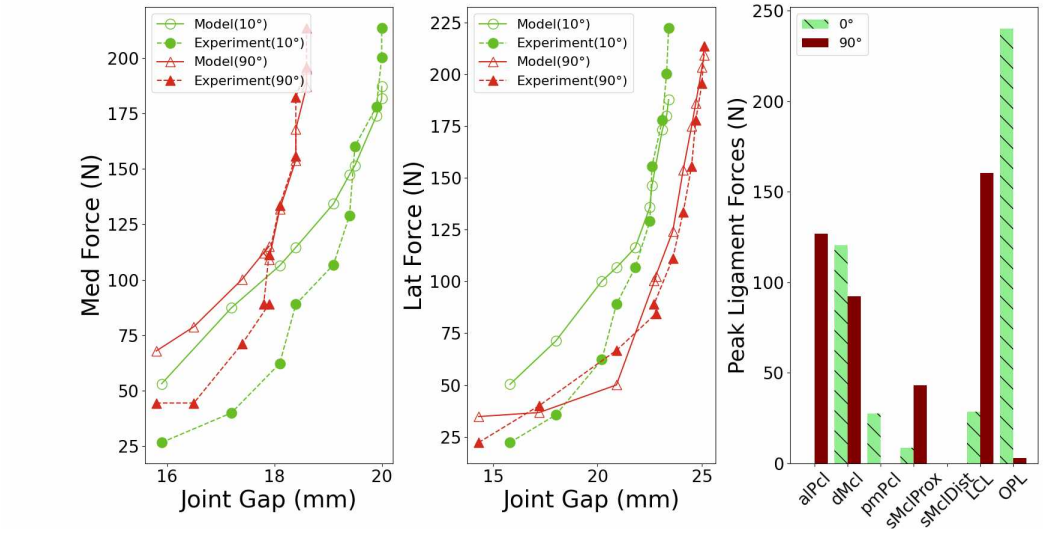

Figure 6.4: Model predicted versus experimental results for PCL intact second specimen (male specimen) as a function of joint gap at 10°and 90°at the medial (Med)-first figure from the right- and the lateral (Lat)-second figure from the right- sides. First figure from the left shows ligament forces at peak condyle reactions.

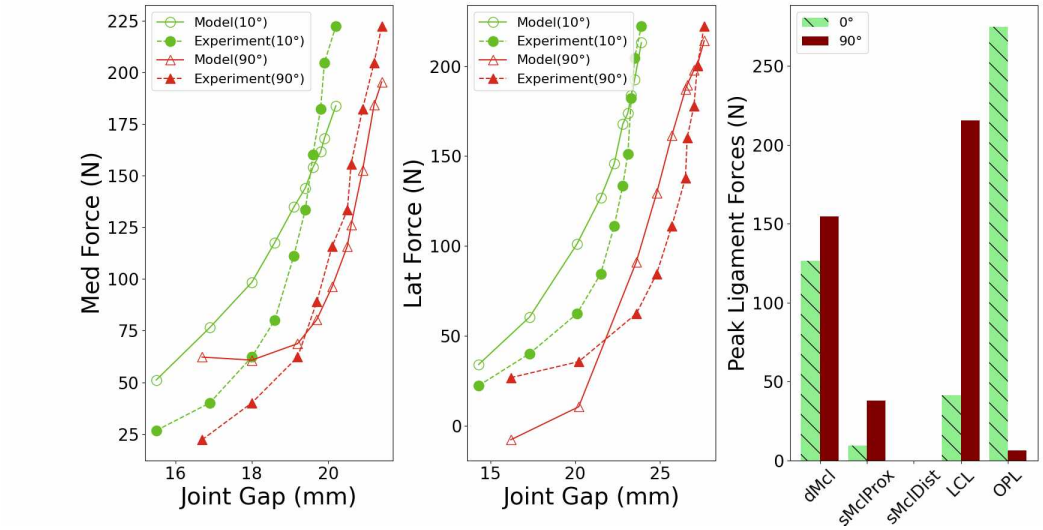

Figure 6.5: Model predicted versus experimental results for PCL resected second specimen (male specimen) as a function of joint gap at 10°and 90°at the medial (Med)-first figure from the right- and the lateral (Lat)-second figure from the right-sides. First figure from the left shows ligament forces at peak condyle reactions.

The model was successfully able to recreate the trend of experimental data with

the following root mean squared (RMSE) errors (Table 6.3).

Specimen	10°	90°	45°
Specimen 1(PCL intact)	23.03	9.15	30.83
Specimen 1(PCL resected)	24.02	19.00	47.12
Specimen 2(PCL intact)	20.45	12.47	40.76
Specimen 2(PCL resected)	28.00	21.90	30.49

Table 6.3: RMSEs (N) between predicted and experimental medial and lateral condylar loads for specimen 1 and 2. Low errors were successfully realized for both data included in calibration (10°and 90°) and for data included in validation (45°).

Preparation of Insertion Sensitivity Samples

A sensitivity analysis of the femoral attachment site locations for ligaments relevant to arthroplasty procedures (LCL, PCL, MCL) was performed on two knee specimens. MRI determined insertion sites were used as the control (C) case, which were perturbated for two levels in four directions to design a computational experiment to test the effect of each ligament, and their interactions, on the predicted condyle reactions (Figure 6.6). Perturbation directions were along primary axes, as determined from the insertion site areas, and the two perturbation levels were based on published MRI determined insertion site location variability (2.5 and 5 mm for the LCL and PCL and 1.25 and 2.5 mm for the MCL) (Rachmat et al. 2014). This resulted in a computational experiment with 3 factors (LCL, PCL, MCL) and 9 levels (2 levels in each direction plus the control, C). All perturbations were performed automatically using Python (Van Rossum and Drake Jr 1995). In short, control case insertion sites were perturbated using two spheres, one for each perturbation distance, then the resulting insertion sites were used to create new ligaments wrapping files to be used in calibration.

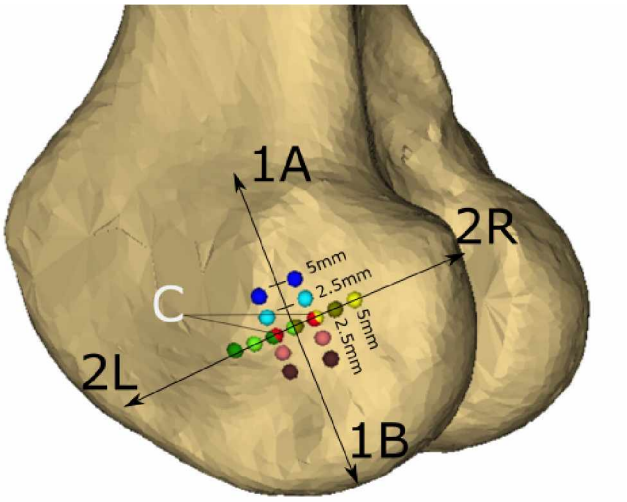

Figure 6.6: Specimen 1's control ("C", red) and the eight perturbed locations along the insertion area determined axes (1 and 2) for the 2 level (5& 2.5 mm) design of experiments sensitivity analysis.

Experiment Model Selection

The goal of this study was to investigate the effect of ligaments insertion sites on the performance of the model versus the experiment. This effect can be a result of a perturbation of single ligament attachments (primary effect) or the result of perturbation of 2 ligaments at the same time (interaction between ligaments insertion sites). Therefore, model with 3 categorical inputs (LCL, PCL and MCL) and their interaction was selected (equation 6.1).

$$\begin{aligned} CondyleReactions \sim 1 + \beta_1 * LCL + \beta_2 * MCL + \beta_3 * PCL \\ +\beta_4 * LCL * MCL + \beta_5 * LCL * PCL + \beta_6 * MCL * PCL \end{aligned} \tag{6.1}$$

Where β_1 to β_6 are the regression coefficients and LCL, MCL, and PCL are insertion site locations for LCL, MCL, and PCL ligaments, respectively.

Selection of Design of Experiments Technique

With 3 factors and 9 levels, full factorial DoE has 729 possible design points, which makes the analysis computationally expensive (Wulff 2003). Therefore, a computer-aided method was selected for this work to reduce the number of design points and reduce the computational expense.

D-optimal design of experiments is a computer-aided design of experiment method, which is based on minimizing the variance in the regression coefficients. D-optimal design criterion with interaction model was selected in this work (Myers, Montgomery, and Anderson-Cook 2016). The goal of the D-optimal algorithm is to generate an information matrix with a pre-specified number of design points. This was accomplished by minimizing the variance of the OLS (ordinary least square) solution predicted response. Thus, D-optimal is an optimization problem. The solution to this problem is provided by maximizing the determinant of the information matrix (more details in 1.3). MATLAB (MATLAB R2019b 2019) *rowexch* was used (Figure 6.7).

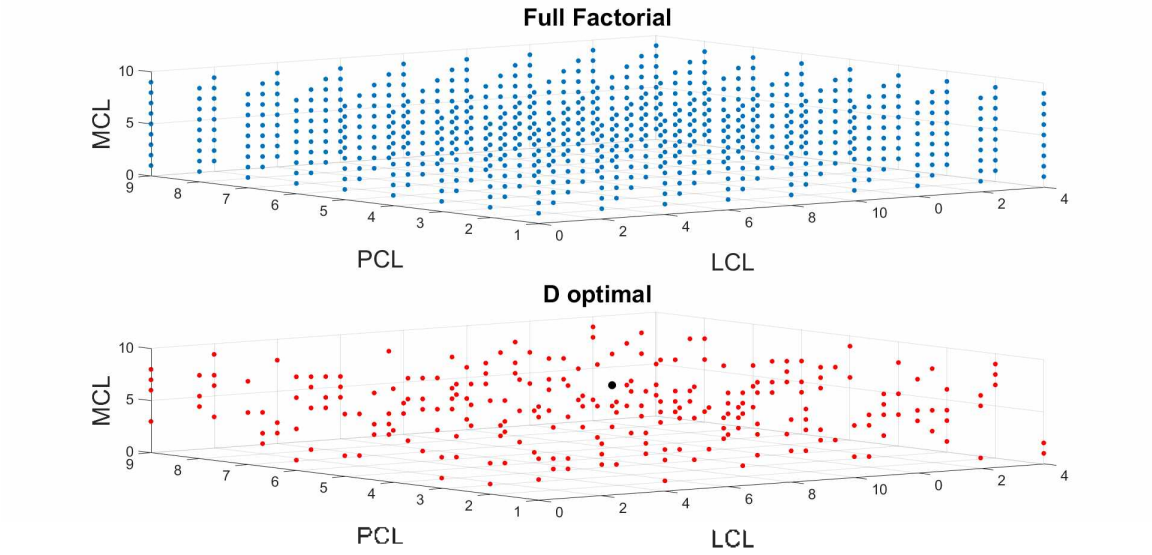

Figure 6.7: D-optimal DoE was used to reduce the number of design points from 729 in case of full factorial DoE (top row) to 220 design points for D-optimal (bottom row). Control case (C) design point highlighted in black.

Sensitivity Analysis Work Flow

The calibrated knee models were recalibrated 220 times (number of design points selected by D-optimal DoE) using a different set of insertion sites (design point) for each calibration. The calibration used CMA-ES optimization (Hansen and Ostermeier 2001) approach to minimize the objective function (equation 6.2).

$$\sum_{i=1}^{2}\sum_{j=1}^{2}\sum_{k=1}^{n}\sum_{l=1}^{2}(M_{ijkl} - E_{ijkl})^2 \tag{6.2}$$

where M is the model predicted condyle reactions, E is the experimentally measured condyle reactions, i is the test case (PCL resected and PCL intact), j is flexion angle, k is the index of the point in the loading cycle, and l are the medial and lateral condyles. The 10° and 90° flexion angles were included in the calibration.

Finally, the Analysis of Variance (ANOVA) was performed using R (R Core Team 2021) using D-optimal design points as independent variables and calibration resulted objective function values as dependent variable to select the statistically significant insertion sites.

6.4 Results

Specimen 1

The insertions sensitivity analysis resulted in ranges between 9.75 N (PCL intact 90°) and 78.04 N (PCL resected 90°) of model versus experiment RMSEs (Table 6.4).

Surgical case	Hi(N)	Lo(N)	C(N)
PCL intact 10°	44.70	18.50	23.03
PCL intact 90°	19.09	9.34	9.15
PCL resected 10°	54.15	23.59	24.02
PCL resected 90°	92.39	14.35	19.00

Table 6.4: RMSEs (N) for control (C), highest (Hi) and lowest (Lo) cases for specimen 1 PCL intact and PCL resected (10°and 90°).

The disparity of RMSEs values through the DoE samples was reflected in the loads each ligament carried. For the PCL intact case at 10°flexion, the variation in the load carried by ligaments ranged between 0 N (no changes in the ligament behavior between low RMSE, high RMSE, and control case) as the case in alPCL and ~50N for dMCL, sMCLDist, and LCL (Figure 6.8). Same behavior was observed for PCL intact case at 90°where ~50 N variation was present for most of load carrying ligaments (Figure 6.9).

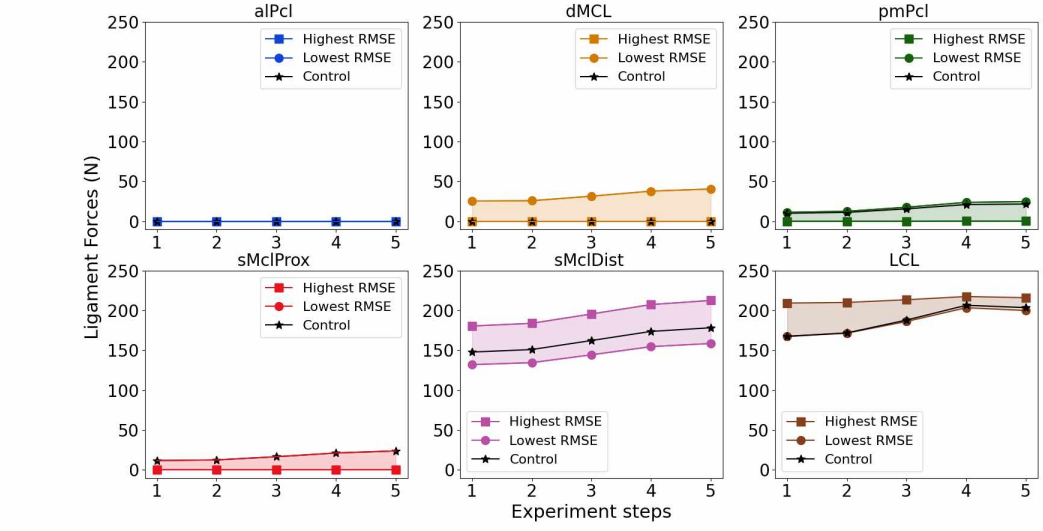

Figure 6.8: The range of loads carried by ligaments for insertion site perturbations with the highest, lowest and control RMSEs for PCL intact case at 10°for specimens 1. The experiment showed a variation of load carried by some ligaments to be as high as 50 N.

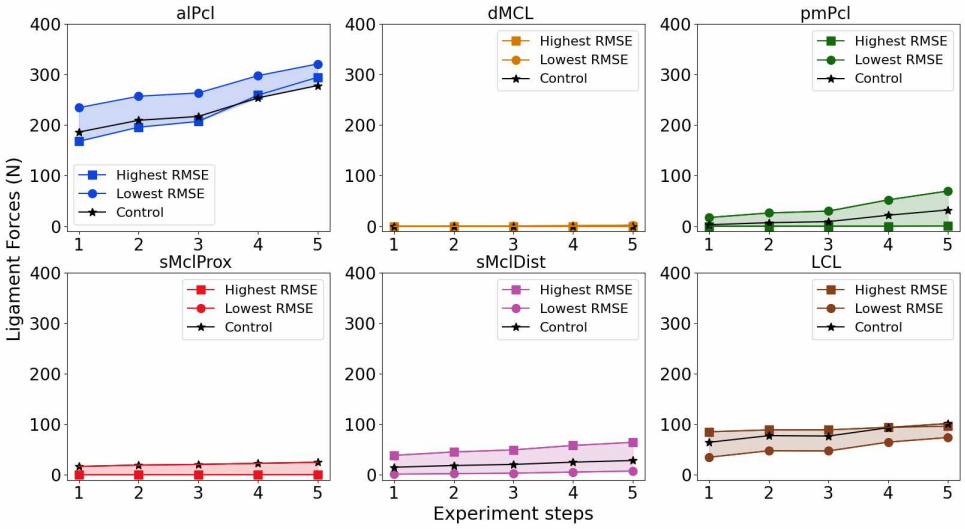

Figure 6.9: The range of loads carried by ligaments for insertion site perturbations with the highest, lowest and control RMSEs for PCL intact case at 90°for specimens 1. The experiment showed a variation of load carried by some ligaments to be as high as 50 N.

The PCL resected cases showed greater variation in loads carried by individual ligaments. For the PCL resected at 10°case, the variation was 100 N (sMCLDist and LCL) (Figure 6.10), while the variation was as high as 200 N for the dMCL in the PCL resected case at 90°(Figure 6.11).

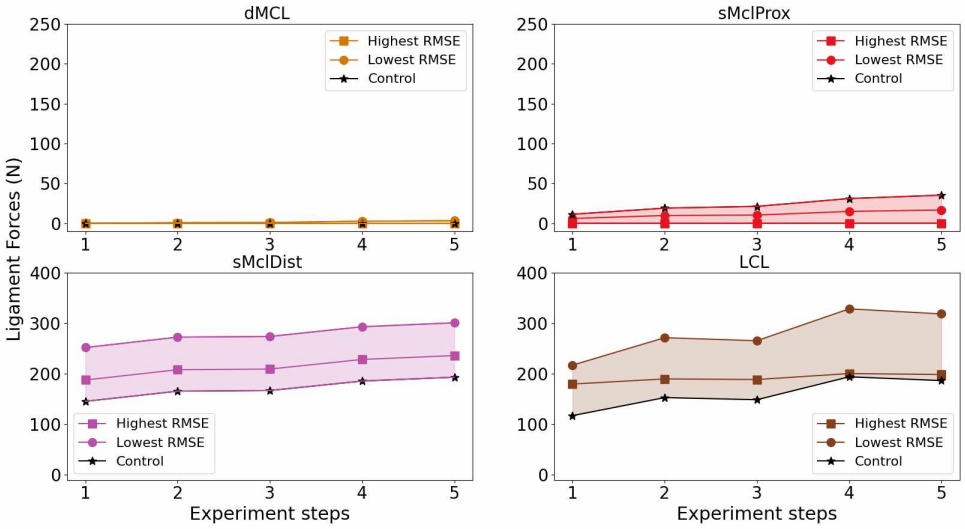

Figure 6.10: The range of loads carried by ligaments for insertion site perturbations with the highest, lowest and control RMSEs for PCL resected case at 10°for specimens 1. The experiment showed a variation of load carried by some ligaments to be as high as 100 N.

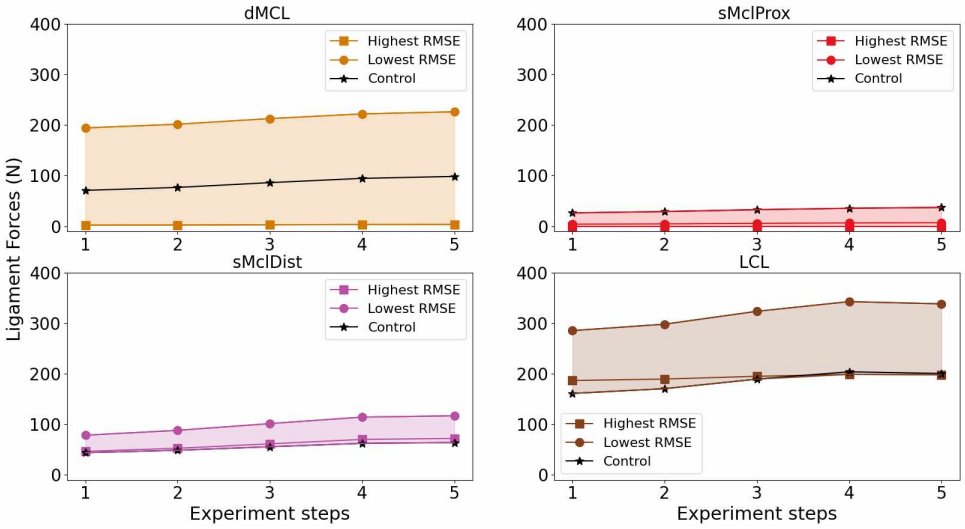

Figure 6.11: The range of loads carried by ligaments for insertion site perturbations with the highest, lowest and control RMSEs for PCL resected case at 90°for specimen 1. The experiment showed a variation of load carried by some ligaments to be as high as 200 N.

These observed changes in ligaments behavior and RMSEs were supported by

the ANOVA, which revealed the LCL and the interaction between LCL and PCL to statistically influence predicted condylar reactions (Table 6.5).

LCL	MCL	PCL	LCL:MCL	LCL:PCL	MCL:PCL
0.00	0.30	0.07	0.15	**0.03**	0.30

Table 6.5: ANOVA p-values for all ligaments and their interactions for specimens 1. insertions of LCL alone as well as its interaction with PCL had a significant effect of predicted condyle reactions (bold text).

Specimen 2

The insertions sensitivity analysis for specimen 2 resulted ranges between 1.44 N (PCL intact 10°) and 5.93 N (PCL intact 90°) of model versus experiment root mean squared errors (RMSEs) (Table 6.6).

Surgical case	Hi(N)	Lo(N)	C(N)
PCL intact 10°	20.5	19.06	20.45
PCL intact 90°	15.25	9.32	12.47
PCL resected 10°	28.44	26.85	28.00
PCL resected 90°	22.36	17.82	21.9

Table 6.6: RMSEs(N) for control(C), highest(Hi) and lowest(Lo) cases for specimen 2 PCL intact and PCL resected (10°and 90°).

In opposite to specimen 1 results, perturbating insertion sites for specimen 2 did not result in a wide range of RMSEs (all less than 10 N), which was reflected in the loads each ligament carried. For the PCL intact case at 10°flexion, most ligaments did not show variation in the load carried by them (alPCL, pmPCL, sMCLProx, and sMclDist) except for the dMCL and LCL which showed a 25 N and 50 N variation, respectively (Figure 6.12). Same behavior was observed for PCL intact case at 90°where most ligaments show small variation (less than 10 N) except for the alPCL which

showed $\sim$ 25 N (Figure 6.13).

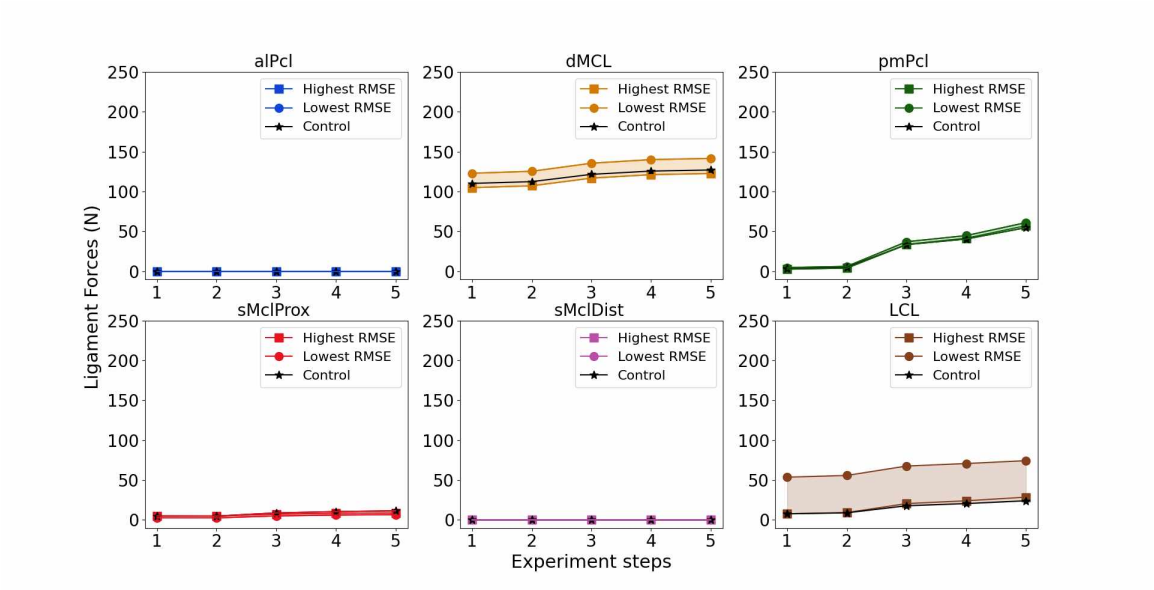

Figure 6.12: The range of loads carried by ligaments for insertion site perturbations with the highest, lowest and control RMSEs for PCL intact case at 10°for specimen 2. The majority of ligament did not show and load variation.

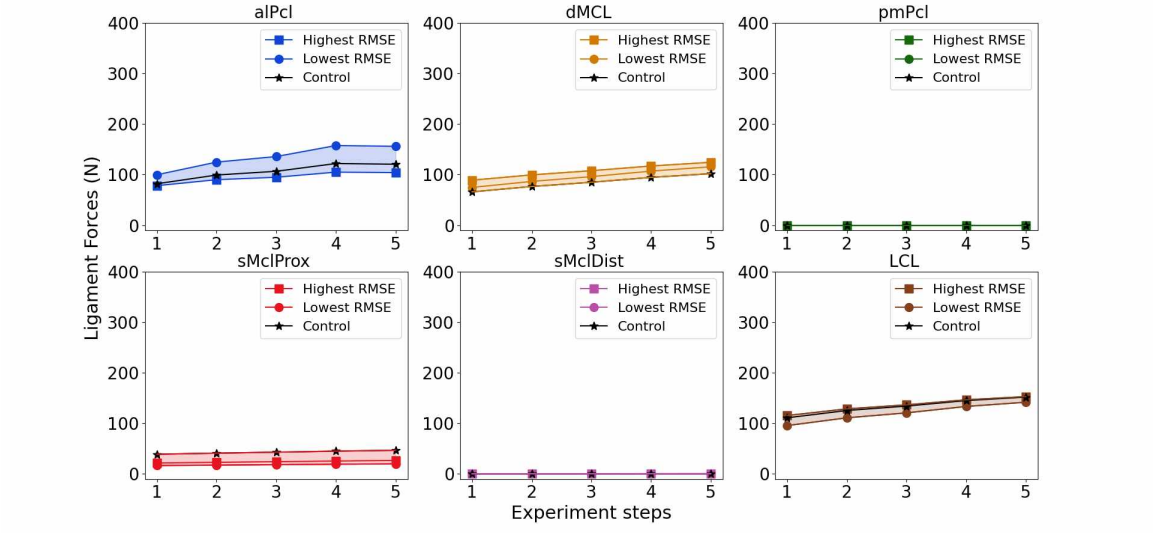

Figure 6.13: The range of loads carried by ligaments for insertion site perturbations with the highest, lowest and control RMSEs for PCL intact case at 90°for specimen 2. The experiment showed a small variation of load carried by the majority of ligaments.

PCL resected cases showed lesser variation in loads carried by individual ligaments.

For the PCL resected at 10°and 90°cases, the variation was less than 10 N for all ligaments except for the dMCL at 90°which had a 20 N load variation (Figures 6.15, 6.14).

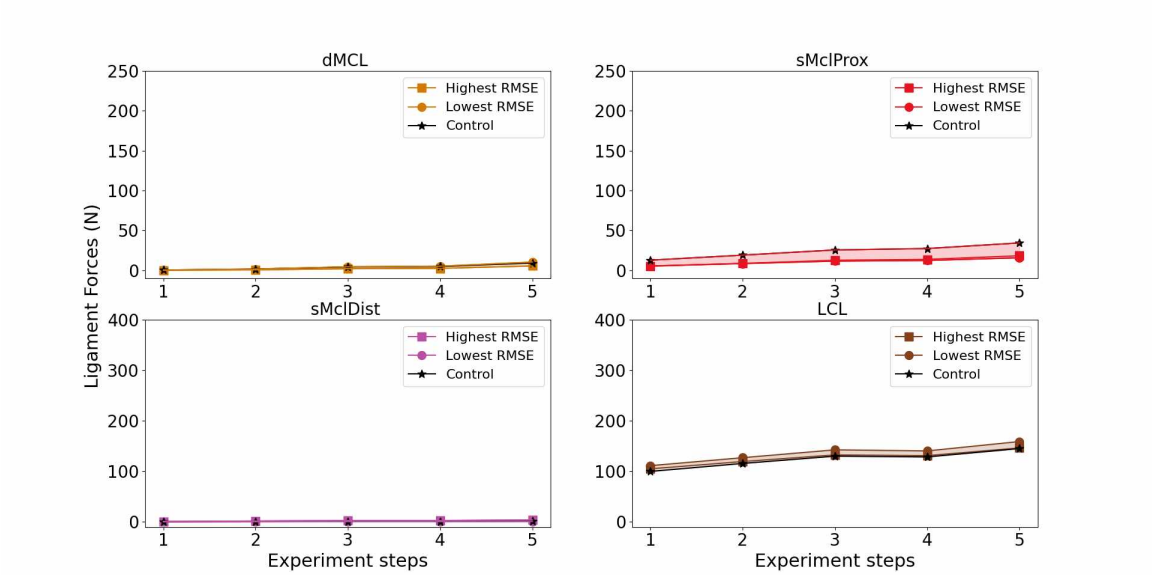

Figure 6.14: The range of loads carried by ligaments for insertion site perturbations with the highest, lowest and control RMSEs for PCL resected case at 10°for specimen 2. The experiment showed a variation of load carried by all ligaments to be less than 10 N.

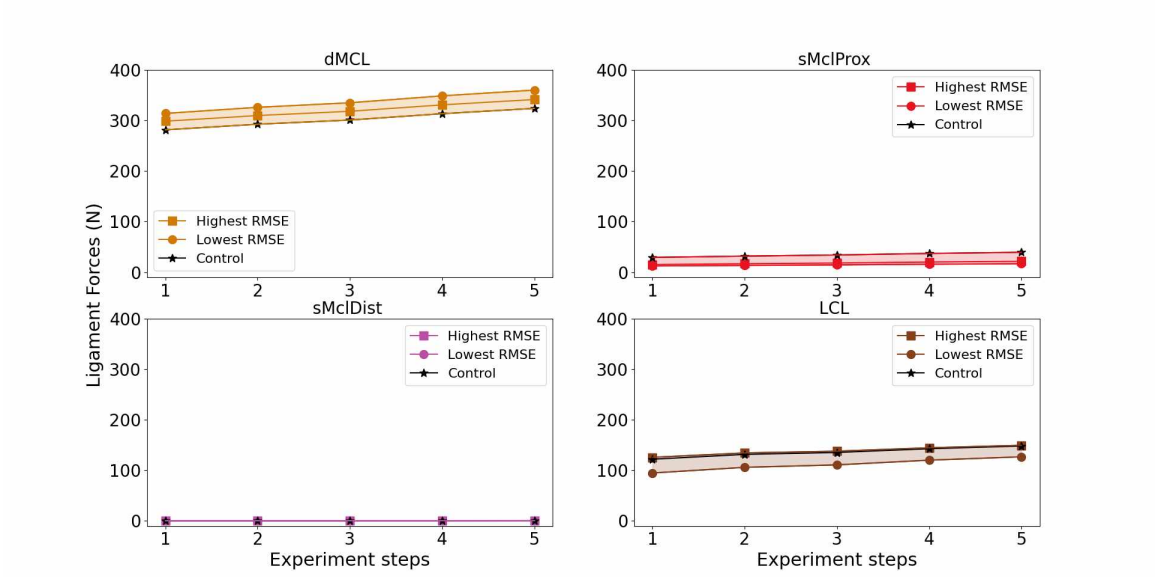

Figure 6.15: The range of loads carried by ligaments for insertion site perturbations with the highest, lowest and control RMSEs for PCL resected case at 90°for specimen 2. The experiment showed a variation of load carried by most ligaments to be as less than 20 N.

These observed changes in ligaments behavior and RMSEs were supported by the ANOVA, which revealed that no insertion location has a statistical influence in predicting condylar reactions (Table 6.7).

LCL	MCL	PCL	LCL:MCL	LCL:PCL	MCL:PCL
0.70	0.58	0.73	0.69	0.87	0.85

Table 6.7: ANOVA p-values for all ligaments and their interactions for specimens 2. Insertions sites showed no significant effect of predicted condyle reactions.

6.5 Discussion

In this work, two calibrated computational knee models were analyzed to investigate the sensitivity of condylar reaction loads to ligaments insertion sites location. The results showed that condyle reaction sensitivity to insertions sites is knee specific. For specimen 1 model, the LCL insertion sites in addition to the interaction between LCL and PCL insertion sites had a significant effect on predicted condyle

reaction loads (Table 6.5), however, no ligament insertion site showed any influence on predicted condyle reactions for specimen 2 (Table 6.7).

This study has several assumptions to reduce the computational cost. Ligaments in computational model used in this work were relatively "simple", where their insertion sites were simplified to four insertion sites, two on the femur and another two on the tibia. In this work, only femoral insertion sites were included in the sensitivity analysis since the ligament recruitment is more sensitive to the location of ligament insertions on the femur (Ali et al. 2017). Individual insertion sites for each ligament were perturbated along two perpendicular axes 2L-2R and 1A-1B (Figure 6.6). Selected axes attempted to follow the native insertion site area which its diameter was based on extreme values from literature (Rachmat et al. 2014). The decision to add another perturbation distance was an attempt to add more design points to better represent the ligament insertion site location with keeping the computational cost feasible.

Investigating the effect of individual ligament insertion sites and their interaction with other ligaments insertion sites are the interest and goal of this study, therefore, a model with interaction terms was adopted which resulted in 729 different combinations (design points) to be evaluated (equation 6.1). Reducing the number of design points was crucial to reduce the experiment's computational cost since every calibration took 2 hours using our dual Xeon 2.4 GHz processors and 64 Gb of RAM work station, thus, D-optimal design of experiments was selected to reduce design points to 220 and subsequently, the computational burden by 69.4% or 1018 hours (Figure 6.7).

Results showed a difference in behavior between specimens, for specimen 1, the insertions sensitivity analysis resulted in ranges between 9.75 N and 78.04 N of model versus experiment RMSEs (Table 6.4). Also, the analysis resulted in a significant change in ligaments behavior as in the case for the PCL intact at 10°when the dMCL

for the lowest RMSE case carried 50 N compared to the control case where the dMCL did not carry any load (Figure 6.8). Results also revealed a significant change in load carried by ligaments up to 100% as the case for sMCLDist and LCL (PCL resected at 10°) (Figure 6.10) and dMCL and LCL (PCL resected at 90°) (Figure 6.11). The change in ligaments behavior was supported by ANOVA analysis where both the LCL and the interaction between LCL and PCL showed a statistical significance in predicting condylar reactions. Perturbating insertion sites for specimen 2 did not result in a wide range of RMSEs, where the range was between 1.44 N and 5.93 N. The analysis also did not reveal any change in ligament behavior even though some ligaments showed an increase in the load carried as in the case of LCL for the PCL intact at 10°(Figure 6.12). Specimen 2 results were supported by ANOVA analysis where no ligaments had statistical significance in predicting condylar reactions.

This study's main goal was to address the uncertainty related to insertion site locations by introducing a framework to investigate the effect of ligament insertion sites on condyler reactions, however, it has multiple limitations to consider for future studies. First, two design points level were selected using perturbation axis, however, there are other possibilities to evaluate such as the use of more levels, the use of different perturbation distances and axis . Second, only three major ligaments femoral insertion sites were included. While these limitations are important to draw a better insight into the goal of this work, the presented analysis is an important step to evaluate computational model's inputs which subsequently improve the model's output prediction by addressing the uncertainty related to insertion site locations.

Quantifying the influence of model's inputs uncertainty by performing sensitivity analysis is critical to establish the credibility of modeling predictions. For this work, selecting each ligament insertion site is a manual process, which depends on many factors such as the quality of MRIs and the user's experience. Our analysis showed a significant effect of insertion site location for specimen 1, which resulted in a wide

range of predicted RMSEs and varied loads across the ligaments. Specimen 2, however, was minimally impacted, which indicates sensitivity to insertion site location may be knee dependent. Our results show the potential influence of insertion site location on prediction of knee-specific ligament loads and condylar reactions, which makes the decision of performing such analysis a decision for the modeler to make depending on the confidence in ligament insertion sites selection process (availability and quality of medical images, experience, available computational resources). The presented analysis is an important part of establishing credibility by addressing one of the sources of knee models uncertainty which ultimately dictates the potential for modeling to support the clinical decision-making process.

Funding

Stryker for initially funding this study.

CHAPTER VII

Conclusion

In this work, two approaches for applying sensitivity analysis to expensive computational knee models were introduced. The first approach was polynomial chaos expansion (PCE) based sensitivity analysis, while the second one was D-optimal design of experiments (DoE) based sensitivity analysis. Both approaches were tested by performing sensitivity analysis on a novel and clinically relevant knee computational model for two specimens. The novelty of the knee model comes from the fact that, to our knowledge, it is the first computational model to evaluate the use of experimentally measured specimen- and condyle-specific distraction forces during calibration of nonlinear ligament properties. While the model's clinical relevance comes from that corresponding predictions of the loads carried by each ligament offer insight into specimen-specific response, which may provide an avenue to accommodate patient-specific tissue mechanics during TKA procedures.

For the first approach, guidelines for the use of PCE-based analysis (aim 1) were provided. Our analysis showed that increasing the PCE order was settled on to create a reliable model versus fixing the PCE order and increasing the number of samples. These results were supported by our analysis of three highly non-linear functions which showed R^2 values grater than 0.9 for all tested functions. The guidelines were

then tested on a knee mechanics problem (aim 2).

A sensitivity analysis was then performed to compare quasi-MC versus PCE sensitivity analyses of predicted condylar reactions that included uncertainty in the mechanical parameters of the ligaments. PCE sensitivity analyses required 3^{rd} PCE with 574 and 170 model evaluations (Tennøe, Halnes, and Einevoll 2018) for PCL intact and PCL resected cases respectively, compared to 12000 and 8000 model evaluations for quasi-MC (Saltelli et al. 2010). The results showed that PCE was practically identical versus quasi-MC with 95% and 98% reductions in model evaluations for analyses with 10 and 6 uncertain variables, respectively. In addition, the PCE-based surrogate model has an additional benefit of low memory size, making it easy to share, disseminate, and embed with other frameworks when a high number of model evaluations may be required (e.g., coupling with musculoskeletal simulations). The specific example used in this study shows that PCE-based sensitivity approach computational efficiency did not affect the quality and accuracy of the results. It also shows the potential to understand the impact of calibrated (or assumed) ligament material properties on predicted articular contact forces by quantifying the proprieties that have the highest contribution. The results revealed differences between specimens, for the medial side, the dMCL consistently showed more involvement in specimen 2 compared to spacemen 1 at 10° flexion for both PCL intact and resected cases. At 90° of knee flexion, reaction forces for specimen 1 were primarily dictated by the alPCL slack length while specimen 2 relied on a combined contribution from the alPCL and the dMCL slack lengths for the PCL intact cases. The PCL resected cases, however, showed combined contributions of the sMCL and dMCL for specimen 1 compared to specimen 2. LCL dominated the later side for both specimens at 10° flexion, with the alPCL showing a significant contribution for specimen 2 compared to specimen 1 at 90° flexion.

Finally, the second approach (DoE based sensitivity analysis) (aim 2) was used to

perform a sensitivity analysis of insertion site locations of the dominant load-carrying ligaments for two knee specimens. The results showed that condyle reaction sensitivity to insertions sites is knee specific. For specimen 1 model, the LCL insertion sites in addition to the interaction between LCL and PCL insertion sites had a significant effect on predicted condyle reaction loads. However, no ligament insertion site showed any influence on predicted condyle reactions for specimen 2. This approach was able to reduce the computational cost by reducing the number of design points from 729 to 220. The presented analysis is an important part of establishing credibility by addressing one of the sources of knee models uncertainty, which ultimately dictates the potential for modeling to support the clinical decision-making process.

References

Ali, Azhar A. et al. (2017). "Combined measurement and modeling of specimen-specific knee mechanics for healthy and ACL-deficient conditions". In: *Journal of Biomechanics* 57, pp. 117–124. ISSN: 18732380. DOI: 10.1016/j.jbiomech.2017.04.008.

Anderson, Colin J. et al. (2012). "Arthroscopically Pertinent Anatomy of the Anterolateral and Posteromedial Bundles of the Posterior Cruciate Ligament". In: *Journal of Bone and Joint Surgery - Series A* 94.21, pp. 1936–1945. ISSN: 15351386. DOI: 10.2106/JBJS.K.01710. URL: http://content.wkhealth.com/linkback/openurl?sid=WKPTLP:landingpage\&an=00004623-201211070-00003.

Babazadeh, Sina et al. (Oct. 2009). "The relevance of ligament balancing in total knee arthroplasty: how important is it? A systematic review of the literature". In: *Orthopedic Reviews* 1.2. ISSN: 2035-8164. DOI: 10.4081/or.2009.e26. URL: https://www.ncbi.nlm.nih.gov/pmc/articles/PMC3143981/ (visited on 08/14/2020).

Baldwin, Mark A et al. (n.d.). "Dynamic finite element knee simulation for evaluation of knee replacement mechanics". In: 45.3 (), pp. 474–483. ISSN: 0021-9290. DOI: 10.1016/j.jbiomech.2011.11.052. URL: http://www.sciencedirect.com/science/article/pii/S0021929011007469.

Baldwin, Mark A. et al. (2009). "Efficient probabilistic representation of tibiofemoral soft tissue constraint". In: *Computer Methods in Biomechanics and Biomedical Engineering* 12.6, pp. 651–659. ISSN: 10255842. DOI: 10.1080/10255840902822550.

Basaga, H B, A Bayraktar, and I Kaymaz (2012). "An improved response surface method for reliability analysis of structures". In: *Structural Engineering and Mechanics* 42.2, pp. 175–189. ISSN: 1225-4568. DOI: 10.12989/sem.2012.42.2.175. URL: http://www.scopus.com/inward/record.url?eid=2-s2.0-84860232789\&partnerID=40\&md5=107679d7f3e0b4ac7868d5009793e31c.

Berveiller, M. and B. Sudret (2004). "Presentation of two methods for computing the response coefficients in stochastic finite element analysis". In: *9th ASCE Specialty Conference on Probabilistic Mechanics and Structural Reliability* 2, pp. 1–7.

Berveiller, Marc, Bruno Sudret, and Maurice Lemaire (2006). "Stochastic finite element: a non intrusive approach by regression". In: *Revue européenne de mécanique numérique* 15.1-2-3, pp. 81–92. ISSN: 17797179. DOI: 10.3166/remn.15.81-92. URL: http://remn.revuesonline.com/article.jsp?articleId=7876.

Blankevoort, L and R Huiskes (1996). "Validation of a three-dimensional model of the knee". In: 29.7, pp. 955–961. ISSN: 0021-9290. DOI: 10.1016/0021-9290(95)00149-2. URL: http://www.sciencedirect.com/science/article/pii/0021929095001492.

Blatman, Géraud and Bruno Sudret (2010a). "An adaptive algorithm to build up sparse polynomial chaos expansions for stochastic finite element analysis". In: *Probabilistic Engineering Mechanics* 25.2, pp. 183–197. ISSN: 02668920. DOI: 10.1016/j.probengmech.2009.10.003.

— (2010b). "Efficient computation of global sensitivity indices using sparse polynomial chaos expansions". In: *John Wiley & Sons* 95.11, pp. 1216–1229. ISSN: 09518320. DOI: 10.1016/j.ress.2010.06.015. URL: http://linkinghub.elsevier.com/retrieve/pii/S0951832010001493.

Blatman, Geraud and Bruno Sudret (2011). "Adaptive sparse polynomial chaos expansion based on least angle regression". In: *Journal of Computational Physics* 230.6, pp. 2345–2367. ISSN: 00219991. DOI: 10.1016/j.jcp.2010.12.021.

Borgonovo, Emanuele and Elmar Plischke (2016). "Sensitivity analysis : A review of recent advances". In: *European Journal of Operational Research* 248.3, pp. 869–887. ISSN: 0377-2217. DOI: 10.1016/j.ejor.2015.06.032. URL: http://dx.doi.org/10.1016/j.ejor.2015.06.032.

Cho, Kyu-Jin, Jong-Keun Seon, Won-Young Jang, et al. (July 2018). "Objective quantification of ligament balancing using VERASENSE in measured resection and modified gap balance total knee arthroplasty". eng. In: *BMC musculoskeletal disorders* 19.1, p. 266. ISSN: 1471-2474. DOI: 10.1186/s12891-018-2190-8.

D'Lima, Darryl D and Clifford W Colwell (2017). "Intraoperative Measurements and Tools to Assess Stability : Journal of the American Academy of Orthopaedic Surgeons". In: 25, S29–S32. URL: http://journals.lww.com/jaaos/Fulltext/2017/02001/Intraoperative_Measurements_and_Tools_to_Assess.8.aspx.

Efron, Bradley et al. (2004). "Least Angle Regression". In: *The Annals of Statistics* 32.2, pp. 407–499. DOI: doi:10.1214/009053604000000067. URL: https://projecteuclid.org/download/pdfview_1/euclid.aos/1083178935.

Ewing, Joseph A., Michelle K. Kaufman, Erin E. Hutter, et al. (Mar. 2016). "Estimating patient-specific soft-tissue properties in a TKA knee". eng. In: *Journal of Orthopaedic Research: Official Publication of the Orthopaedic Research Society* 34.3, pp. 435–443. ISSN: 1554-527X. DOI: 10.1002/jor.23032.

Ewing, Joseph A. et al. (2016). "Estimating patient-specific soft-tissue properties in a TKA knee". In: *Journal of Orthopaedic Research* 34.3, pp. 435–443. ISSN: 1554527X. DOI: 10.1002/jor.23032.

Factorial, Fractional, Jon Herman, and Will Usher (2018). "SALib : Sensitivity Analysis Library in Python (Numpy). Contains Sobol , SALib : An open-source

Python library for Sensitivity Analysis". In: 41.April, pp. 2015–2017. DOI: 10.1016/S0010-1.

Fajraoui, N., S. Marelli, and B. Sudret (2017). "On optimal experimental designs for Sparse Polynomial Chaos Expansions". In: *Retrieved from http://arxiv.org/abs/1703.05312*, pp. 1–32. arXiv: 1703.05312. URL: http://arxiv.org/abs/1703.05312.

Feinberg, Jonathan and Hans Petter Langtangen (2015). "Chaospy: An open source tool for designing methods of uncertainty quantification". In: *Journal of Computational Science* 11, pp. 46–57. ISSN: 18777503. DOI: 10.1016/j.jocs.2015.08.008.

Field, R. V. and M. Grigoriu (2004). "On the accuracy of the polynomial chaos approximation". In: *Probabilistic Engineering Mechanics* 19.1, pp. 65–80. ISSN: 02668920. DOI: 10.1016/j.probengmech.2003.11.017.

Flom, Peter L and David L Cassell (2009). "NESUG 2009 Statistics & Analysis Stopping stepwise : Why stepwise and similar selection methods are bad , and what you should use". In: *Nesug*, pp. 1–7. DOI: 10.1.1.110.8353.

Ghanem, R. G. and P. D. Spanos (2012). *Stochastic finite elements - A spectral approach*. Revised Ed. Mineola, New York.: Dover Publications, Inc.

Giunta, Anthony A., Steven F. Wojtkiewicz, and Michael S. Eldred (2003). "Overview of modern design of experiments methods for computational simulations". In: *41st Aerospace Sciences Meeting and Exhibit* July 2014. DOI: 10.2514/6.2003-649.

Grau, Luis, Max Lingamfelter, Danielle Ponzio, et al. (Dec. 2019). "Robotic arm assisted total knee arthroplasty workflow optimization, operative times and learning curve". eng. In: *Arthroplasty Today* 5.4, pp. 465–470. ISSN: 2352-3441. DOI: 10.1016/j.artd.2019.04.007.

Grau, Luis et al. (2019). "Robotic arm assisted total knee arthroplasty workflow optimization, operative times and learning curve". In: *Arthroplasty Today* 5.4, pp. 465–470. ISSN: 23523441. DOI: 10.1016/j.artd.2019.04.007. URL: https://doi.org/10.1016/j.artd.2019.04.007.

Griffin, Frankie M., John N. Insall, and Giles R. Scuderi (Dec. 2000a). "Accuracy of soft tissue balancing in total knee arthroplasty". English. In: *The Journal of Arthroplasty* 15.8. Publisher: Elsevier, pp. 970–973. ISSN: 0883-5403, 1532-8406. DOI: 10.1054/arth.2000.6503. URL: https://www.arthroplastyjournal.org/article/S0883-5403(00)34521-1/abstract (visited on 08/14/2020).

— (2000b). "Accuracy of soft tissue balancing in total knee arthroplasty". In: *Journal of Arthroplasty* 15.8, pp. 970–973. ISSN: 08835403. DOI: 10.1054/arth.2000.6503.

Grood, E. S. and W. J. Suntay (1983). "A joint coordinate system for the clinical description of three-dimensional motions: Application to the knee". In: *Journal of Biomechanical Engineering* 105.2, pp. 136–144. ISSN: 15288951. DOI: 10.1115/1.3138397. URL: http://dx.doi.org/10.1115/1.3138397.

Halloran, Jason P, Anthony J Petrella, and Paul J Rullkoetter (2005). "Explicit finite element modeling of total knee replacement mechanics". In: 38.2, pp. 323–331. ISSN: 0021-9290, 1873-2380. DOI: 10.1016/j.jbiomech.2004.02.046. URL: http://www.jbiomech.com/article/S0021-9290(04)00092-2/abstract.

Halloran, Jason P et al. (2005). "Comparison of Deformable and Elastic Foundation Finite Element Simulations for Predicting Knee Replacement Mechanics". In: 127.5, pp. 813–818. ISSN: 0148-0731. DOI: 10.1115/1.1992522. URL: http://dx.doi.org/10.1115/1.1992522.

Hansen, N. and A. Ostermeier (2001). "Completely derandomized self-adaptation in evolution strategies." In: *Evolutionary computation* 9.2, pp. 159–195. ISSN: 10636560. DOI: 10.1162/106365601750190398.

Harris, Michael D et al. (2016). "A Combined Experimental and Computational Approach to Subject-Specific Analysis of Knee Joint Laxity". In: *Journal of Biomechanical Engineering* 138.8, p. 81004. ISSN: 0148-0731. DOI: 10.1115/1.4033882. URL: http://dx.doi.org/10.1115/1.4033882.

Hirschmann, Michael T. and Henrik Behrend (Oct. 2018). "Functional knee phenotypes: a call for a more personalised and individualised approach to total knee arthroplasty?" en. In: *Knee Surgery, Sports Traumatology, Arthroscopy* 26.10, pp. 2873–2874. ISSN: 1433-7347. DOI: 10.1007/s00167-018-4973-8. URL: https://doi.org/10.1007/s00167-018-4973-8 (visited on 08/14/2020).

Huang, Shuping and Xinjian Kou (2007). "An extended stochastic response surface method for random field problems". In: *Acta Mechanica Sinica* 23.4, pp. 445–450. ISSN: 0567-7718. DOI: 10.1007/s10409-007-0090-5. URL: http://link.springer.com/10.1007/s10409-007-0090-5.

Innocenti, Bernardo et al. (2016). "How accurate and reproducible are the identification of cruciate and collateral ligament insertions using MRI?" In: *Knee* 23.4, pp. 575–581. ISSN: 18735800. DOI: 10.1016/j.knee.2015.07.015. URL: http://dx.doi.org/10.1016/j.knee.2015.07.015.

Jalalpour, Mehdi and Mazdak Tootkaboni (2016). "An efficient approach to reliability-based topology optimization for continua under material uncertainty". In: *Structural and Multidisciplinary Optimization* 53.4, pp. 759–772. ISSN: 16151488. DOI: 10.1007/s00158-015-1360-7.

Keshavarzzadeh, Vahid, Felipe Fernandez, and Daniel A. Tortorelli (2017). "Topology optimization under uncertainty via non-intrusive polynomial chaos expansion". In: *Computer Methods in Applied Mechanics and Engineering* 318, pp. 120–147. ISSN: 00457825. DOI: 10.1016/j.cma.2017.01.019. URL: http://linkinghub.elsevier.com/retrieve/pii/S0045782516313019http://dx.doi.org/10.1016/j.cma.2017.01.019.

Krstajic, Damjan et al. (2014). "Cross-validation pitfalls when selecting and assessing regression and classification models". In: *Journal of Cheminformatics* 6.1, pp. 1–15. ISSN: 17582946. DOI: 10.1186/1758-2946-6-10. URL: JournalofCheminformatics.

LaPrade, Matthew D. et al. (June 2015). "Anatomy and Biomechanics of the Medial Side of the Knee and Their Surgical Implications". en-US. In: *Sports Medicine and Arthroscopy Review* 23.2, pp. 63–70. ISSN: 1062-8592. DOI: 10.1097/JSA.0000000000000054. URL: https://journals.lww.com/sportsmedarthro/Fulltext/2015/06000/Anatomy_and_Biomechanics_of_the_Medial_Side_of_the.5.aspx (visited on 09/28/2020).

LaPrade, Robert F et al. (n.d.). "The posterolateral attachments of the knee". In: 31.6 (), pp. 854–860. URL: http://journals.sagepub.com/doi/abs/10.1177/03635465030310062101.

LaPrade, Robert F. et al. (2003). "The Posterolateral Attachments of the Knee. A Qualitative and Quantitative Morphologic Analysis of the Fibular Collateral Ligament, Popliteus Tendon, Popliteofibular Ligament, and Lateral Gastrocnemius Tendon". In: *American Journal of Sports Medicine* 31.6, pp. 854–860. ISSN: 03635465. DOI: 10.1177/03635465030310062101.

LaPrade, Robert F. et al. (2007a). "The anatomy of the medial part of the knee". In: *Journal of Bone and Joint Surgery - Series A* 89.9, pp. 2000–2010. ISSN: 00219355. DOI: 10.2106/JBJS.F.01176. URL: http://jbjs.org/cgi/doi/10.2106/JBJS.F.01176.

LaPrade, Robert F. et al. (2007b). "The anatomy of the posterior aspect of the knee: An anatomic study". In: *Journal of Bone and Joint Surgery - Series A* 89.4, pp. 758–764. ISSN: 00219355. DOI: 10.2106/JBJS.F.00120.

Li, Guoan et al. (Sept. 2004). "In vivo elongation of the anterior cruciate ligament and posterior cruciate ligament during knee flexion". eng. In: *The American Journal of Sports Medicine* 32.6, pp. 1415–1420. ISSN: 0363-5465. DOI: 10.1177/0363546503262175.

Loeser, Richard F. et al. (June 2012). "Osteoarthritis: A Disease of the Joint as an Organ". In: *Arthritis and Rheumatism* 64.6, pp. 1697–1707. ISSN: 0004-3591. DOI:

10.1002/art.34453. URL: https://www.ncbi.nlm.nih.gov/pmc/articles/PMC3366018/ (visited on 08/14/2020).

Logan, Daryl L et al. (2007). *A First Course in the Finite Element Method Fourth Edition*. Vol. 147. 3, pp. 1–836. ISBN: 0534552986. DOI: 10.1016/0022-460X(91)90505-E. URL: http://books.google.com/books?hl=en\&lr=\&id=wjr3ArdvAc4C\&oi=fnd\&pg=PA1\&dq=A+First+Course+in+the+Finite+Element+Method\&ots=nan0HIK3bt\&sig=gBLYugWkMJyh3mNku0VTrfsWfww.

MATLAB R2019b (2019). *The MathWorks. Inc.* Natick, Massachusetts, United States.

Mazzoni, Silvia et al. (2007). "OpenSees Command Language Manual". In.

McKay, M. D., R. J. Beckman, and W. J. Conover (2000). "A comparison of three methods for selecting values of input variables in the analysis of output from a computer code". In: *Technometrics* 42.1, pp. 55–61. ISSN: 15372723. DOI: 10.1080/00401706.2000.10485979.

McKenna, F., G. L. Fenves, and M. H. Scott (2000). *Open System for Earthquake Engineering Simulation*. URL: http://opensees.berkeley.edu..

Mommersteeg, T J, L Blankevoort, R Huiskes, et al. (Feb. 1996). "Characterization of the mechanical behavior of human knee ligaments: a numerical-experimental approach". In: *Journal of biomechanics* 29.2, pp. 151–160. ISSN: 0021-9290. URL: http://www.ncbi.nlm.nih.gov/pubmed/8849808 (visited on 08/28/2012).

Mommersteeg, T. J.A. A et al. (1996). "Characterization of the mechanical behavior of human knee ligaments: A numerical-experimental approach". In: *Journal of Biomechanics* 29.2, pp. 151–160. ISSN: 00219290. DOI: 10.1016/0021-9290(95)00040-2. URL: http://www.sciencedirect.com/science/article/pii/0021929095000402.

Mootanah, R et al. (2014). "Development and validation of a computational model of the knee joint for the evaluation of surgical treatments for osteoarthritis". In:

17.13, pp. 1502–1517. ISSN: 1025-5842. DOI: 10.1080/10255842.2014.899588. URL: https://doi.org/10.1080/10255842.2014.899588.

Morris, Max D and Toby J Mitchell (1992). "Exploratory designs for computational experiments". In.

Myers, Raymond H., Douglas C. Montgomery, and Christine M. Anderson-Cook (2016). *Response Surface Methodology: Process and Product Optimization Using Designed Experiments, 4th Edition*. 4th Editio, p. 856. ISBN: 978-1-118-91601-8.

Nowak, Andrzej S. and Kevin R. Collins (2000). *Reliability of Structures*. The McGraw-Hill Companies, Inc. ISBN: 0-07-048163-6.

Papannagari, Ramprasad, Louis E. DeFrate, Kyung W. Nha, et al. (Sept. 2007). "Function of posterior cruciate ligament bundles during in vivo knee flexion". eng. In: *The American Journal of Sports Medicine* 35.9, pp. 1507–1512. ISSN: 1552-3365. DOI: 10.1177/0363546507300061.

Pedregosa, F. et al. (2011). "Scikit-learn: Machine Learning in Python". In: *Journal of Machine Learning Research* 12, pp. 2825–2830.

Posik, P., W. Huyer, and L. Pal (2012). "A comparison of global search algorithms for continuous black box optimization". In: *Evolutionary Computation* 20.4, pp. 509–541. ISSN: 10636560. DOI: 10.1162/EVCO_a_00084.

R Core Team (2021). *R: A Language and Environment for Statistical Computing*. R Foundation for Statistical Computing. Vienna, Austria. URL: https://www.R-project.org/.

Rachmat, H. H. et al. (2014). "Generating finite element models of the knee: How accurately can we determine ligament attachment sites from MRI scans?" In: *Medical Engineering and Physics* 36.6, pp. 701–707. ISSN: 18734030. DOI: 10.1016/j.medengphy.2014.02.016. URL: http://dx.doi.org/10.1016/j.medengphy.2014.02.016.

Rajashekhar, Malur R. and Bruce R. Ellingwood (1993). "A new look at the response surface approach for reliability analysis". In: *Structural Safety* 12.3, pp. 205–220. ISSN: 01674730. DOI: 10.1016/0167-4730(93)90003-J.

Saltelli, Andrea et al. (2010). "Variance based sensitivity analysis of model output. Design and estimator for the total sensitivity index". In: *Computer Physics Communications* 181.2, pp. 259–270. ISSN: 00104655. DOI: 10.1016/j.cpc.2009.09.018. URL: http://dx.doi.org/10.1016/j.cpc.2009.09.018.

Shalhoub, Sami, Wayne E. Moschetti, Leonid Dabuzhsky, et al. (Sept. 2018). "Laxity Profiles in the Native and Replaced Knee—Application to Robotic-Assisted Gap-Balancing Total Knee Arthroplasty". en. In: *The Journal of Arthroplasty* 33.9, pp. 3043–3048. ISSN: 0883-5403. DOI: 10.1016/j.arth.2018.05.012. URL: http://www.sciencedirect.com/science/article/pii/S0883540318304807 (visited on 08/14/2020).

Shin, Yeonjong and Dongbin Xiu (2016). "Nonadaptive quasi-optimal points selection for least squares linear regression". In: *SIAM Journal on Scientific Computing* 38.1, pp. 385–411. ISSN: 1064-8275. DOI: 10.1137/15M1015868.

Smith, Colin R et al. (2016a). "Influence of Ligament Properties on Tibiofemoral Mechanics n Walking". In: 29.2, pp. 99–106. ISSN: 1538-8506. DOI: 10.1055/s-0035-1558858.

Smith, Colin R. et al. (2016b). "The Influence of Component Alignment and Ligament Properties on Tibiofemoral Contact Forces in Total Knee Replacement". In: *Journal of Biomechanical Engineering* 138.2, pp. 21010–21017. ISSN: 0148-0731. DOI: 10.1115/1.4032464. URL: http://dx.doi.org/10.1115/1.4032464.

Sobo, I M (2001). "Global sensitivity indices for nonlinear mathematical models and their Monte Carlo estimates". In: *Mathematics and Computers in Simulation* 55.1–3, pp. 271–280. DOI: http://dx.doi.org/10.1016/S0378-4754(00)

00270-6. URL: http://www.sciencedirect.com/science/article/pii/S0378475400002706.

Stefanou, George (2009). "The stochastic finite element method: Past, present and future". In: *Computer Methods in Applied Mechanics and Engineering* 198.9-12, pp. 1031–1051. ISSN: 00457825. DOI: 10.1016/j.cma.2008.11.007. URL: http://dx.doi.org/10.1016/j.cma.2008.11.007.

Stoltze, Jonas Stensgaard, John Rasmussen, and Michael Skipper Andersen (2018). "On the biomechanical relationship between applied hip, knee and ankle joint moments and the internal knee compressive forces". In: *International Biomechanics* 5.1, pp. 63–74. ISSN: 23335432. DOI: 10.1080/23335432.2018.1499442. URL: https://doi.org/10.1080/23335432.2018.1499442.

Sudret, Bruno (2014). "Polynomial Chaos Expansions and Stochastic Finite Element Methods". In.

Taguchi, G., S. Chowdhury, and S. Taguchi (2000). *No Robust EngineeringTitle.* McGraw-Hill, New York.

Tanzer, Michael and Asim M. Makhdom (Apr. 2016). "Preoperative Planning in Primary Total Knee Arthroplasty". en-US. In: *JAAOS - Journal of the American Academy of Orthopaedic Surgeons* 24.4, pp. 220–230. ISSN: 1067-151X. DOI: 10.5435/JAAOS-D-14-00332. URL: https://journals.lww.com/jaaos/Fulltext/2016/04000/Preoperative_Planning_in_Primary_Total_Knee.2.aspx (visited on 08/14/2020).

Tennøe, Simen, Geir Halnes, and Gaute T. Einevoll (2018). "Uncertainpy: A Python Toolbox for Uncertainty Quantification and Sensitivity Analysis in Computational Neuroscience". In: *Frontiers in Neuroinformatics* 12.August, pp. 1–29. ISSN: 16625196. DOI: 10.3389/fninf.2018.00049.

Tibshirani, Robert (1996). "Regression Shrinkage and Selection via the Lasso". In: *Journal of the Royal Statistical Society* 58.1, pp. 267–288.

Unitt, L et al. (2008a). "Knee Short-term outcome in total knee replacement after soft-tissue release and balancing". In: 90.2, pp. 159–165. DOI: 10.1302/0301-620X.90B2.19327.

Unitt, L. et al. (Feb. 2008b). "Short-term outcome in total knee replacement after soft-tissue release and balancing". In: *The Journal of Bone and Joint Surgery. British volume* 90-B.2. Publisher: The British Editorial Society of Bone & Joint Surgery, pp. 159–165. ISSN: 0301-620X. DOI: 10.1302/0301-620X.90B2.19327. URL: https://online.boneandjoint.org.uk/doi/full/10.1302/0301-620X.90B2.19327 (visited on 08/14/2020).

Van Rossum, Guido and Fred L Drake Jr (1995). *Python reference manual*. Centrum voor Wiskunde en Informatica Amsterdam.

Verstraete, Matthias A et al. (2017). "Contact forces in the tibiofemoral joint from soft tissue tensions: Implications to soft tissue balancing in total knee arthroplasty". In: 58, pp. 195–202. ISSN: 00219290. DOI: 10.1016/j.jbiomech.2017.05.008. URL: http://linkinghub.elsevier.com/retrieve/pii/S0021929017302609.

Völlner, Florian, Tim Weber, and Markus others Weber (Mar. 2019). "A simple method for determining ligament stiffness during total knee arthroplasty in vivo". en. In: *Scientific Reports* 9.1. Number: 1 Publisher: Nature Publishing Group, p. 5261. ISSN: 2045-2322. DOI: 10.1038/s41598-019-41732-x. URL: https://www.nature.com/articles/s41598-019-41732-x (visited on 08/14/2020).

Wasielewski, Ray C., Daniel D. Galat, and Richard D. Komistek (Feb. 2005a). "Correlation of compartment pressure data from an intraoperative sensing device with postoperative fluoroscopic kinematic results in TKA patients". en. In: *Journal of Biomechanics*. Knee Mechanics: An Update of Theoretical and Experimental Analyses 38.2, pp. 333–339. ISSN: 0021-9290. DOI: 10.1016/j.jbiomech.2004.02.040. URL: http://www.sciencedirect.com/science/article/pii/S0021929004000934 (visited on 08/14/2020).

Wasielewski, Ray C, Daniel D Galat, and Richard D Komistek (2005b). "Correlation of compartment pressure data from an intraoperative sensing device with postoperative fluoroscopic kinematic results in TKA patients". In: 38, pp. 333–339. DOI: 10.1016/j.jbiomech.2004.02.040.

Wulff, Shaun S (2003). *A First Course in Design and Analysis of Experiments*. Vol. 57. 1, pp. 66–67. ISBN: 0716735105. DOI: 10.1198/tas.2003.s210.

Xiu, Dongbin (2009). "Fast numerical methods for stochastic computations: A review". In: *Communications in Computational Physics* 5.2-4, pp. 242–272. ISSN: 18152406. DOI: 10.1.1.148.5499.

— (2010). *Numerical Methods for Stochastic Computations*, p. 142. ISBN: 9780691142128.

Yao, Jiang et al. (2006). "Sensitivities of medial meniscal motion and deformation to material properties of articular cartilage, meniscus and meniscal attachments using design of experiments methods". In: *Journal of Biomechanical Engineering* 128.3, pp. 399–408. ISSN: 01480731. DOI: 10.1115/1.2191077.

Zaylor, William and Jason P. Halloran (2021). "Wraptmor: Confirmation of an approach to estimate ligament fiber length and reactions with knee-specific morphology". In: *Journal of Biomechanical Engineering* 143.8, pp. 1–8. ISSN: 15288951. DOI: 10.1115/1.4050810.

Zaylor, William, Bernard N. Stulberg, and Jason P. Halloran (2019). "Use of distraction loading to estimate subject-specific knee ligament slack lengths". In: *Journal of Biomechanics* 92, pp. 1–5. ISSN: 0021-9290. DOI: 10.1016/j.jbiomech.2019.04.040. URL: https://doi.org/10.1016/j.jbiomech.2019.04.040http://www.sciencedirect.com/science/article/pii/S0021929019303161.

Zein, Samih, Benoît Colson, and François Glineur (2013). "An efficient sampling method for regression-based polynomial chaos expansion". In: *Communications in Computational Physics* 13.4, pp. 1173–1188. ISSN: 18152406. DOI: 10.4208/cicp.020911.200412a.

Zhang, X. Y. et al. (2015). "Sobol sensitivity analysis: A tool to guide the development and evaluation of systems pharmacology models". In: *CPT: Pharmacometrics and Systems Pharmacology* 4.2, pp. 69–79. ISSN: 21638306. DOI: 10.1002/psp4.6.